MOBILITY POWER FLOW ANALYSIS OF A THICK PLATE STRUCTURE

J.M. Cuschieri
Center For Acoustics and Vibration
Department of Ocean Engineering
Florida Atlantic University.

N00014-89-J-3140

INTRODUCTION

The flow of vibrational power through structures is an important characteristic in understanding the behavior and the dynamic response of an elastic structure. In the case of thick or curved structural components, the vibrational power can be transmitted by different wave types which have different propagation characteristics through the structure and which can propagate at different speeds. A wave propagating through a structure can be scattered into other wave types when the wave encounters discontinuities in the structure, such as changes in cross section, stiffeners or bulkheads, etc. If the structure is fluid loaded, some of these waves propagate at supersonic speeds and can therefore very efficiently loose some of their energy to acoustic radiation. The efficiency of noise radiation from a structure is very much dependent on the presence of wavenumber components which are supersonic relative to the acoustic fluid that surrounds the structure. The supersonic wavenumber components can be associated with either waves that propagate at supersonic speeds or with supersonic wavenumber components created due to the presence of discontinuities. Consequently, for noise control purposes, it would be required to differentiate between the relative contribution and strength of the structural intensity that can be associated with different wave types or wavenumbers.

Additionally, dissipation mechanisms introduced to dissipate the propagating vibrational power can be wave type dependent. Dissipation efficiency is different according to the type of wave and certain type of waves can act as short circuiting paths for the energy transmission. Therefore, an understanding of the power propagated by different wave components and how the power propagated by one wave type can be scattered into other wave types, is an essential element in the design for vibration control. A formulation is required to relate the scattering of vibrational power from one wave type to another based on the characteristics of the discontinuity. The control of scattering of vibrational power into those wave components which are either efficient radiators or can act as short circuits around energy dissipation mechanisms can reduce the sound radiated by a structural component.

The objectives of this work, as defined at the beginning of the project, were to develop analytical and experimental techniques for the analysis of power flow through thick connected plate

structures and to identify the components of vibrational power flow that can propagate across a discontinuity in a thick plate structure. The emphasis was to be placed on the interaction and scattering between the different wave components in the presence of structural discontinuities. An approach was to be developed that can directly provide the structural intensity components associated with the different wave types. The influence of fluid loading was to be considered based on the progress of the research. Specifically the objectives were as follows:

1. Using the formulation for analytically describing the interaction between in–plane and out–of–plane waves developed in the previous work, formulate the basis for determining the influence of discontinuity characteristics on the scatter of vibrational power across the discontinuity.
2. Experimentally measure the components of the structural intensity associated with the different wave components.
3. Develop the formulation for integrating the influence of fluid loading, and the additional coupling that exists through the fluid for coupled structures for finite coupled plates.

At the beginning of this research program, no techniques were available, in the open literature that can be used to evaluate the flow of vibrational power through thick connected structures, especially if the structure is finite and mode dependent results are required. Some work had been done previously for two plates joined in an L–shaped configuration [1] which did take into account both the in–plane and the out–of–plane waves. However in that analysis [1], a thin plate formulation was used for the representation of the in–plane waves and the coupling between the in–plane and out–of–plane waves only existed because of the configuration of the structure being analyzed.

Furthermore, the concept of structural intensity or power flow had not been fully explored as a method by which one can describe the behavior of elastic structures. The type of information that can be obtained from structural intensity analysis includes:

1. Location of vibration sources and sinks
2. Critical power flow paths
3. Locations on the structure with a high level of energy loss associated with either acoustic radiation or mechanical dissipation.
4. Identification of the dominant wave components (with a component decomposition of the structural intensity) that are involved in the mechanism by which the vibrational power is transmitted.

had not been considered.

With regards to experimental analysis of the power flow, past work generally has been limited to thin plates or beams of infinite extent. Some work has been done by Williams [2] that considers thin elastic shells and which takes into account propagation by both in–plane and out–of–plane waves. The work by Pavic [3] on thick structures concentrates on developing a measurement techniques using strain gauges and velocity transducers to measure the in–plane velocities. While this paper contains a very good discussion on the errors associated with the measurements, the approach is not easy to implement because of the required installation of the strain gauges and the way the in–plane motions are being detected. Berthelot and Jarzynski [4] designed a laser probe for the measurement of in–plane structural motion. Using two interfering laser beams the out–of–plane motion of the structure is filtered out of the measurement. Both frequency domain results and time domain results have been obtained. By scanning the laser probe, the in–plane structural intensity can be determined. While this is one of the most useful techniques for measuring in–plane motion or structural intensity, different probes or processing would be required to measure simultaneously the out–of–plane structural intensity. It would be desirable to have a single probe that can simultaneously measure both the in–plane and the out–of–plane wave motion and thus structural intensity. None of the available experimental techniques can distinguish between structural intensity components propagated by different wave types.

The work done can be classified under three categories:

1. Analytical
2. Simulated and direct experiments
3. Signal Processing.

ANALYTICAL WORK

Thick Plate Analysis

The analytic approach used in the research under this grant is based on the Mobility Power Flow (MPF) method [5]. In this approach a complex structural element is divided into subsystems where each subsystem represents either a physical subcomponent of the global structure or a wave component within a physical substructure. Mechanical mobility functions are then derived for each of the subsystems without reference to the other subsystems or the type of loading. Assumptions can be introduced on the junction loading to simplify the problem by reducing the number of mobility functions included in the analysis. the response of the global structure is then obtained by developing a mobility matrix equation based on continuity of forces and displacements (velocity) at the junctions between the subsystems. This approach has the advantage that by dividing the global

structure into subcomponents, analytical solutions can be obtained for relative complex structural systems which would be difficult to analytically model otherwise. Additionally, since the mobility function required in the matrix equations are generated for the subsystems independent of the influence of the external loading or the other systems, the MPF approach is very efficient when performing parametric analysis on the response of the global structure, for variation of one of the parameters of one of the subsystems. Only the mobility functions associated with that subsystem needs to be re–evaluated.

The MPF technique is particularly applicable in the middle frequency range, where the middle frequency range is defined as being higher than the first one or two modes of the global structure which can be very effectively determined using finite element (FE) analysis, but below the region where the modes become strongly coupled and other techniques such as Statistical Energy Analysis (SEA) would be more appropriate. Beyond the first couple of modes of the global structure, the computational requirements of the FE approach may be prohibitive while the results generated by the SEA method would be too generic possibly leaving out some important characteristic of the response of the global structure.

Using the MPF method, a solution has been found for the determination of the structural power flow between two coupled finite plates of different thickness. In the solution coupling between the in–plane vibrational motion or power flow and the out–of–plane loading has been achieved. Initially the solution was based on the Mindlin [6] and Kane and Mindlin [7] solutions for out–of–plane and in–plane analysis, respectively, of thick plates, and by defining the out–of–plane external load acting on one of the surfaces of the plate as being made up of two components, acting on opposite surfaces of the plate. These two forces have two resultant at the mid–plane of the plate where the solutions of Mindlin are derived. One resultant load is a transverse force and the second resultant load is a "pinching" [72] force. The influence of this decomposition is that the out–of–plane load acting on one of the surfaces of the plate imparts vibrational power to both the in–plane and out–of–plane waves. Using this set up, a solution for the structural power flow is obtained for a number of different thickness combinations of two coupled finite plates. The thickness variations range form equal thickness to a thickness of the receiving plate, which is the plate with no external excitation, being two times thicker than the source plate, which is the plate with the external excitation. The thickness of the source plate is kept constant in the analysis.

The results of the first analysis [8] show that for the out–of–plane flow of vibrational power between the two plates, any variations in thickness will reduce the magnitude of the vibrational power flow. Maximum vibrational power transfer occurs when the two plate components are of equal thickness. The results for the in–plane power flow are however different. In this case, as the receiver plate thickness increases, the magnitude of the vibrational power flow increases, reaching

a maximum for a thickness ratio of between 2 and 4. With further increase in the thickness ratio, the flow of vibrational power between the two plates decreases. The increase in the magnitude of the power flow is more significant at low frequencies, where the product of the longitudinal wavenumber and thickness (kh) is less than approximately 0.5. Because of the fact that the flow of vibrational power associated with the in–plane waves increases as kh increases (for $kh < 0.5$), and the rate of decrease of the power flow associated with the in–plane waves for $kh > 0.5$ is slower than that for the power flow components associated with the out–of–plane waves, more of the available vibrational power goes into in–plane waves as the plate thickness changes. Therefore changes in structural thickness to control the flow of out–of–plane waves vibrational power may result in more power being placed in the in–plane waves.

From initial the work based on the equations of Mindlin's [6] and Kane and Mindlin's [7], a modified version has been developed which uses the approach of Mindlin and Medick [9] which includes the second thickness harmonic for the in–plane waves. The frequency at which the second harmonic becomes important is comparable to the frequency of the first thickness stretch mode for structures with a material which has a value of poisson's ratio of order 0.3. This is common for most materials and therefore Mindlin and Medick's approach is more appropriate. Based on this approach, the same type of analysis for determining the coupling between the out–of–plane and the in–plane waves have been used. In general the results are comparable with previous results. That is, for the problem of the two coupled plates with different thicknesses, the ratio of the in–plane wave power to the out–of–plane wave power increases as the thickness of the plates increases. The ratio of the transmitted power to the input power generally varies in the same way as was previously obtained.

The results obtained thus far are for a discontinuity between two coupled finite plates consisting of a change in the thickness between the two plates. The same approach can be extended to other types of discontinuities in a rather straight forward manner. There is a limitation on the maximum frequency or thickness that can be considered in the analysis, if the Kane and Mindlin [7] approach is used. However, this limitation is removed if the approach by Mindlin and Medick [9] is used.

One interesting new feature which was observed while performing the analysis using the modified approach, but which is not a result of this new approach is that no scattering takes place between the vibrational power of one wave type to another at the discontinuity. Initially this was thought to be a problem with the analysis but when analyzing the governing equations of motion and the results more closely it was observed that scattering would only take place when a load, external to the plate is applied at the discontinuity. The change in the plate thickness discontinuity, because of the fact that the Mindlin approaches are for the mid–plane of the plates, with a Legendre

polynomial expansion to describe the thickness dependency, no additional loading at the surface of the plates is induced by the presence of the discontinuity. The discontinuity only influences the flow of vibration power by one wave type or the another. Any additional loads are created at the mid–plane of the two plates which therefore do not couple the in–plane with the out–of–plane waves. This results in no interaction between the wave types at the discontinuity and hence no scattering of vibrational power. For scattering to take place, a discontinuity which creates an external loading on the surface of the plates, such as would be obtained from a stiffener or a bulkhead, is required. If this is considered, there is scattering and the significance of the scattering increases as the force or moment created by the discontinuity increases.

The force or moment created by the discontinuity (stiffener or bulkhead) is a function of the impedance of the discontinuity and the velocity of the plate along the line of attachment of the discontinuity. A complete analysis on the variation of the strength of the scattering with changes in the impedance or mobility of the discontinuity as a function of frequency has not yet been completed. From this analysis it would be expected that the optimum impedance or mobility for minimum scattering of the vibrational power from the out–of–plane waves to the in–plane waves can be obtained.

To verify the approach used for coupling the in–plane and out–of–plane waves when a load is applied to the surface of the plate, based on the Legendre polynomial expansion, the results from the Mindlin and Mindlin and Medick analysis have been compared to results obtained from a solution of the three dimensional stress equations using an approach similar to the one proposed by Hutchinson [10]. There are some restrictions when using the 3–D stress solution without the approximation of Mindlin [6,9]. One of the most significant is the limitation on the types of boundary conditions that can be described. The results that have been obtained are for a plate with all edges free. Another limitation is the complexity of the solution. Comparing the results obtained for the response using the 3–D stress approach to the results from the Mindlin approach, when a load is applied on the surface of a narrow thick plate, the results from the two approaches are comparable. This suggests that the approaches of Mindlin and Mindlin and Medick can provide the required results without having to deal with the full 3–D stress equations, which are much more complex to solve. Also, the agreement between the two sets of results verifies the approach that has been developed here to couple the in–plane and out–of–plane waves with the excitation applied on the surface of the plate.

Fluid–Loaded Plate

The influence of the fluid loading was investigated using the same MPF technique as for the thick plate analysis. The purpose of the analysis is to investigate the influence of fluid loading on

the power flow between coupled plates across a discontinuity. The analysis is performed for finite plates which create some severe complexities in the solution. Furthermore, since the analysis of the interaction through the fluid between coupled fluid loaded structural elements had not been done in the past, this analysis was restricted to thin plate systems. The objective is to use the results obtained here as a building block for future work that would include both the in–plane and the out–of–plane waves for a thick plate structure or a shell structure. The extension to thick plates with both the in–plane and the out–of–plane waves can be accomplished using the developed approach as a basis. The complexity in the solution arises because of the boundaries of the plate, especially if the boundaries are arbitrary. To deal with the arbitrary boundary conditions, the equations of motion for the plate and the fluid are spatial Fourier transformed into the wavenumber domain. This eliminates the need for assuming a known mode shape. Having performed the spatial transform a relationship can be established between the scattered pressure and the motion of the plate. Since the plate is finite, when taking the spatial transform of the elastic part of the equation of motion of the plate, eight response related parameters are obtained in the result of the transform. From knowledge of the boundary conditions a set of four equations can be derived. The other four equations are obtained from the condition that due to the presence of the fluid–loading, the response of the plate must always remain finite for all frequencies, even if the structural damping is equal to zero. From the two sets of four equations, 8 simultaneous equations are set up and solved to evaluate the unknown parameters in the transform of the equation of motion.

In solving for the scattered pressure part of the equation of motion, this equation only holds over the surface of the plate. Outside the plate surface, different parameters have to be introduced in the equation. For example if the plate is surrounded by an rigid baffle, the stiffness term in the equation of motion outside of the boundaries of the plate should be made infinite. The spatial transform of the elastic part of the equation of motion is thus a truncated transform creating the eight parameters ,mentioned in the previous paragraph. Mathematically the same truncated transform should be applied to the scattered pressure component of the equation of motion. the relationship between the scattered pressure and the plate surface velocity is however based on the full transform. Therefore the spatial transform of the surface velocity cannot be directly substituted for the truncated transform of the scattered pressure. This difference between the full and truncated transforms is analogous to an edge effect. If the scattered pressure waves decay very quickly away from the edge of the plate on the surface of the baffle, then the differences between the full and truncated transforms of the scattered pressure are insignificant. For light fluid–loading the differences between the truncated transform and the full transform, are not significant. Physically this implies that the edge effects are insignificant, which is expected. Furthermore, for light fluid loading the solution including the truncation of the scattered pressure can be readily obtained by

expanding the solution in a taylor series which converges. The series has a fluid density term in the numerator which for light fluid loading is very small and thus the solution converges. For heavy fluid loading, as expected the edge effects are more significant. The difference between the full and partial transform of the scattered cannot be neglected. In this case however, expanding the solution in a similar series as in the light fluid loading case, the solution diverges. The fluid density term in the numerator is significant and the terms of the expansion diverge. A solution including the truncation can still be obtained, but it is more complex mathematically. The complete solution is in the form of a Friedholm integral of the third kind, which can be reduced to a Friedholm integral of the second kind. The solution can then be obtained using a projection method where the first approximation is the solution without scattering. This approach has been successfully implemented and a solution obtained for two end coupled plates and two plates coupled to form an L–shaped configuration. In the case of the L–shaped plate, the diffraction from the outside corner is not considered.

EXPERIMENTAL ANALYSIS

Simulation Results

In the experimental phase of the work, simulation experiments were performed on a thick, L–shaped, finite plate. The L–shaped plate configuration was selected since the analytical solution which can be modified to evaluate the components of structural intensity at each location on the plates, was already available. Using the derived expressions from the analytical solution, structural intensity maps are generated for each of the components of the wave motion in the thick finite plates. An analysis was performed on the influence of thickness and frequency or mode number on the structural intensity maps. The results of the analysis show that the out–of–plane structural intensity components decrease with increasing wavenumber and thickness product (kh), for a fixed mode number, while the in–plane structural intensity components increase as the kh value value increases. Less vibrational power is imparted to the out–of–plane motion with increases in the thickness of the plates. This result is consistent with some of the results obtained in the analytical section. Also, as would be expected, for thin plates the components of structural intensity associated with the in–plane motion are insignificant when compared to the structural intensity components associated with the out–of plane motion. As the thickness increases, out–of–plane motion structural intensity components become the dominating components. The changes with the mode number are very similar to the changes with thickness. The controlling parameter is the kh product, which is modified by either changes in the thickness or the frequency.

The simulation analysis also allowed for the determination of the required spacing of the measurement locations to evaluate the spatial transforms for the computation of the structural intensity components using finite differences. It is concluded that to obtain meaningful estimates

of the spatial derivatives, spatial distances of the order of 1% of the minimum wavelength are required. This can make the separation distance very small. In developing the simulation results a separation distance for the measurements of 1 mm on a 0.5 m by 1.0 m plates is considered.

Experimental Measurements

Apart from the simulation experiments, direct experimental measurements of structural intensity were performed on a thick plexiglass beam of thickness 0.025 m, with one of its ends embedded in sand, to damp some of the out–of–plane motion, and with an external load applied at the free end. The external load consists of an in–plane load applied slightly off axis to induce both in–plane and out–of–plane waves. The vibrational power associated with either the in–plane or the out–of–plane waves propagate at different speeds, with different wavenumbers. Therefore a frequency–wavenumber decomposition can be used to decompose the structural intensity values into components associated with the different wave types. The decomposition of the intensity components is performed at the cross spectrum stage, before the final intensity vector is computed. The structural intensity vectors can then be plotted as a function of frequency and wavenumber, with the magnitude at each frequency and wavenumber value representing the relative fraction of power flow associated with the corresponding wave type.

In implementing this concept for the measurement of structural intensity on a thick beam, vibration measurements were taken at a number of equally spaced locations along the length of the beam. The in–plane and out–of–plane motions are measured by a single transducer mounted on the surface of the beam. The in–plane waves induce an out–of–plane motion due to the poisson effect. The magnitude of this out–of–plane motion is significant for thick structures. With the mainly in–plane excitation induced in the beam, the out–of–plane motion associated with in–plane waves is of the same order of magnitude as the out–of–plane motions associated with the out–of–plane waves. Frequency cross spectra were formed for each of the measurement locations and by performing a spatial transform on these measured cross spectra, the frequency–wavenumber structural intensity spectrum is obtained. In the case of the beam, in–plane longitudinal waves and out–of–plane transverse waves are the predominant wave motions, thus the frequency–wavenumber spectrum of the structural intensity shows two distinct set of peaks, one set for the out–of–plane waves, where the relationship of wavenumber with frequency at the location of the peaks shows the characteristic dispersive curve, and the second set of peak corresponding to in–plane longitudinal waves, where the propagation speed is independent of frequency. If instead of the beam a plate was considered, then apart from the longitudinal in–plane waves, in–plane shear waves would also have been present.

Additionally, measurements were performed on a semi–infinite thick beam with and without a discontinuity. The measurements of the beam response were in this case obtained using a

stereophonic magnetic head mounted on a scanning table. Discrete cross–spectral density data between the response at selected locations on the surface of the beam and the input load were first determined and then spatial Fourier transformed to obtain a frequency – wavenumber cross spectra of the response. The cross spectra are manipulated to obtain the frequency – wavenumber plots of the structural intensity. A stereophonic pickup was used to simplify the acquisition of the data.

The experimental results obtained for the semi–infinite beam show the expected two components of the structural intensity which propagate with different wave speed, hence different wavenumbers, in the frequency–wavenumber plot. One component is associated with the in–plane waves (fast wave speed) and the other component is associated with the out–of–plane waves (slower wave speed). These results verify the technique that the scattering of vibration power can be determined experimentally by using a frequency–wavenumber decomposition of the structural intensity flow.

Signal Processing

Work was also performed on the signal processing approach required to manipulate the acquired experimental data on a two dimensional, finite surface to deduce the frequency–wavenumber spectrum of the structural intensity. In the case of a two dimensional structure, wavenumber components exist for each dimension of the structure. For a structure with both in–plane and out–of–plane wave motion, wavenumber components will also exist for each wave type in every direction. The proper combination of the components in one direction with the components in the orthogonal direction will result in the wavenumber values for the selected frequency, and for the particular wave type. Without a priori knowledge, the wave number components cannot be properly combined, however this problem can be worked around by using a two dimensional transform. In this case, the peaks in the two dimensional wavenumber spectrum will combine to represent the proper values for the wavenumbers for each of the existing wave types in the structure. For example if a wavenumber spectrum is computed at a fixed frequency, for a finite plate with both in–plane and out–of–plane motion, then the two–dimensional spectrum will have three peaks, one corresponding to the out–of–plane wavenumber, another for the in–plane longitudinal wavenumber and the third for the in–plane shear wavenumber. If multiple two–dimensional spectra are obtained as a function of frequency, the trace of the peaks in these spectra will represent the dispersion characteristics of the respective wave type. These result have been obtained for the structural intensity frequency–wavenumber spectrum for a finite thick plate structure, using simulated measured data.

An issue which is of concern when performing spatial data processing with finite structures, especially for low order modes, is the proper identification of the wavenumber components given

the sever truncation of the vibration motion shapes. In the work performed here, to better distinguish wavenumber components, the measured data is extended by either duplicating the data using replicas of the measured data or by zero padding. Padding with zeros increases the resolution but does not eliminate the side band effects. On the other hand, duplication by mirror imaging the data such that discontinuities are not introduced eliminates or minimizes the side band effects. Either of these two techniques are used in the processing of the simulated data to generate the two–dimensional frequency wavenumber structural intensity plots. Using this approach, it is shown that [11] a good estimate of the wavenumber of the mode is obtained. This is demonstrated by the consistency of the dispersion characteristics obtained for a particular wave type with what is expected from theory. This issue will not be a problem for large structures or for high order modes.

Non–Contacting Measurement Technique

A laser based approach has been developed to perform measurements of structural intensity associated with different wave components. In developing the approach, efforts were made to determine not only the motion of the structure but also the first, second and third order derivatives. The reason behind this requirements are twofold. First, to eliminate errors that are typically introduced in the evaluation of the derivative through multiplying the wavenumber spectrum of the response by the wavenumber. Since the wavenumber spectrum is derived from measurements, estimates of high order derivatives based on these measurement have a high level of error [12]. Second, by directly measuring the derivatives, real time estimates of the structural intensity are possible without further post processing, if a wavenumber decomposition is not required. If more than one component of the structural intensity is present and it is required to discriminate the components using a wavenumber decomposition, then post processing is required to obtain the wavenumber spectra.

The approach used to estimate the derivatives is based on finite differences. With this approach it is required that the response at multiple locations is measured simultaneously by the laser system. The simultaneous measurements require a high degree of accuracy especially with regards to the phase of the signal. The importance of phase accuracy in the measurement of the structural intensity is well documented [13]. The determination of the derivatives using finite differences would require the same level of accuracy as if the structural intensity is being directly measured. Another aspect of the finite difference approach for the determination of the response derivatives is that the separation distance between the measurement locations must be less than 10% of the minimum wavelength for which measurements are required. To be able to extend the measurement up to as high a frequency as possible, the finite difference spacing is reduced. With a laser based approach, since the thickness of the laser beam is very small, the spacing can also be made very

small. However this creates a larger constraint on the maximum error that is allowed in the measurement of the amplitude and the phase between the measuring channels.

Fiber optic techniques are commonly used in laser vibrometers. However if the fiber is strained, such as would be the case if the fiber is bent, an unknown static phase shift is introduced in the signal passing through the fibre optic cable. If only one measurement is being performed by one single fibre, since the phase shift is static, this will not influence the measurement. However when multiple point measurements, with different optical fibers, are performed, a non–recoverable static phase error is introduced in each fiber optic cable. This phase shift destroys the accuracy between the channels and thus the relative measurements between the channels. Finally the laser based system had to be capable of handling more than one frequency component. That is for the frequency wavenumber scheme to discriminate between different wave components of the structural intensity an broad band frequency analysis is required.

With the above requirements established, a compact laser based measuring set–up with all the laser components right up at the measuring front end, to eliminate as much as possible static phase and magnitude errors has been developed. The set–up would be capable of measuring up to the third derivative. However significant difficulties were encountered with the set–up and to–date the set–up is still non functional. Outside companies were asked to help in this set–up, (United technologies Optical Systems and Advanced Acoustics Concepts), supplying expertise in optics and high frequency electronic circuitry. Instabilities in the electronic circuitry, caused by high frequency interference on the measurement signals, that conditions the optical signal before it is passed to the data acquisition system have not been eliminated.

The set–up of this laser consists of a diode laser source mounted at the head of the multi channel system. The single source is then divided into 13 channels through a series of aperture plates and lenslets. The front end set of the lenslets will focus the multiple beams on the vibrating target which is 5 to 10 cm away. The total size of the head which includes all the optics is 0.33 m by 0.33 m. The selected set–up optimizes phase accuracy between the channels. The back scattered light from the target is collected by two sets of detectors. The output of the detectors feeds to a processing unit with a one channel handling each pair of detectors. By combining the signals from the pair of detectors, the absolute phase of the channel can be estimated to an accuracy of a few milli radians. Whether the processing can be done in real time is dependent on how fast the collected data can be transferred from the memory on the processing boards for each pair of detectors to the processing system, and how fast the processing system can manipulate this data to compute the structural intensity results and store these results on some medium.

This part of the project, to set up a laser based measurement approach to measure the surface response and its derivatives from which both the in–plane and the out–of plane structural intensity components can be simultaneously measured in frequency and wavenumber has not been very successful. The main reason for this is an underestimate of the time and expense required to develop an untested approach and set–up an experimental measurement technique by which all components of the structural intensity can be measured. Development of this approach and set–up will continue even after the end date of this project. Given the effort that has already been put into the development, and the fact that now only engineering type problems remain, work will continue to be able to perform some measurements. It has been shown by using, other forms of measurements of structural intensity, that the data that will be generated by this laser based set–up can be used to discriminate between the intensity components associated with different wave types.

REFERENCES

1. McCollum M. D., "Vibrational Power Flow in Thick Connected Plates", Ph. D. Dissertation, Florida Atlantic University, 1988.
2. Williams E. G., "Structural Intensity in Thin Cylindrical Shells", Proceedings of the Third International Congress on Intensity Techniques, Senlis, 1990.
3. Pavic G., "Structural Surface Intensity: An alternative Approach in Vibration Analysis and Diagnostics", Journal Of Sound and Vibration, 115(3), 1987.
4. Berthelot, Y. H., Jarzynski J., "A Laser Probe for Measurement of in–plane structural Vibrations", Proceedings of the Third International Congress on Intensity Techniques, Senlis, 1990.
5. Cuschieri J. M., "Structural Power Flow analysis using a Mobility Approach of an L–shaped Thick Plate", Journal of the Acoustical Society of America, 87(3), 1990.
6. Mindlin R.D., "Influence of Rotary Inertia and Shear on Flexural Motions of Isotropic Plates", Journal of Applied Mechanics, Vol: 18, 31–38, 1951.
7. Kane T.R., Mindlin R.D., "High Frequency Extensional Vibration of Plates", Journal of Applied Mechanics, Vol: 23, 277–283, 1956.
8. Faivre D'Arcier E., "Mobility Power Flow Analysis of Connected Thick Plates with Step Discontinuity", M. S. Thesis, Florida Atlantic University, 1990.
9. Mindlin R.D., Medick M.A., "Extensional Vibration of Elastic Plates", Journal of Applied Mechanics, Vol: 26, 561–569, 1959.
10. Hutchinson J. R., Zillmer S. D. "Vibration of a free rectangular parallelepiped", Journal of Applied Mechanics, Vol: 50, 123–130, 1983.
11. Grandclement C., "In–Plane and Out–of–Plane Components of Structural Intensity in Thick Structures", M. S. Thesis, Florida Atlantic University, 1990.
12. A. L. Pate et al. "Determination of structure–borne intensity in plates from acoustic imaging". Proc. of the third international congress on intensity techniques, 1990, 189–196.
13. W. Redman–White. "The measurement of structural wave intensity". 1983. Ph. D dissertation, Univ. of Southampton.

FUTURE WORK

Analytical and experimental tools have been developed which can be used to better understand the flow of vibrational power across structural discontinuities in thick connected plate like structures. The work done thus far, while establishing the basis, is by no means complete. Work should be continued in this area to generate results for different thick plate and discontinuities combinations. A more extensive experimental program is also required. Finally the techniques should be extended to cylindrical shell structures including fluid–loading effects.

LIST OF PUBLICATIONS, PRESENTATIONS AND THESIS

Under this research grant, three Master's thesis and two Ph.D. Dissertations have been completed. Copies of the Master's thesis have already been submitted to the program monitor. Copies of the Ph.D. dissertations will be submitted as they become available. A number of Presentations have been given at meeting of the Acoustical Society of America. Up to this point no papers have been published from this work in refereed journals but a number of papers are in preparation for submission to technical journals.

1. "Acoustic Wave Scattering from Fluid–loaded Plates with Arbitrary Boundary Conditions", jointly with R. Kaina, A.S.A. 123rd Meeting, Salt Lake City, Utah, May 1992.

2. "Coupling of In–plane and Out–of–plane Waves in a Thick Flat Plate Structure Subjected to a Transverse Load", A.S.A. 123rd Meeting, Salt Lake City, Utah, May 1992.

3. "Experimental Measurement of Structural Intensity in the frequency–wavenumber Domain", jointly with S. Padiyar, A.S.A. 123rd Meeting, Salt Lake City, Utah, May 1992.

4. "In–plane and Out–of–plane Propagation of Structural Intensity on Thick Plate Structures", M.S. Thesis, Ocean Engineering Department, Florida Atlantic University, April 1991.

5. "Structural Intensity Measurements in Thick Structures", M.S. Thesis, Ocean Engineering Department, Florida Atlantic University, April 1991.

6. "Mobility Power Flow Analysis of Connected Thick Plates with a Step Discontinuity", M.S. Thesis, Ocean Engineering Department, Florida Atlantic University, April 1991.

7. "Interaction of Acoustic Waves Generated by Coupled, Finite Fluid–Loaded Plates", Ph. D. Dissertation, Ocean Engineering Department, Florida Atlantic University, August 1993.

8. "The Decomposition of Structural Intensity by Wave Type using Experimental Techniques", Ph. D. Dissertation, Ocean Engineering Department, Florida Atlantic University, expected date to completion December 1993.

Power Flow Through The Junction Between Two End Coupled Plates

In previous work [1] equations were developed for the power flow across the junction between two plates joined in an L–shaped configuration. In that case the two plates were joined at right angle which coupled the in–plane waves with the out–of–plane waves at the junction. The out–of–plane waves of the first plate would couple with the in–plane waves of the second plate at the junction and vice versa. The solution was developed in terms of mobility functions which were derived from Mindlin's thick plate equations for flexural out–of–plane motion [2] and thin plate in–plane equations of motion in which only the thickness stretch motion was considered. An improvement to this analysis uses Kane and Mindlin's [3] in–plane wave equations of motion. Essentially these equations apply for the mid–plane of the plate with assumptions made regarding the variation of the displacement as a function of the thickness direction. All forms of loading, both for the in–plane and the out–of–plane waves are describe with respect to the mid–plane of the plate. The consequence of this is that in–plane and out–of–plane waves remain uncoupled. This issue is important when trying to obtain a solution for end coupled plates.

In the case of the end coupled plates (figure 1), because the junction between the two plates is in the same plane as that of the plates, there is no angle which couples the in–plane with the out–of–plane waves. That is, if the plates are subjected to a transverse load this would only induce out–of–plane motion. While if the plate is subjected to an in–plane load it would only induce in–plane motion. This is contrary to what would be expected physically. Intuitively it would be expected that if a force is applied perpendicular to the surface of a thick plate slab, the force will induce both in–plane and out–of–plane motion.

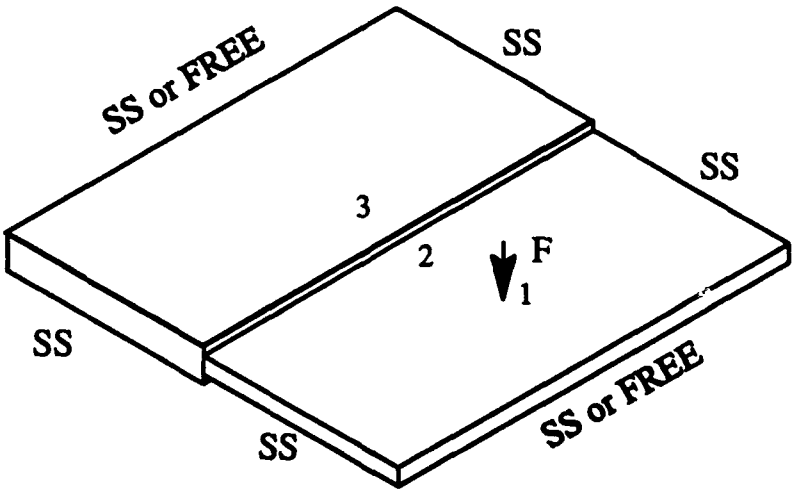

Figure 1. Configuration for end coupled plates.

Various approaches were considered to work around this problem [4]. The literature was surveyed and while solutions based on 3–D stress analysis were found, these were very restrictive in their use, especially the type of boundary conditions that can be considered. Using a variational approach it is shown that the Mindlin [2] and Kane and Mindlin [3], approaches for out–of–plane and in–plane waves can be simultaneously derived from the 3–D stress equations, using the assumption of linear variation for the deformations and the strains in the thickness direction of the plate. Even though the equations where derived from the same 3–D stress equations, the results are two sets of independent uncoupled equations, one set describing the in–plane motion and another set describing the out–of–plane motion, with the solution being in terms of the deformation of the mid–plane of the thick plate. The deformation at planes away from the mid–plane are derived from the assumed linear variation in the thickness direction.

Therefore, the decoupling between the two wave forms is a consequence of the linear dependency in the thickness direction. Furthermore, the two waveforms remain uncoupled even when external forces are introduced. This is because the solution, external forces and boundary conditions are all being defined with respect to the plate mid–plane. If the forces and boundary conditions are to be defined relative to one of the plate surfaces and the same type of variation assumed over the thickness as that for the deformation and strain, then coupling would be obtained between the in–plane and out–of–plane motions [4]. This approach for coupling the two wave motions is here implemented together with a refinement of the variation along the thickness direction by using a Legendre polynomial expansion as used by Mindlin and Medick [5].

COUPLED IN–PLANE AND OUT–OF–PLANE WAVES USING MINDLIN'S APPROACH.

In Mindlin and Medick's approach [5], variations along the thickness direction are expanded using a Legendre Polynomial. That is,

$$\begin{Bmatrix} U(x,y,z) \\ V(x,y,z) \\ W(x,y,z) \end{Bmatrix} = \sum_{i=0}^{i=\infty} P_n\left(\frac{z}{h}\right) \begin{Bmatrix} U_n \\ V_n \\ W_n \end{Bmatrix} (x,y) \qquad 1.$$

where $P_0\left(\frac{z}{h}\right) = 1$, $P_1\left(\frac{z}{h}\right) = \frac{z}{h}$, and $P_2\left(\frac{z}{h}\right) = \frac{1}{2}\left(\frac{3z^2}{h^2} - 1\right)$, etc. These displacements represented by the first few terms of the expansion for all the plate motions, including those for the out–of–plane waves, are graphically shown in figure (2).

The equations of motion from Mindlin [2] and Mindlin and Medick [5] are given by,

$$G\nabla^2 u_0 + (\lambda + G)\frac{\partial}{\partial x}\left(\frac{\partial u_0}{\partial x} + \frac{\partial v_0}{\partial y}\right) + \frac{\lambda \varkappa_1}{h}\frac{\partial w_1}{\partial x} = \varrho \frac{\partial^2 u_0}{\partial t^2} \qquad 2.$$

$$G\nabla^2 v_0 + (\lambda + G)\frac{\partial}{\partial y}\left(\frac{\partial u_0}{\partial x} + \frac{\partial v_0}{\partial y}\right) + \frac{\lambda \varkappa_1}{h}\frac{\partial w_1}{\partial y} = \varrho\frac{\partial^2 v_0}{\partial t^2} \qquad 3.$$

$$G\varkappa_2{}^2\,\nabla^2 w_1 - \frac{3\lambda\varkappa_1}{h}\left(\frac{\partial u_0}{\partial x} + \frac{\partial v_0}{\partial y}\right) - \frac{3\varkappa_1{}^2}{h^2}(\lambda + 2G)w_1 +$$

$$\frac{3G\varkappa_2{}^2}{h}\left(\frac{\partial u_2}{\partial x} + \frac{\partial v_2}{\partial y}\right) = \varrho\varkappa_3{}^2\frac{\partial^2 w_1}{\partial t^2} \qquad 4.$$

$$\frac{E'}{2}\left[(1 - \nu)\nabla^2 u_2 + (1 + \nu)\frac{\partial}{\partial x}\left(\frac{\partial u_2}{\partial x} + \frac{\partial v_2}{\partial y}\right)\right] -$$

$$\frac{5G\varkappa_2{}^2}{h}\left(\frac{\partial w_1}{\partial x} + \frac{3u_2}{h}\right) = \varrho\varkappa_4{}^2\frac{\partial^2 u_2}{\partial t^2} \qquad 5.$$

$$\frac{E'}{2}\left[(1 - \nu)\nabla^2 v_2 + (1 + \nu)\frac{\partial}{\partial y}\left(\frac{\partial u_2}{\partial x} + \frac{\partial v_2}{\partial y}\right)\right] -$$

$$\frac{5G\varkappa_2{}^2}{h}\left(\frac{\partial w_1}{\partial y} + \frac{3v_2}{h}\right) = \varrho\varkappa_4{}^2\frac{\partial^2 v_2}{\partial t^2} \qquad 6.$$

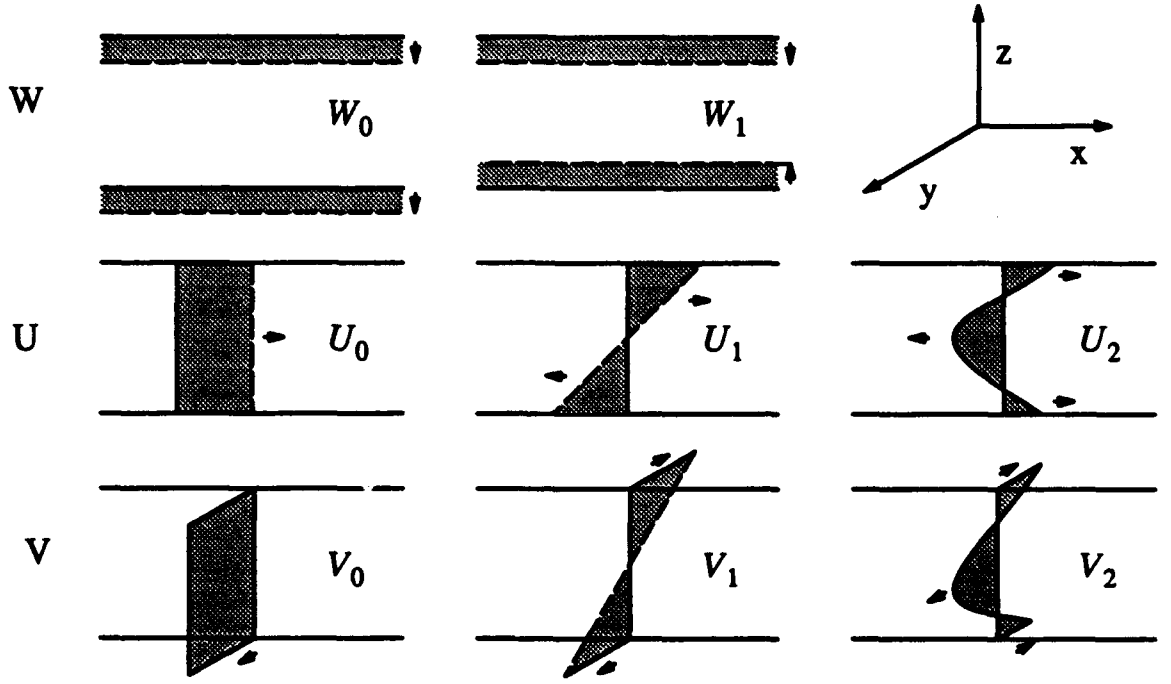

Figure 2. Displacement modes.

$$\frac{D}{2}\left[(1-\nu)\nabla^2 u_1 + (1+\nu)\frac{\partial}{\partial x}\left[\frac{\partial u_1}{\partial x} + \frac{\partial v_1}{\partial y}\right]\right] - \varkappa^2 Gh\left(u_1 + \frac{\partial w_0}{\partial x}\right) = \frac{\varrho h^3}{12}\frac{\partial^2 u_1}{\partial t^2} \quad 7.$$

$$\frac{D}{2}\left[(1-\nu)\nabla^2 v_1 + (1+\nu)\frac{\partial}{\partial y}\left[\frac{\partial u_1}{\partial x} + \frac{\partial v_1}{\partial y}\right]\right] - \varkappa^2 Gh\left(v_1 + \frac{\partial w_0}{\partial y}\right) = \frac{\varrho h^3}{12}\frac{\partial^2 v_1}{\partial t^2} \quad 8.$$

$$\varkappa^2 Gh\left[\nabla^2 w_0 + \left(\frac{\partial u_1}{\partial x} + \frac{\partial v_1}{\partial y}\right)\right] = \varrho h\frac{\partial^2 w_0}{\partial t^2} \quad 9.$$

where equations (2) to (6) describe the in–plane motion of the plate and equations (7) to (9) describe the out–of–plane plate motion. The solution to these equations of motion is obtained by defining two potential functions for the out–of–plane displacement (θ and ψ_0) and five potentials for the in–plane displacements (ϕ_1, ϕ_2, ϕ_3 ψ_1 and ψ_2).

That is for the out–of–plane displacements u_1 and v_1 can be described by the two potentials:

$$u_1 = \frac{\partial\theta}{\partial x} + \frac{\partial\psi_0}{\partial y} \quad 10.$$

$$v_1 = \frac{\partial\theta}{\partial y} - \frac{\partial\psi_0}{\partial x} \quad 11.$$

which when substituted into the equations of motion results in the following three equations of equilibrium.

$$\frac{\partial}{\partial x}\left[\nabla^2\theta + \left(R\delta_0{}^4 - S^{-1}\right)\theta - S^{-1}w_0\right] + \frac{1-\nu}{2}\frac{\partial}{\partial y}\left[\nabla^2\delta_3{}^2\right]\psi_0 = 0 \quad 12.$$

$$\frac{\partial}{\partial y}\left[\nabla^2\theta + \left(R\delta_0{}^4 - S^{-1}\right)\theta - S^{-1}w_0\right] + \frac{1-\nu}{2}\frac{\partial}{\partial x}\left[\nabla^2\delta_3{}^2\right]\psi_0 = 0 \quad 13.$$

$$\nabla^2(\theta + w_0) + S\delta_0{}^4 w_0 = 0 \quad 14.$$

Eliminating ϕ and ψ,

$$\nabla^2\left(\nabla^2 + \delta_3{}^2\right)\psi_0 = 0 \quad 15.$$

$$\left(\nabla^2 + \delta_1{}^2\right)\left(\nabla^2 + \delta_2{}^2\right)w_0 = 0 \quad 16.$$

$$\left(\nabla^2 + \delta_1{}^2\right)\theta_1 = 0 \tag{17.}$$

$$\left(\nabla^2 + \delta_1{}^2\right)\theta_2 = 0 \tag{18.}$$

from which alternative expressions for the out–of–plane displacements are given by,

$$u_1 = (\sigma_1 - 1)\frac{\partial\theta_1}{\partial x} + (\sigma_2 - 1)\frac{\partial\theta_2}{\partial x} + \frac{\partial\psi_0}{\partial y} \tag{19.}$$

$$v_1 = (\sigma_1 - 1)\frac{\partial\theta_1}{\partial y} + (\sigma_2 - 1)\frac{\partial\theta_2}{\partial y} + \frac{\partial\psi_0}{\partial x} \tag{20.}$$

$$w_0 = \theta_1 + \theta_2 \tag{21.}$$

where $R = \frac{h^2}{12}$, $S = \frac{D}{\varkappa^2 Gh}$, $\delta_0{}^4 = \frac{\varrho\omega^2 h}{D}$, $\varkappa = \frac{\pi}{\sqrt{12}}$, $\sigma_{1,2} = \frac{\delta_{1,2}{}^2}{R\delta_0{}^4 - S^{-1}}$

$\delta_{1,2}{}^2 = \frac{1}{2}\delta_0{}^4\left(R + S \pm \sqrt{(R - S) + 4\delta_0{}^{-4}}\right)$ and $\delta_3{}^2 = 2\frac{R\delta_0{}^4 - S^{-1}}{1 - \nu}$

For the in–plane displacements,

$$w_1 = \alpha_1\phi_1 + \alpha_2\phi_2 + \alpha_3\phi_3 \tag{22.}$$

$$u_0 = \frac{\partial\phi_1}{\partial x} + \frac{\partial\phi_2}{\partial x} + \frac{\partial\phi_3}{\partial x} - \frac{\partial\psi_1}{\partial y} \tag{23.}$$

$$u_2 = \beta_1\frac{\partial\phi_1}{\partial x} + \beta_2\frac{\partial\phi_2}{\partial x} + \beta_3\frac{\partial\phi_3}{\partial x} - \frac{\partial\psi_2}{\partial y} \tag{24.}$$

$$v_0 = \frac{\partial\phi_1}{\partial y} + \frac{\partial\phi_2}{\partial y} + \frac{\partial\phi_3}{\partial y} + \frac{\partial\psi_1}{\partial x} \tag{25.}$$

$$v_2 = \beta_1\frac{\partial\phi_1}{\partial y} + \beta_2\frac{\partial\phi_2}{\partial y} + \beta_3\frac{\partial\phi_3}{\partial y} + \frac{\partial\psi_2}{\partial x} \tag{26.}$$

which when substituted into the equations of motion results in the following five equations of equilibrium.

$$\nabla^2\psi_1 + \frac{\varrho\omega^2}{G}\psi_1 = 0 \tag{27.}$$

$$\nabla^2\psi_2 + \left[\frac{\varkappa_4^2\varrho\omega^2}{G} - \frac{15\varkappa_2{}^2}{h}\right]\psi_2 = 0 \qquad 28.$$

$$\nabla^2\phi_i + \xi_i{}^2\phi_i = 0\ , \quad i = 1,2,3 \qquad 29.$$

where $\alpha_i = \dfrac{h[(\lambda + 2G)\xi_i{}^2 - \varrho\omega^2]}{\varkappa_1\lambda}$, $\beta_i = \dfrac{\alpha_i\, h}{0.75(\Omega^2 - 4) - \frac{E'h^2\xi_i{}^2}{5G\varkappa_2{}^2}}$, $\Omega = \dfrac{\omega}{\frac{\pi}{2h}\sqrt{\frac{G}{\varrho}}}$,

$E' = \dfrac{E}{1-\nu^2}$, $\dfrac{\varkappa_2^2}{\varkappa_1^2} = \dfrac{48(\mathcal{K}^2-4)}{\pi^3\mathcal{K}^4}\left[\pi(\mathcal{K}^2-1) + 4\mathcal{K}\cot\left(\dfrac{\pi\mathcal{K}}{2}\right)\right]$,

$\dfrac{1}{\varkappa_1^2} = \dfrac{5\mathcal{K}^2\varkappa_2^2}{4\varkappa_1^2(\mathcal{K}^1-1)(\mathcal{K}^2-4)}\left[\dfrac{\varkappa_2^2}{\varkappa_1^2} + \dfrac{6(\mathcal{K}^2-4)}{\pi^3}\left(\dfrac{\pi}{2} - \dfrac{4}{\mathcal{K}}\tan\dfrac{\pi}{\mathcal{K}}\right)\right]$ $\dfrac{\varkappa_1}{\varkappa_3} = \dfrac{\pi}{\sqrt{12}}$,

$\dfrac{\varkappa_2}{\varkappa_4} = \dfrac{\pi}{\sqrt{15}}$, $\mathcal{K}^2 = \dfrac{2(1-\nu)}{1-2\nu}$, and ξ_i are the roots of the equation,

$$\begin{vmatrix} a_{11} & a_{12} & 0 \\ a_{12} & a_{22} & a_{23} \\ 0 & a_{23} & a_{33} \end{vmatrix} = 0 \qquad 30.$$

where for a plate of thickness 2h

$$a_{11} = \mathcal{K}^2\left(\frac{2\,\xi\,h}{\pi}\right)^2 - \Omega^2 \quad a_{22} = \frac{\varkappa_2^2}{3}\left(\frac{2\,\xi\,h}{\pi}\right)^2 + \frac{\varkappa_1^2\,\mathcal{K}^2}{\pi^2} - \frac{\varkappa_3^2\,\Omega^2}{3}$$

$$a_{33} = \frac{E'}{3G}\left(\frac{2\,\xi\,h}{\pi}\right)^2 + \frac{12\varkappa_2^2}{\pi^2} - \frac{\varkappa_4^2\,\Omega^2}{5}$$

$$a_{12} = \frac{2\varkappa_1(\mathcal{K}^2-2)}{\pi}\left(\frac{2\,\xi\,h}{\pi}\right) \quad a_{23} = \frac{-2\varkappa_2^2}{\pi}\left(\frac{2\,\xi\,h}{\pi}\right) \qquad 31.$$

In equations (27) to (31), ν is poisson's ratio and E and G are respectively the modulus of elasticity and the shear modulus.

For a plate simply supported along two edges (y = 0 and a) and free on the other two edges (x = 0 or b), the solutions that satisfy the boundary conditions are given by

$$\theta_1 = \left(C_1e^{\hat{k}_1x} + D_1e^{-\hat{k}_1x}\right)\sin\left(\frac{n\pi y}{b}\right) \qquad 32.$$

$$\theta_2 = \left(C_2 e^{\hat{k}_2 x} + D_2 e^{-\hat{k}_2 x}\right) \sin\left(\frac{n\pi y}{b}\right) \tag{33.}$$

$$\psi_0 = \left(C_3 e^{\hat{k}_3 x} + D_3 e^{-\hat{k}_3 x}\right) \cos\left(\frac{n\pi y}{b}\right) \tag{34.}$$

$$\phi_i = \left(A_i e^{\tilde{k}_i x} + B_i e^{-\tilde{k}_i x}\right) \cos\left(\frac{n\pi y}{b}\right) \tag{35.}$$

$$\psi_1 = \left(A_4 e^{\tilde{k}_4 x} + B_4 e^{-\tilde{k}_4 x}\right) \sin\left(\frac{n\pi y}{b}\right) \tag{36.}$$

$$\psi_2 = \left(A_5 e^{\tilde{k}_5 x} + B_5 e^{-\tilde{k}_5 x}\right) \sin\left(\frac{n\pi y}{b}\right) \tag{37.}$$

where $\hat{k}_i$, (i = 1, 2, 3) are the out–of–plane wavenumber components and $\tilde{k}_i$ (i = 1 to 5) are the in–plane wavenumber components, respectively defined by

$$\left(\frac{n\pi}{b}\right)^2 + \hat{k}_{1,2,3}^2 = \delta_{1,2,3}^2 \tag{38.}$$

$$\left(\frac{n\pi}{b}\right)^2 + \tilde{k}_{1,2,3}^2 = \xi_{1,2,3}^2 \tag{39.}$$

$$\left(\frac{n\pi}{b}\right)^2 + \tilde{k}_4^2 = \frac{\varrho\omega^2}{G} \tag{40.}$$

$$\left(\frac{n\pi}{b}\right)^2 + \tilde{k}_5^2 = \left[\frac{\varkappa_4^2 \varrho\omega^2}{G} - \frac{15\varkappa_2{}^2}{h}\right] \tag{41.}$$

For a force applied on one of the surfaces of the plate,

$$F(x,\ y,\ z) = F(x,\ y)\ \delta(z - h) \tag{42.}$$

This force can be decomposed using the same Legendre polynomial expansion as for the deformation and the strains.

$$F(x,\ y,\ z) = \sum_{i=0}^{i=\infty} P_n\left(\frac{z}{h}\right)\ F_n(x,\ y) \tag{43.}$$

The results of this expansion with different number of terms retained in the expansion is shown in figure (3). As the number of terms increases, the result approaches a delta function at the

surface of the plate (z/h = 1) . This expansion gives the coupling between the in–plane and the out–of–plane waves is obtained. For a force applied as shown in figure (4), retaining only the first two terms of the Legendre polynomial expansion,

$$F(x,\ y,\ z) = F(x,\ y) + F(x,\ y)\frac{z}{b} + \ldots\ldots\ldots \qquad 44.$$

That is, the force is described by a force of equal magnitude applied at the mid–plane of the plate and two forces with apposite direction applied on either surface of the plate creating a squeezing load [5]. The transverse force applied at the plate mid–plane only induces out–of–plane motion, while because of the symmetry about the plate mid–plane the squeezing force only induces in–plane motion. This same type of approach was used by Lyamyshev [6].

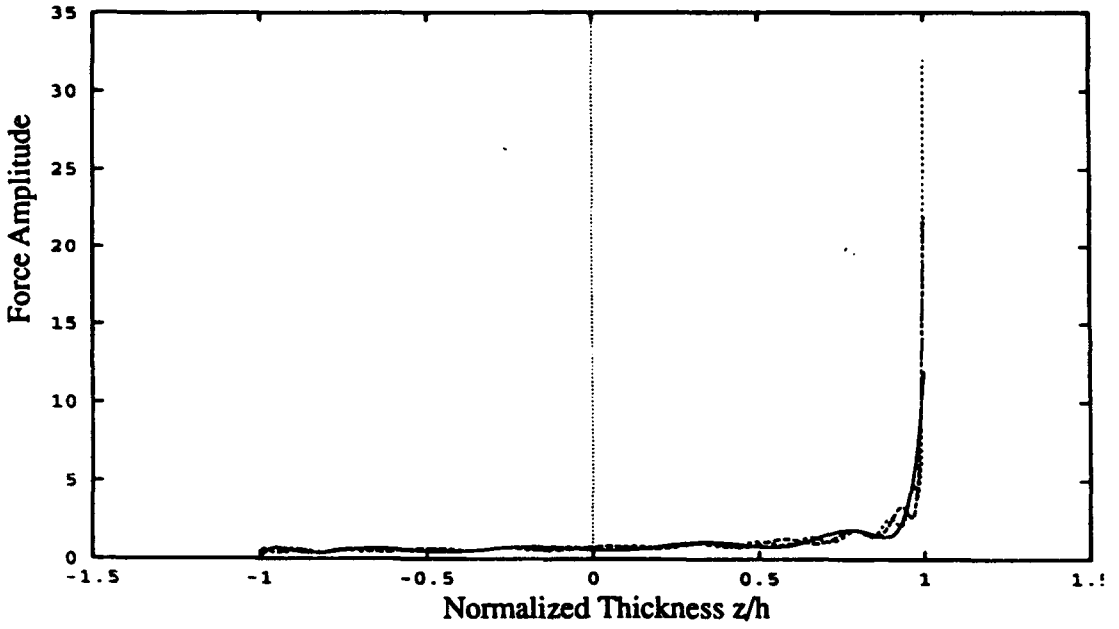

Figure 3. Sum of contribution from elements of the Legendre Polynomial expansion for the surface applied load. ———: 5 terms; – – –: 10 terms; - - - - -: 20 terms.

The first few terms of the expansion match the linearly assumed variation in the Mindlin [2] and Kane and Mindlin [3] solutions. The terms of the polynomial expansion describe both the out–of–plane wave motion (W_0, U_1, V_1) and the in–plane wave motion (W_0, U_0, U_2, V_0, V_2), where W_i is the displacement perpendicular to the plate surface and U_i and V_i are the displacements in the plane of the plate.

To check the validity of this approach, especially the expansion of the surface force using the Legendre polynomials, the solution for the response of a narrow and long plate (equivalent to a thick beam) with an edge transverse load applied on the top surface of the plate has been obtained using the above approach and compared to a solution obtained a 3–D stress analysis similar to the

one used by Hutchinson and Zillmer [7]. The Mindlin and Mindlin and Medick plate equations (equations (19) to (26)) are used in this solution for the thick beam by letting n in the sine and cosine functions of equations (32) to (37) to be equal to zero.

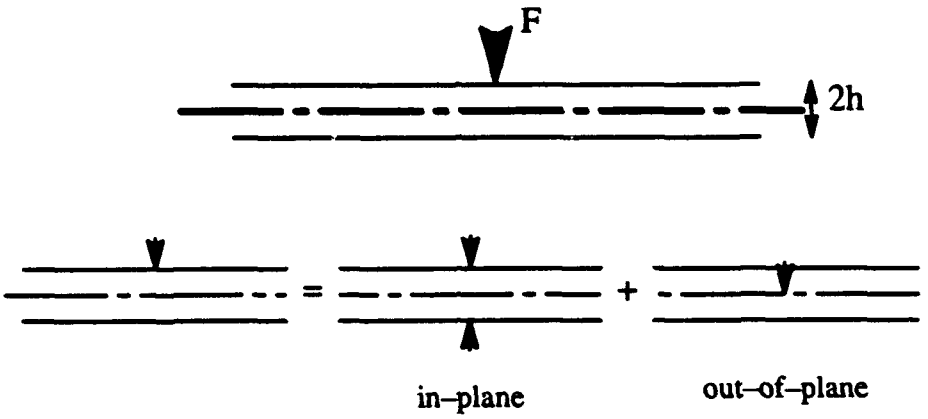

Figure 4. First two terms in the surface load expansion.

3–D ELASTICITY SOLUTION

Considering a 3–D slab as shown in figure (5) where 2a and 2b are much smaller than 2c (thick long beam equivalent to a plate with very narrow width) with free boundary conditions at its ends and with a transverse force applied at one of the ends on the surface of the slab.

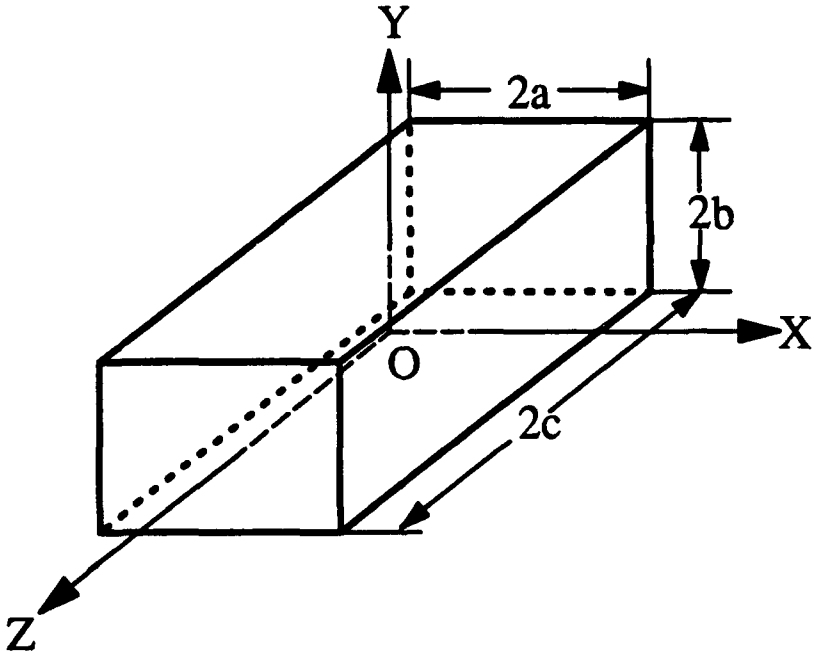

Figure 5. Geometry for 3–D elasticity analysis.

The 3–D elasticity solution starts from the basic 3–D stress equations,

$$(\lambda + G)\,\vec{\nabla}\,(\vec{\nabla}.\vec{u}) + G(\nabla^2\,\vec{u}) = \varrho\left(\frac{\partial^2\vec{u}}{\partial t^2}\right) \qquad 45.$$

The solution to this equation is obtained in terms of Helmholtz displacement potentials,

$$\vec{u} = \vec{\nabla}\phi + \nabla \times \vec{\psi} \qquad 46.$$

where $\vec{u}$ is the displacement vector given by,

$$\vec{u} = (u\,\hat{i} + v\,\hat{j} + w\,\hat{k}) \qquad 47.$$

and ϕ and $\vec{\psi}$ are scalar and vector potential functions respectively. These potentials must satisfy wave equations of the form,

$$\nabla^2\vec{\psi} = \frac{1}{c_2^2}\left[\frac{\partial^2\vec{\psi}}{\partial t^2}\right] \qquad 48.$$

$$\nabla^2\phi = \frac{1}{c_1^2}\left(\frac{\partial^2\phi}{\partial t^2}\right) \qquad 49.$$

where c_1 is the dilatational wave velocity and c_2 is the shear wave velocity.

The solutions for the two potentials in Cartesian coordinates are given by,

$$\phi = \begin{Bmatrix}\sin(\alpha x)\\ \cos(\alpha x)\end{Bmatrix}\begin{Bmatrix}\sin(\beta y)\\ \cos(\beta y)\end{Bmatrix}\begin{Bmatrix}\sin(\delta z)\\ \cos(\delta z)\end{Bmatrix} \qquad 50.$$

$$\psi_i = \begin{Bmatrix}\sin(\overline{\alpha} x)\\ \cos(\overline{\alpha} x)\end{Bmatrix}\begin{Bmatrix}\sin(\overline{\beta} y)\\ \cos(\overline{\beta} y)\end{Bmatrix}\begin{Bmatrix}\sin(\overline{\delta} z)\\ \cos(\overline{\delta} z)\end{Bmatrix} \qquad 51.$$

The terms in the 3 sets of brackets have 8 combinations, only four of which are independent. The solution for the displacement vector is thus

$$\vec{U} = \underbrace{\left[\frac{\partial\phi}{\partial x}\,\hat{i} + \frac{\partial\phi}{\partial y}\,\hat{j} + \frac{\partial\phi}{\partial z}\,\hat{k}\right]}_{\text{I}\quad\text{I}\quad\text{I}} + \underbrace{\left[\frac{\partial\psi_z}{\partial y} - \frac{\partial\psi_y}{\partial z}\right]\hat{i}}_{\text{II}\quad\text{III}} + \underbrace{\left[\frac{\partial\psi_x}{\partial z} - \frac{\partial\psi_z}{\partial x}\right]\hat{j}}_{\text{IV}\quad\text{II}} + \underbrace{\left[\frac{\partial\psi_y}{\partial x} - \frac{\partial\psi_x}{\partial y}\right]\hat{k}}_{\text{III}\quad\text{IV}} \qquad 52.$$

The overall response, as given by the above equation is divided into four components as indicated by the roman numerals.

Similar expressions can be derived for the stresses solutions which for the direct stresses these are given by,

$$\sigma_i = \lambda e + 2G\varepsilon_i \qquad 53.$$

where $e = \sum \varepsilon_i = \sum \partial u_i/\partial x_i$ and for the shear stresses these are given by.

$$\tau_{ij} = G\gamma_{ij} \qquad 54.$$

where $\gamma_{ij} = \partial u_i/\partial x_j + \partial u_j/\partial x_i$. The combinations of all the solutions are shown tabulated in Table I which is taken from [7] In this table $\Omega = \omega^2\lambda/c_1^2$.

Table I:
Solution Components in Cartesian Coordinates

	I	II	III	IV
u	$\alpha\begin{Bmatrix}-s\\c\end{Bmatrix}\begin{Bmatrix}s\\c\end{Bmatrix}\begin{Bmatrix}c\\s\end{Bmatrix}$	$\beta\begin{Bmatrix}s\\c\end{Bmatrix}\begin{Bmatrix}-s\\c\end{Bmatrix}\begin{Bmatrix}c\\s\end{Bmatrix}$	$-\delta\begin{Bmatrix}s\\c\end{Bmatrix}\begin{Bmatrix}s\\c\end{Bmatrix}\begin{Bmatrix}-c\\s\end{Bmatrix}$	0
v	$\beta\begin{Bmatrix}c\\s\end{Bmatrix}\begin{Bmatrix}-c\\s\end{Bmatrix}\begin{Bmatrix}c\\s\end{Bmatrix}$	$-\alpha\begin{Bmatrix}-c\\s\end{Bmatrix}\begin{Bmatrix}c\\s\end{Bmatrix}\begin{Bmatrix}c\\s\end{Bmatrix}$	0	$\delta\begin{Bmatrix}c\\s\end{Bmatrix}\begin{Bmatrix}c\\s\end{Bmatrix}\begin{Bmatrix}-c\\s\end{Bmatrix}$
w	$\delta\begin{Bmatrix}c\\s\end{Bmatrix}\begin{Bmatrix}s\\c\end{Bmatrix}\begin{Bmatrix}-s\\c\end{Bmatrix}$	0	$\alpha\begin{Bmatrix}-c\\s\end{Bmatrix}\begin{Bmatrix}s\\c\end{Bmatrix}\begin{Bmatrix}s\\c\end{Bmatrix}$	$-\beta\begin{Bmatrix}c\\s\end{Bmatrix}\begin{Bmatrix}-s\\c\end{Bmatrix}\begin{Bmatrix}s\\c\end{Bmatrix}$
σ_x	$-(\Omega + 2G\alpha^2)\begin{Bmatrix}c\\s\end{Bmatrix}\begin{Bmatrix}s\\c\end{Bmatrix}\begin{Bmatrix}c\\s\end{Bmatrix}$	$2G\alpha\beta\begin{Bmatrix}-c\\s\end{Bmatrix}\begin{Bmatrix}-s\\c\end{Bmatrix}\begin{Bmatrix}c\\s\end{Bmatrix}$	$-2G\alpha\delta\begin{Bmatrix}-c\\s\end{Bmatrix}\begin{Bmatrix}s\\c\end{Bmatrix}\begin{Bmatrix}-c\\s\end{Bmatrix}$	0
σ_y	$-(\Omega + 2G\beta^2)\begin{Bmatrix}c\\s\end{Bmatrix}\begin{Bmatrix}s\\c\end{Bmatrix}\begin{Bmatrix}c\\s\end{Bmatrix}$	$-2G\alpha\beta\begin{Bmatrix}-c\\s\end{Bmatrix}\begin{Bmatrix}-s\\c\end{Bmatrix}\begin{Bmatrix}c\\s\end{Bmatrix}$	0	$2G\beta\delta\begin{Bmatrix}c\\s\end{Bmatrix}\begin{Bmatrix}-s\\c\end{Bmatrix}\begin{Bmatrix}-c\\s\end{Bmatrix}$
σ_z	$-(\Omega + 2G\delta^2)\begin{Bmatrix}c\\s\end{Bmatrix}\begin{Bmatrix}s\\c\end{Bmatrix}\begin{Bmatrix}c\\s\end{Bmatrix}$	0	$2G\alpha\delta\begin{Bmatrix}-c\\s\end{Bmatrix}\begin{Bmatrix}s\\c\end{Bmatrix}\begin{Bmatrix}-c\\s\end{Bmatrix}$	$2G\beta\delta\begin{Bmatrix}c\\s\end{Bmatrix}\begin{Bmatrix}-s\\c\end{Bmatrix}\begin{Bmatrix}-c\\s\end{Bmatrix}$
τ_{xy}	$2G\alpha\beta\begin{Bmatrix}-s\\c\end{Bmatrix}\begin{Bmatrix}-c\\s\end{Bmatrix}\begin{Bmatrix}c\\s\end{Bmatrix}$	$G(\alpha^2-\beta^2)\begin{Bmatrix}s\\c\end{Bmatrix}\begin{Bmatrix}c\\s\end{Bmatrix}\begin{Bmatrix}c\\s\end{Bmatrix}$	$-G\beta\delta\begin{Bmatrix}s\\c\end{Bmatrix}\begin{Bmatrix}-c\\s\end{Bmatrix}\begin{Bmatrix}-c\\s\end{Bmatrix}$	$G\alpha\delta\begin{Bmatrix}-s\\c\end{Bmatrix}\begin{Bmatrix}c\\s\end{Bmatrix}\begin{Bmatrix}-c\\s\end{Bmatrix}$
τ_{yz}	$2G\beta\delta\begin{Bmatrix}c\\s\end{Bmatrix}\begin{Bmatrix}-c\\s\end{Bmatrix}\begin{Bmatrix}-s\\c\end{Bmatrix}$	$-G\alpha\delta\begin{Bmatrix}-c\\s\end{Bmatrix}\begin{Bmatrix}c\\s\end{Bmatrix}\begin{Bmatrix}-s\\c\end{Bmatrix}$	$G\alpha\beta\begin{Bmatrix}-c\\s\end{Bmatrix}\begin{Bmatrix}-c\\s\end{Bmatrix}\begin{Bmatrix}s\\c\end{Bmatrix}$	$G(\beta^2-\delta^2)\begin{Bmatrix}c\\s\end{Bmatrix}\begin{Bmatrix}c\\s\end{Bmatrix}\begin{Bmatrix}s\\c\end{Bmatrix}$
τ_{zx}	$2G\alpha\delta\begin{Bmatrix}-s\\c\end{Bmatrix}\begin{Bmatrix}s\\c\end{Bmatrix}\begin{Bmatrix}-s\\c\end{Bmatrix}$	$G\beta\delta\begin{Bmatrix}s\\c\end{Bmatrix}\begin{Bmatrix}-s\\c\end{Bmatrix}\begin{Bmatrix}-s\\c\end{Bmatrix}$	$G(\delta^2-\alpha^2)\begin{Bmatrix}s\\c\end{Bmatrix}\begin{Bmatrix}s\\c\end{Bmatrix}\begin{Bmatrix}s\\c\end{Bmatrix}$	$-G\alpha\beta\begin{Bmatrix}-s\\c\end{Bmatrix}\begin{Bmatrix}-s\\c\end{Bmatrix}\begin{Bmatrix}s\\c\end{Bmatrix}$

The contributions from each of the solutions of the vector and scalar potential functions, for the four combinations, are arranged is such a way that a physical explanation can be attributed to these contributions.

For example, if the upper terms in each set of brackets are considered, u is an odd function of x, an odd function of y, and an even function of z. v is an even function of x, an even function of y and even function of z., and w is even function of x, an odd function of y and an odd function

of z. This contribution for a structure with one dimension much longer than the others, corresponds to the even out–of–plane beam modes. The other combinations would correspond to odd out–of–plane modes, even in–plane modes and odd in–plane modes.

For each of the selected combination, the solutions for the displacements or the stresses are written in terms of a linear combination of 3 double series. For example, for displacement u,

$$u = \sum_{m=1}^{NX} \sum_{n=1}^{NY} A_{mn} f_{mn}(z) \sin(\alpha_m x) \sin(\beta_n y)$$

$$+ \sum_{n=1}^{NY} \sum_{p=1}^{NZ} B_{np} g_{np}(x) \sin(\beta_n y) \cos(\delta_p z)$$

$$+ \sum_{p=1}^{NZ} \sum_{m=1}^{NX} C_{pm} h_{pm}(y) \cos(\delta_p z) \sin(\alpha_m x) \qquad 55.$$

where

$$f_{mn} = \left(- A_1 \alpha_m \cos(\delta z) + \left[- A_2 \bar{\beta}_n - A_3 \bar{\delta} \right] \cos(\bar{\delta} z) \right) \qquad 56.$$

$$g_{np} = \left(- B_1 \alpha \sin(\alpha x) + \left[- B_2 \bar{\beta}_n - B_3 \bar{\delta}_p \right] \sin(\bar{\alpha} x) \right) \qquad 57.$$

$$h_{pm} = \left(- C_1 \alpha_m \sin(\beta y) + \left[- C_2 \bar{\beta} - C_3 \bar{\delta}_p \right] \sin(\bar{\beta} y) \right) \qquad 58.$$

The singly subscripted constants and the values of α_m, $\bar{\alpha}_m$, β_n, $\bar{\beta}_n$ δ_p and $\bar{\delta}_p$ are chosen to satisfy the boundary conditions.

For free–free boundaries, that is all surfaces free of any stresses, the boundary conditions are given by $\tau_{yx}(a, y, z) = 0$, $\tau_{xz}(a, y, z) = 0$ and $\sigma_x(a, y, z) = 0$ for the surfaces in the x–plane, that is the surfaces perpendicular to the x–axis (figure 5). Similar conditions can be defined for the surfaces in the y and z planes. The 6 shear stress boundary conditions are satisfied term–by–term by selecting the parameters α_m, $\bar{\alpha}_m$, β_n, $\bar{\beta}_n$ δ_p and $\bar{\delta}_p$ to satisfy the conditions,

$$\alpha_m = \bar{\alpha}_m = (m - 1)\frac{\pi}{a} \qquad 59.$$

$$\beta_n = \bar{\beta}_n = (2n - 1)\frac{\pi}{2b} \qquad 60.$$

$$\delta_p = \bar{\delta}_p = (p - 1)\frac{\pi}{c} \qquad 61.$$

from which

$$\alpha^2 = \frac{\omega^2}{c_1^2} - \beta_m^2 - \delta_p^2 \qquad 62.$$

$$\overline{\alpha}^2 = \frac{\omega^2}{c_2^2} - \overline{\beta}_m^2 - \overline{\delta}_p^2 \qquad 63.$$

and similar expressions can be derived for β, $\overline{\beta}$, δ, $\overline{\delta}$.

For the singly subscripted constants, arbitrary functions are selected that must also satisfy the 6 shear stress boundary conditions. The functions for the singly subscripted constants selected by Hutchinson and Zillmer [7] for the case of a plate or beam slab with all edges free are as follows,

$$A_1 = \frac{\alpha_m^2 + \beta_n^2 - \overline{\delta}^2}{2\delta \sin(\delta c)}, \quad A_2 = 0, \quad A_3 = \frac{\alpha_m}{\sin(\overline{\delta} c)}, \quad A_4 = \frac{\beta_n}{\sin(\overline{\delta} c)},$$

$$B_1 = \frac{\beta_n^2 + \delta_p^2 - \overline{\alpha}^2}{2\alpha \sin(\alpha a)}, \quad B_2 = \frac{-2\beta_n}{\sin(\overline{\alpha} a)}, \quad B_3 = \frac{-2\delta_p}{\sin(\overline{\alpha} a)}, \quad B_4 = 0,$$

$$C_1 = \frac{\delta_p^2 + \alpha_m^2 - \overline{\beta}^2}{2\beta \sin(\beta b)}, \quad C_2 = \frac{2\alpha_m}{\cos(\overline{\beta} b)}, \quad C_3 = 0, \quad C_4 = \frac{-2\delta_p}{\cos(\overline{\beta} b)} \qquad 64.$$

The remaining 3 normal stress boundary conditions are satisfied by orthogonalization over the area of the respective faces on which they act. If no normal external load is applied to a particular surface, then the integral from the orthogonalization over the area of the surface is equal to zero. If an external normal load is applied on the the surface, the orthogonalized normal stress on the loaded surface is equal to the orthogonalization of the external load.

For an external normal load applied to the surface in the y–plane (force along the y–axis direction), the integral of the stress function multiplied by the corresponding cosine or sine functions, over the surface in the y–plane is equal to the integral of the applied external load, that is

$$\int_0^a \int_0^c \sigma_y(x, b, z) \cos(\alpha_i y) \cos(\delta_j z)\, dz\, dx = \int_0^a \int_0^c q(x, z) \cos(\alpha_i x) \cos(\delta_j z)\, dz\, dx \qquad 65.$$

where q(x,z) is the external load applied on the surface y = b. If the external applied load is a point load of magnitude F_0 applied at (x_0, z_0), then

$$q(x,z) = F_0\delta(x - x_0)\delta(z - z_0) \qquad 66.$$

This procedure generates a system of linear equations. The number of equations generated by the loading in each of the three orthogonal directions is equal to the number of modes considered in that directions. Combining all the linear equations a system of (NX*NY + NY*NZ + NZ*NX) equations is obtained, where NX, NY and NZ are the number of modes in the x, y and z directions respectively. The solution to this system of equations yields the values for the A_{mn}, B_{np} and C_{pm} terms in equation (55). Having solved for these coefficients, the displacements or stresses can be computed using equations of the form of equation (55).

Results for the response of a long thick beam have been obtained using the above approach and the modified Mindlin and Mindlin and Medick approach. The results are shown in figure (6). There are some discrepancies in the results, but these mainly stem from scaling factors and an insufficient number of modes in the three orthogonal directions (see equation 55). What is of importance is the fact that in relative levels the solutions from the two approaches match in as far as the shape and ratio of in–plane response to out–of–plane response.

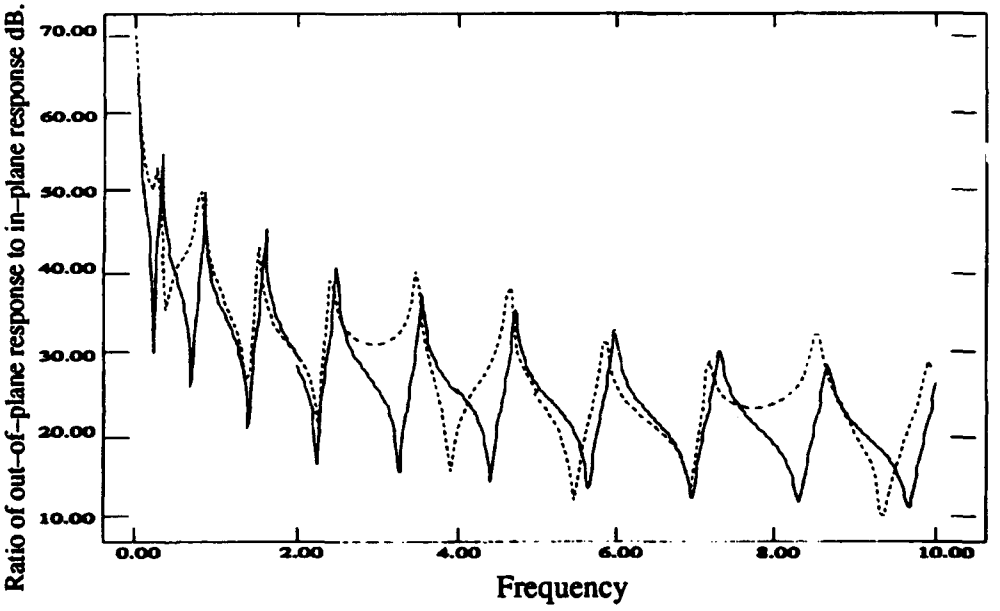

Figure 6. Ratio of out–of–plane response to in–plane response. _____: result from approach based on Mindlin's solutions; . . . . . : result from approach based on 3–D elasticity analysis.

Mindlin [2], and Mindlin and Medick's [5] approach is much more efficient than the 3–D stress analysis approach [7] and can be adapted to a number of different boundary conditions. Therefore this method is used to analyze the flow of vibrational power across the junction between two plates.

POWER FLOW

To evaluate the power flow across the junction between two end coupled plates, (figure 1) the solutions in equations (19) to (26) are used to obtain the mobility functions that relate the different motions ($\dot{W}_0$, $\dot{W}_1$, $\dot{U}_0$, $\dot{U}_1$, $\dot{U}_2$, $\dot{V}_0$,$\dot{V}_1$, $\dot{V}_2$) to the all possible types of forces (T_6^0, T_6^1, T_1^0, T_1^1, T_1^2, T_5^0, T_5^1, T_5^2) where the same convention as the one used in [5] is used here and extended to include the forces associated with the out–of–plane motion (see figure 7).

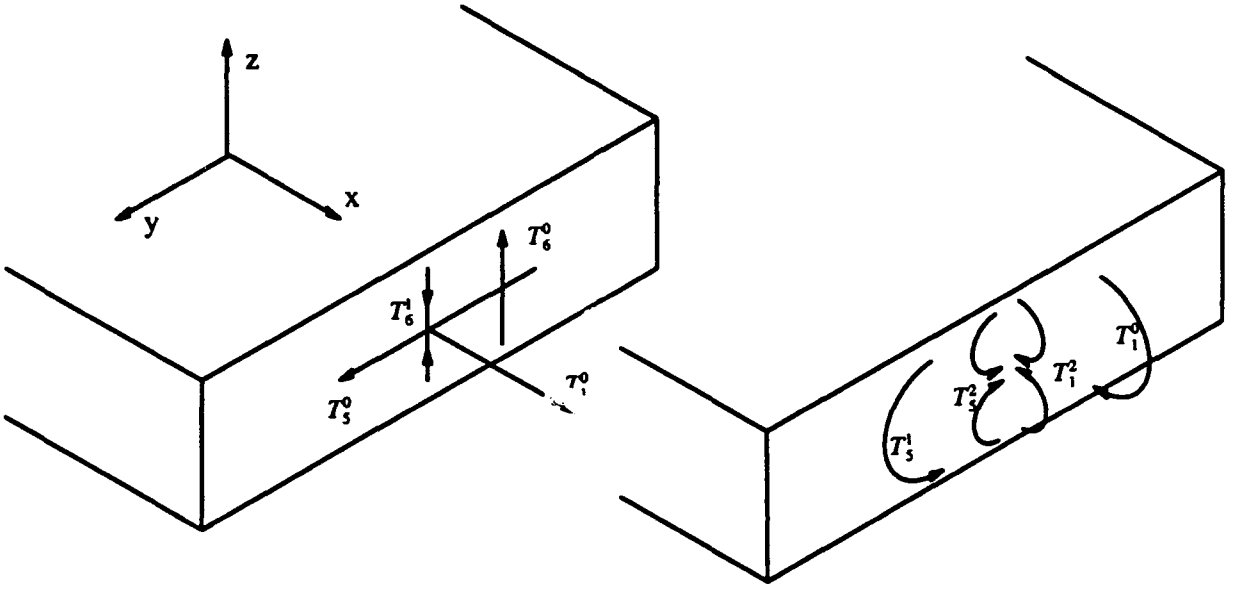

Figure 7. Convention for forces representation.

It should be noted that the discontinuity at the junctions between the two plates considered in this analysis is a change in the thickness between the two plates. The discontinuity does not include an external mobility (or impedance) element which when attached to the surface of the plate would create a surface force due to the relative motion between the plate and the discontinuity. It is important to remember this point when analyzing the results since the absence of any external forces at the junction will keep the in–plane and out–of–plane motions uncoupled at the junction.

To simplify the displacement notation, a numerical subscript representation will be used, where subscripts 1,2 and 3 will denote the x ,y and z directions respectively. That is the response in the $\dot{W}_0$ direction will be represented by the subscript 30.

Since the interaction between forces and displacements or velocities can only take place if both the forces and the motions belong to the same type of wave motion, – in–plane or out–of–plane – and there are 3 out–of–plane velocities (or displacements) with three corresponding force directions and 5 in–plane velocities (or displacements) with five corresponding force directions, then 9 plus 25 mobility functions have to be generated. Furthermore the solution for the in–plane

and out–of–plane waves can be treated separately. Therefore, to solve for the power flow across the junction between two end coupled plates, two sets of matrix equations can be formulated. One set solving for the junction in–plane motions and forces and the other set solving for the out–of–plane motion and forces. The two set of matrix equations, respectively for the out–of–plane waves and the in–plane waves, are as following,

$$\begin{bmatrix} M_{2i3011} + M_{3i3011} & M_{2i3051} + M_{3i3051} & M_{2i3060} + M_{3i3060} \\ M_{2i1111} + M_{3i1111} & M_{2i1151} + M_{3i1151} & M_{2i1160} + M_{3i1160} \\ M_{2i2111} + M_{3i2111} & M_{2i2151} + M_{3i2151} & M_{2i2160} + M_{3i2160} \end{bmatrix} \begin{bmatrix} T_1^1 \\ T_5^1 \\ T_6^0 \end{bmatrix} = \begin{bmatrix} - M_{21i3060} \\ - M_{21i1160} \\ - M_{21i2160} \end{bmatrix} \tag{67.}$$

$$\begin{bmatrix} \dot{W}_0 \\ \dot{U}_1 \\ \dot{V}_1 \end{bmatrix} = \begin{bmatrix} M_{3i3011} & M_{3i3051} & M_{3i3060} \\ M_{3i1111} & M_{3i1151} & M_{3i1160} \\ M_{3i2111} & M_{3i2151} & M_{3i2160} \end{bmatrix} \begin{bmatrix} T_1^1 \\ T_5^1 \\ T_6^0 \end{bmatrix} \tag{68.}$$

$$\begin{bmatrix} M_{2i3110} + M_{3i3110} & M_{2i3112} + M_{3i3112} & M_{2i3150} + M_{3i3150} & M_{2i3152} + M_{3i3152} & M_{2i3161} + M_{3i3161} \\ M_{2i1010} + M_{3i1010} & M_{2i1012} + M_{3i1012} & M_{2i1050} + M_{3i1050} & M_{2i1052} + M_{3i1052} & M_{2i1061} + M_{3i1061} \\ M_{2i1210} + M_{3i1210} & M_{2i1212} + M_{3i1212} & M_{2i1250} + M_{3i1250} & M_{2i1252} + M_{3i1252} & M_{2i1261} + M_{3i1261} \\ M_{2i2010} + M_{3i2010} & M_{2i2012} + M_{3i2012} & M_{2i2050} + M_{3i2050} & M_{2i2052} + M_{3i2052} & M_{2i2061} + M_{3i2061} \\ M_{2i2210} + M_{3i2210} & M_{2i2212} + M_{3i2212} & M_{2i2250} + M_{3i2252} & M_{2i2252} + M_{3i2252} & M_{2i2261} + M_{3i2261} \end{bmatrix} \begin{bmatrix} T_1^0 \\ T_1^2 \\ T_5^0 \\ T_5^2 \\ T_6^1 \end{bmatrix} = \begin{bmatrix} - M_{21i3161} \\ - M_{21i1061} \\ - M_{21i1261} \\ - M_{21i2061} \\ - M_{21i2261} \end{bmatrix} \tag{69.}$$

$$\begin{bmatrix} \dot{W}_1 \\ \dot{U}_0 \\ \dot{U}_2 \\ \dot{V}_0 \\ \dot{V}_2 \end{bmatrix} = \begin{bmatrix} M_{3i3110} & M_{3i1010} & M_{3i1210} & M_{3i2010} & M_{3i2210} \\ M_{3i3112} & M_{3i1012} & M_{3i1212} & M_{3i2012} & M_{3i2212} \\ M_{3i3150} & M_{3i1050} & M_{3i1250} & M_{3i2050} & M_{3i2250} \\ M_{3i3152} & M_{3i1052} & M_{3i1252} & M_{3i2052} & M_{3i2252} \\ M_{3i3161} & M_{3i1061} & M_{3i1261} & M_{3i2061} & M_{3i2261} \end{bmatrix} \begin{bmatrix} T_1^0 \\ T_1^2 \\ T_5^0 \\ T_5^2 \\ T_6^1 \end{bmatrix} \tag{70.}$$

where the notation used for the mobility terms consists of the first number indicating the location on the structure for the response and the input load if its an input mobility function or the response location followed by the force location if its a transfer mobility function, following is an i or a t to indicate whether the mobility function is an input or transfer mobility and then the numerical representation of the motion followed by the subscript and superscript of the force. For example M_{2i3060} represents an input mobility at location 2 for the 30 response due to a force T_6^0 and $M_{21i3161}$ would represent the transfer mobility for the 31 response at location 2 due to a force T_6^1 at location 1. The combination of the result for the force vectors, from equations (67) and (69), and the velocity response vectors from equations (68) and (70) will give the transferred power across the junction between the two plates by the in–plane and out–of–plane waves.

RESULTS

The input and transferred power flow results for two different thickness ratios are shown in figures (8) (9) and (10). An interesting observation from these results is that while changes in the plates thickness ratio changes the modal frequency of the out–of–plane waves, the change in thickness ratio has no influence on the modal frequencies of the in–plane waves. The change in the thickness changes the mass and bending stiffness and thus influences the out–of–plane motion of the plates. However the modal frequencies for the in–plane waves are mainly controlled by the width and length of the plates which is not modified in the above analysis. The power input and power transfer associated with the out–of–plane waves shows variations with thickness while the power input and power transfer associated with the in–plane waves remains in general the same.

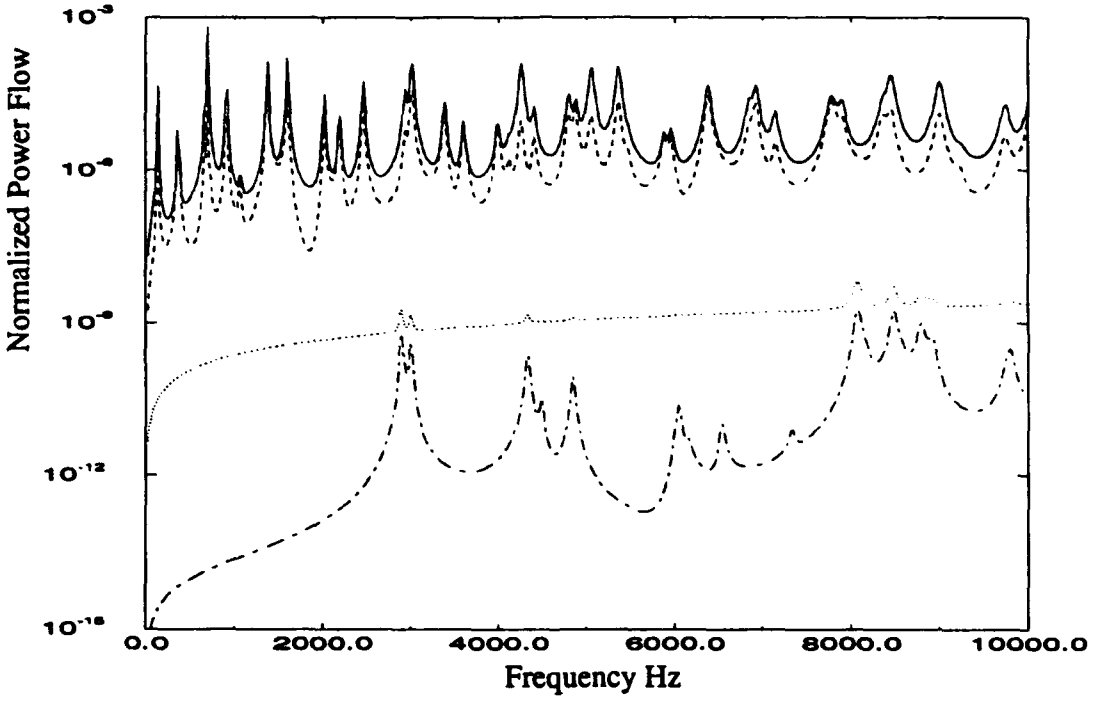

Figure 8. Power Flow for the coupled plate problem for a thickness ratio of 0.5. _____: Input power to out–of–plane waves; _ _ _ _: transferred power by out–of–plane waves; . . . . . : Input power to in–plane waves; ____ . _: transferred power by in–plane waves.

Another observation which is the result of the previously mentioned fact that there is no coupling between the in–plane and out–of–plane waves can also be seen from the results. This decoupling between the in–plane and out–of–plane waves is indicated by the fact that while the power flow associated with the out–of–plane waves type changes with the thickness ratio, that associated with the in–plane waves type remains the same. The in–plane waves are induced in the plate by the application of a transverse load because of that the load is applied on the surface of the plate.

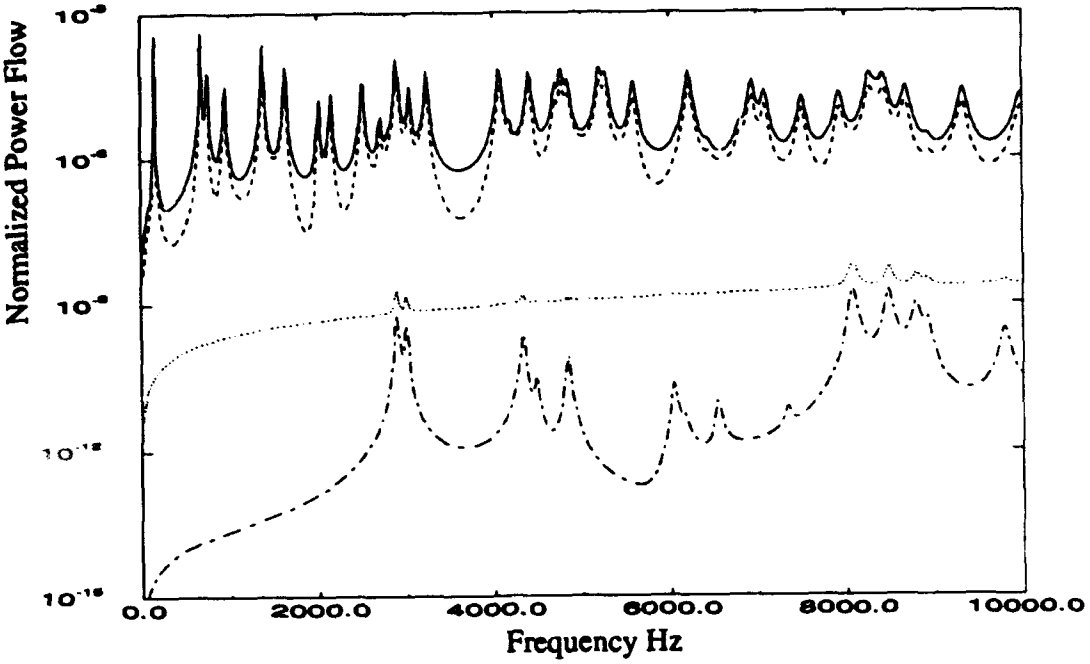

Figure 9. Power Flow for a thickness ratio of 1.0. _____: Input power to out–of–plane waves; _ _ _ _: transferred power by out–of–plane waves; . . . . . : Input power to in–plane waves; _ _ . _ _ : transferred power by in–plane waves.

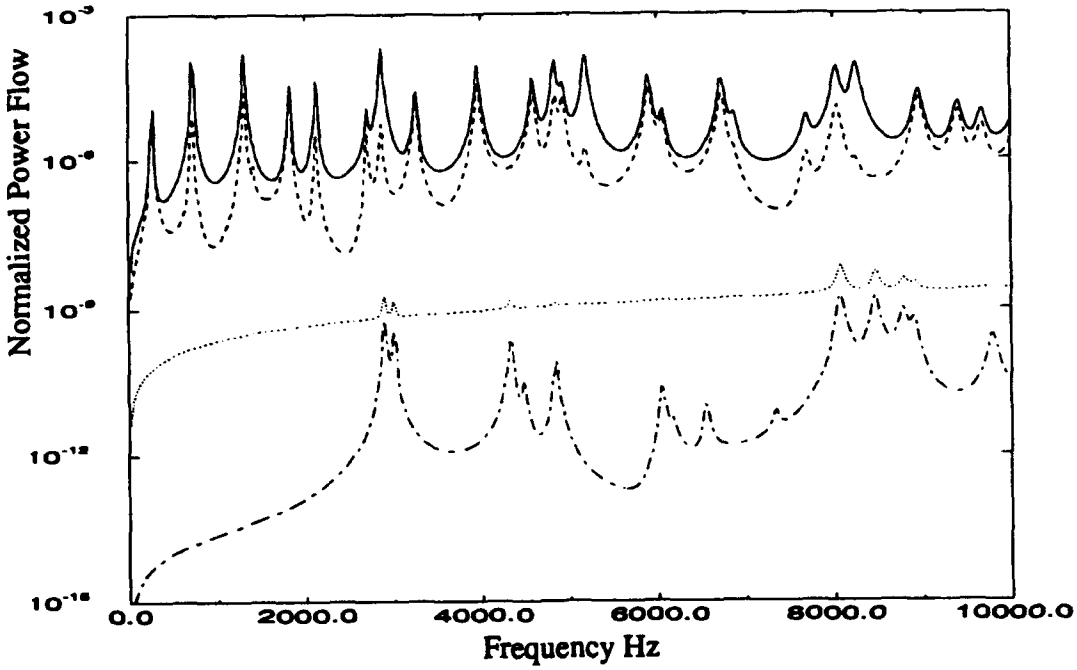

Figure 10. Power Flow for a thickness ratio of 2.0. _____: Input power to out–of–plane waves; _ _ _ _: transferred power by out–of–plane waves; . . . . . : Input power to in–plane waves; _ _ . _ _ : transferred power by in–plane waves.

At the junction, since the solution is based on the mid–plane of the plates, the edge effects due to the unequal thickness are not taken into consideration. There are therefore no external or induced forces at the junction between the two plates which would couple the out–of–plane waves with the in–plane waves. Out–of–plane wave energy or power is not scattered into in–plane waves energy or power and vice versa because of the presence of the junction which has been selected here. This will not however be the case if the discontinuity at the junction was a bulkhead or stiffener which due to its mobility will induce a force on the surface of the two plates. In this case the magnitude of this force will be dependent on the combined motion at the plate surface which thus couples the two wave types. If the bulkhead or stiffener had only lateral stiffness in the direction perpendicular to the plate surface and the mobility of the bulkhead is M_B, then the induced force at the junction will have a magnitude of $(\dot{W}_0 + \dot{W}_1)/M_B$. Since this force is applied on one of the plate surfaces the two waves would be coupled. In this case a solution similar to the one developed in [8] can be applied.

CONCLUSIONS

A solution for the power flow across the junction between two plates has been developed based on Mindlin and Mindlin and Medick approaches for the the response of a thick plate. In these approaches a Legendre Polynomial expansion is used in the thickness direction to simplify the governing equations of motion. Solutions are obtained for the equations of motion in the mid–plane of the plate with the Legendre Polynomials describing the distribution of the displacements in the thickness direction. The components of this expansion are orthogonal and the consequence is that the in–plane and out–of–plane wave equations become uncoupled.

To couple the in–plane and out–of plane waves due to the actions of an externally applied load on the plate surface, the load is also expanded into components using the same Legendre Polynomial expansion. The results from this approach are verified by comparison to results obtained using 3–D elasticity equations without simplifying assumptions. The solution for the out–of–plane and the in–plane wave motions is developed in this case based on a superposition of dilatational and shear motions. General agreement is obtained for the ratio of the out–of–plane response to the in–plane response between the approach based on Mindlin's solutions and the 3–D elasticity approach. There are some discrepancies in the the agreement between the 2 techniques, but this is mainly attributed to insufficient number of modes considered in the 3–D elasticity solution. The number of terms required to obtain adequate representation of the physical behavior requires the size of the matrix equation to be very large, requiring significant computation time. The approach based on Mindlin's in–plane and out–of–plane wave solutions is computationally much more efficient.

When using Mindlin's approach, without external loads – direct loading or loading from externally attached structures (stiffeners or bulkheads) – the in–plane waves and out–of–plane waves remain uncoupled at the junction. This is a deficiency of the model due to the fact that the solution is described relative to the plate mid–plane. In the case of the two end coupled plates, with different thickness, with external transverse load applied on one of the plate surfaces, vibrational power is input to each wave type, however no scatter from one wave type to the other occurs at the junction. Coupling between the in–plane and out–of–plane waves – which may result in the scattering of vibrational power from one wave type to the other – would be obtained at the junction if the junction includes a discontinuity which would create loading on one of the plate surfaces.

REFERENCES

14. "Vibrational Power Flow in Thick Connected Plates", M. D. McCollum, Ph.D. Dissertation, Ocean Engineering Department, Florida Atlantic University, 1988.

15. Mindlin R.D., "Influence of Rotary Inertia and Shear on Flexural Motions of Isotropic Plates", Journal of Applied Mechanics, Vol: 18, 31–38, 1951.

16. Kane T.R., Mindlin R.D., "High Frequency Extensional Vibration of Plates", Journal of Applied Mechanics, Vol: 23, 277–283, 1956.

17. "Mobility Power Flow Analysis of Connected Thick Plates with a Step Discontinuity", E. Faivre D'Arcier, M. S. Thesis, Ocean Engineering Department, Florida Atlantic University, April 1991.

18. Mindlin R.D., Medick M.A., "Extensional Vibration of Elastic Plates", Journal of Applied Mechanics, Vol: 26, 561–569, 1959.

19. Lyamyshev L.M., "Reflection of Sound by Thin Plates and Shells in Liquids", partial translation from Russian, (1955).

20. Hutchinson J. R., Zillmer S. D. "Vibration of a free rectangular parallelepiped", Journal of Applied Mechanics, Vol: 50, 123–130, 1983.

21. J.M. Cuschieri, "Vibration Transmission Through Periodic Structures Using a Mobility Power Flow Approach", Journal of Sound and Vibration, Vol. 143(1), 65–74, (1990).

ACOUSTIC SCATTERING FROM FLUID–LOADED PLATES WITH ARBITRARY BOUNDARY CONDITIONS.

Acoustic radiation from infinite fluid loaded plates have been extensively considered in the past [1,2]. Similarly for finite fluid–loaded plates where the boundary conditions allow for a modal decomposition of the plate response [3]. In other work which deals with fluid–loaded plates where the boundary conditions are arbitrary, generally the influence of the scattering is neglected. In this paper, the dynamic response and acoustic scattering from a finite, fluid–loaded, rectangular plate, simply supported on two edges and with arbitrary boundary conditions on the remaining edges and set in an infinite rigid baffle, is considered. It is assumed that compressible fluids are present on both sides of the plate and the plate is excited by an obliquely incident acoustic plane wave. Because of the complexity in the solution, in this paper the plate is considered a thin plate with no in–plane waves and negligible shear and rotary inertia effects. In future work a thick plate will be considered. The work presented here is a step towards the analysis of the power flow between two coupled plates including both the mechanical and acoustic coupling.

4. GOVERNING EQUATIONS

Consider a rectangular plate set in the plane z=0, bounded by $0 \leq x \leq a$ and $0 \leq y \leq b$, and set in an infinite rigid baffle. The plate is assumed to be simply supported along two of the edges (x = 0 and a), with arbitrary boundary conditions on the remaining two edges. The semi–infinite spaces z > 0 and z < 0 are occupied respectively by compressible fluids with density ϱ_1 and $\varrho_2$and sound speeds c_1 and c_2. The plate is characterized by a mass per unit area D, thickness h and bending stiffness B. An incident plane wave with angles of incidence ϕ and θ to the z and x–axes respectively, excites the plate into flexural motion (figure 1).

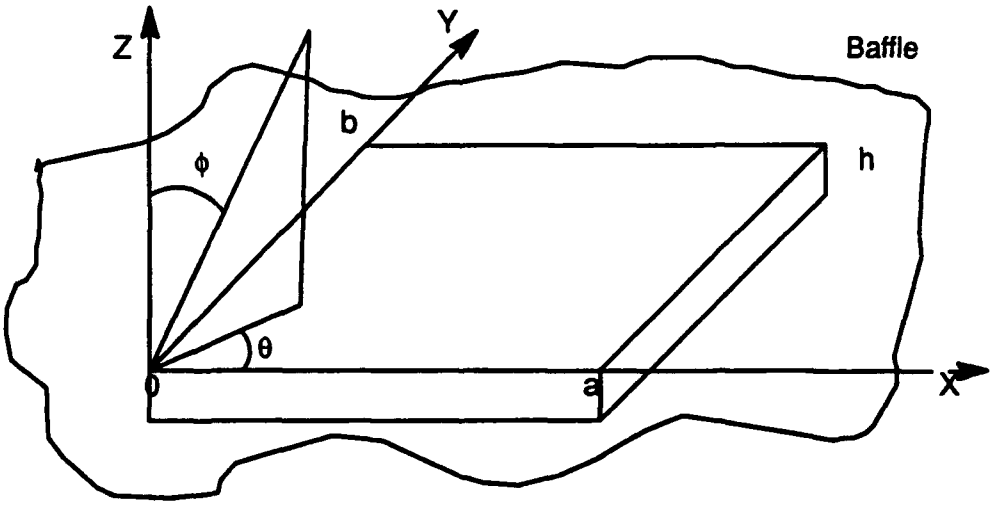

Figure 1. Plate and Baffle configuration.

For a thin plate, the bending stiffness is given by $B = Eh^3/12(1-\nu^2)$, where $E = E_0(1 + j\eta)$ is Young's Modulus, η is the structural damping, and ν is Poisson's ratio.

The incident wave obeys the Helmholtz equation in the half space z > 0. The incident acoustic wave is therefore governed by the equation,

$$P_i = P_0 e^{j(\omega t + k_x x + k_y y + k_z z)} \tag{71.}$$

where $k_x = k\sin\phi\cos\theta$, $k_y = k\sin\phi\sin\theta$, $k_z = k\cos\phi$ and $k = \omega/c_1$ is the acoustic wave number.

$$k^2 = k_x^2 + k_y^2 + k_z^2 \tag{72.}$$

All field variables are considered to be time harmonic with the convention $e^{i\omega t}$, this time dependency $e^{i\omega t}$ is however suppressed in the following derivations.

The equation governing small amplitude flexural vibrations of a thin elastic plate in the region $0 \le x \le a$ and $0 \le y \le b$, is given by,

$$B\nabla^4 W(x,y) - D\omega^2 W(x,y) = [P] \tag{73.}$$

where W(x,y) is the transverse displacement of the plate at position (x,y), ∇^4 is the square of the laplacian operator and [P] is the total pressure acting on the plate due to the incident and reflected acoustic waves and the scattered waves,

$$[P] = \left[P_{s_2}(x,y,z)\right]_{z=0^-} - \left[P_i(x,y,z) + P_r(x,y,z) + P_{s_1}(x,y,z)\right]_{z=0^+} \tag{74.}$$

$P_i(x,y,z)$ and $P_r(x,y,z)$ are respectively the incident and the reflected wave pressures if the plate is rigid and $P_{s_1}(x,y,z)$ and $P_{s_2}(x,y,z)$ are the scattered pressure components satisfying the Helmholtz equation and the radiation condition [3]. It has been shown [3] that the reflected pressure from a rigid surface is equal to the incident pressure, and therefore equation (4) can be simplified to,

$$[P] = \left[P_{s_2}(x,y,z)\right]_{z=0^-} - \left[2P_i(x,y,z) + P_{s_1}(x,y,z)\right]_{z=0^+} \tag{75.}$$

In determining the response of the plate, only the value of the pressure on the plate surfaces is considered, that is all pressure components are evaluated at z=0. and therefore for simplicity the z dependency will be dropped from the notation used in the analysis. At the plate–fluid interface the normal particle velocity of the fluid must be equal to that of the plate [3], that is for $0 \le x \le a$ and $0 \le y \le b$,

$$\left(\frac{\partial P_{s_{1,2}}(x,y,z)}{\partial z}\right)_{z=0^+} + j\varrho_{1,2}\omega^2 W(x,y) = 0 \qquad 76.$$

On the rigid baffle the normal velocity must vanish and the gradient of the pressure must be equal to zero.

$$\left(\frac{\partial P_{s_{1,2}}(x,y,z)}{\partial z}\right)_{z=0^+} = 0 \qquad 77.$$

If the plate is simply supported on two of its edges, the boundary conditions along the simply supported edges are given by: $W(0,y) = 0$, $\partial^2 W(0,y)/\partial x^2 = 0$, $W(a,y) = 0$ and $\partial^2 W(a,y)/\partial x^2 = 0$. The boundary conditions on the other two edges are arbitrary. However to demonstrate the approach and to generate expressions which can be used for the analysis of two end coupled plate with a stiff support at the junction, it will be assumed that the two remaining edges are also simply supported together with an edge moment at y=0, that is $W(x,0) = 0$, $\partial^2 W(x,0)/\partial y^2 = 0$, $W(x,b) = 0$ and $\partial^2 W(x,b)/\partial y^2 = 0$ *or* $-M(x)/B$ depending on whether the edge is just simply supported or loaded with an edge moment.

The solution is derived in the wavenumber domain. This is necessary to take into proper consideration the influence of the scattered pressure. The forward and reverse spatial transforms are defined by the Fourier transform pair,

$$\tilde{F}(\alpha) = \int_{-\infty}^{\infty} f(x)e^{j\alpha x}dx \text{ and } f(x) = \frac{1}{2\pi}\int_{-\infty}^{\infty} \tilde{F}(\alpha)e^{-j\alpha x}d\alpha \qquad 78.$$

5. METHOD OF SOLUTION

In the solution of the equation of motion, equation (3), a modal decomposition is assumed in the direction perpendicular to the simply supported edges, that is along the x–axis direction

$$W(x,y) = \sum_{m=0}^{m=\infty} W_m(y)\sin\left(\frac{m\pi x}{a}\right) \qquad 79.$$

Substituting into equation (3),

$$\sum_{m=0}^{m=\infty}\left\{B\left[\frac{d^4W_m(y)}{d^4y} - 2k_m{}^2\frac{d^2W_m(y)}{d^2y} + k_m{}^4W_m(y)\right] - D\omega^2 W_m(y)\right\}\sin\left(\frac{m\pi x}{a}\right) = [P(x,y)] \qquad 80.$$

where $k_m = m\pi/a$, is the modal wavenumber along the x–axis. Multiplying equation (10) by $\sin(n\pi x/a)$, and integrating from 0 to a,

$$\frac{d^4W_m(y)}{d^4y} - 2k_m{}^2\frac{d^2W_m(y)}{d^2y} + \left(k_m{}^4 - k_p{}^4\right)W_m(y) = \frac{1}{B}\left[-2P_{i_m}(y) - P_{s_{1_m}}(y) + P_{s_{2_m}}(y)\right] \qquad 81.$$

where $k_p^4 = D\omega^2/B$ is the in–vacuo plate flexural wavenumber and $P_{i_m}(y)$, $P_{s_{1_m}}(y)$ and $P_{s_{2_m}}(y)$ are respectively defined by

$$P_{i_m}(y) = \frac{2}{a}\int_o^a P_i(x,y)\sin(\frac{m\pi x}{a})dx = \frac{2P_0}{a}jJ_m e^{jk_y y} \qquad 82.$$

$$P_{s_{1_m}}(y) = \frac{2}{a}\int_o^a P_{s_1}(x,y)\sin(\frac{m\pi x}{a})dx \qquad 83.$$

$$P_{s_{2_m}}(y) = \frac{2}{a}\int_o^a P_{s_2}(x,y)\sin(\frac{m\pi x}{a})dx \qquad 84.$$

In the above equations use has been made of the orthogonality condition

$$\int_0^a \sin\left(\frac{m\pi x}{a}\right)\sin\left(\frac{n\pi x}{a}\right)dx = \begin{Bmatrix} 0 & \text{if } m \neq n \\ \frac{a}{2} & \text{if } m = n \end{Bmatrix} \qquad 85.$$

In equation (12)

$$J_m = jk_m\frac{(-1)^m e^{jk_x a} - 1}{k_m^2 - k_x^2} \qquad 86.$$

When the acoustic wavenumber in the x direction is equal to the plate mode wavenumber in the x direction, that is $k_m = \pm k_x$, the coefficient J_m is not singular, but is given by,

$$J_m = \begin{cases} \frac{a}{2} & \text{if } k_m = k_x \\ -\frac{a}{2} & \text{if } k_m = -k_x \end{cases} \qquad 87.$$

Because of the nonlinear form of equation (11), there is no exact simple analytical solution to this equation. If the scattering pressure components can be neglected, then an analytical solution

is possible. Otherwise a numerical approximation method has to be used for the solution. The following sections present solutions to the coupled equations of motion of the finite fluid–loaded plate.

6. NEGLIGIBLE SCATTERING COMPONENT

Neglecting the scattered pressure component, equation (11) can be solved analytically and the solution can be written in the form,

$$W_{0_m}(y) = W_p(y) + W_h(y) \tag{88.}$$

where W_p is the particular solution of equation (11),

$$W_p(y) = \frac{-4P_0}{a} j \frac{J_m}{B} \frac{e^{jk_y y}}{\left(k_m^2 + k_y^2\right)^2 - k_p^4} \tag{89.}$$

and Wg is the general solution of the homogeneous equation,

$$W_h(y) = Y_1 e^{jK_1 y} + Y_2 e^{-jK_1 y} + Y_3 e^{jK_2 y} + Y_4 e^{-jK_2 y} \tag{90.}$$

In equation (20), Y_i ($i = 1$ *to* 4) are arbitrary constants which are determined from the boundary conditions. K_1 and K_2 are the roots of the dispersion equation and are given by $K_1 = \pm j\sqrt{k_p^2 + k_m^2}$ and $K_2 = \pm \sqrt{k_p^2 - k_m^2}$. K_1 and K_2 are selected such that the imaginary part is positive.

In the case of a simply supported plate, the coefficients Y_i ($i = 1$ *to* 4) are given by,

$$Y_{1A} = \frac{k_y^2 - K_2^2}{4k_p^2 j \sin(K_1 b)} \left(e^{jk_y b} - e^{-jK_1 b}\right) W_p(0)$$

$$Y_{2A} = -\frac{k_y^2 - K_2^2}{4k_p^2\, j \sin(K_1 b)} \left(e^{jk_y b} - e^{jK_1 b}\right) W_p$$

$$Y_{3A} = -\frac{k_y^2 - K_1^2}{4k_p^2 j \sin(K_2 b)} \left(e^{jk_y b} - e^{-jK_2 b}\right) W_p(0)$$

$$Y_{4A} = \frac{k_y^2 - K_1^2}{4k_p^2 j \sin(K_2 b)} \left(e^{jk_y b} - e^{jK_2 b}\right) W_p(0) \tag{91.}$$

where the additional subscript A is introduced for the simply supported case.

For a plate with an edge moment excitation M(x) at the edge y=0, the coefficients Y_i ($i = 1$ *to* 4) are given by,

$$Y_{1M} = \frac{\frac{M}{B} e^{-jK_1 b}}{4k_p^2\, j\sin(K_1 b)}, \; Y_{2M} = -\frac{\frac{M}{B} e^{jK_1 b}}{4k_p^2\, j\sin(K_1 b)},$$

$$Y_{3M} = -\frac{\frac{M}{B} e^{-jK_2 b}}{4k_p^2\, j\sin(K_2 b)} \text{ and } Y_{4M} = \frac{\frac{M}{B} e^{jK_2 b}}{4k_p^2\, j\sin(K_2 b)} \qquad 92.$$

the subscript M is to indicate the presence of the edge moment. In equation (22),

$$M = \frac{a}{2}\int_0^a M(x)\sin\left(\frac{m\pi x}{a}\right)dx \qquad 93.$$

Other boundary conditions can be considered using a similar approach.

7. SOLUTION INCLUDING SCATTERING

When the scattered pressure components are not neglected, a relation between the scattered pressures and the plate displacement is required in the solution. From equation (6), the relation between the displacement W and the scattered pressure in the wavenumber domain is given by

$$\gamma' \tilde{P}_s(\alpha',\beta') = j\varrho\omega^2 \tilde{W}(\alpha',\beta') \qquad 94.$$

where γ' is the acoustic wavenumber in the z–axis direction

$$\gamma' = \pm\sqrt{k^2 - \alpha'^2 - \beta'^2} \qquad 95.$$

The appropriate sign and phase are determined by the physics of the problem. Fourier transforming equation (11)

$$\left[\left(\beta^2 + {k_m}^2\right)^2 - {k_p}^4\right]\tilde{W}_m(\beta) - \left(\beta^2 + 2{k_m}^2\right)\left[W_m'(b)e^{jb\beta} - W_m'(0)\right] +$$

$$j\beta\left(\beta^{2+2}{k_m}^2\right)\left[W_m(b)e^{jb\beta} - W_m(0)\right] - j\beta\left[W_m''(b)e^{jb\beta} - W_m''(0)\right] +$$

$$W_m'''(b)e^{jb\beta} - W_m'''(0) = \frac{1}{B}\left[-2\tilde{P}_{i_m}(\beta) - \tilde{P}_{s_{1_m}}(\beta) + \tilde{P}_{s_{2_m}}(\beta)\right] \qquad 96.$$

where

$$\tilde{W}_m(\beta) = \int_0^b W_m(y)e^{jy\beta}dy\,,\quad \tilde{P}_{s_{1_m}}(\beta) = \int_0^b P_{s_{1_m}}(y)e^{jy\beta}dy,$$

$$\tilde{P}_{s_{2_m}}(\beta) = \int_0^b P_{s_{2_m}}(y)e^{jy\beta}dy \text{ and } \tilde{P}_{i_m}(\beta) = \int_0^b P_{i_m}(y)e^{jy\beta}dy \qquad 97.$$

The W primed terms in equation (26) are a result of the fact that the plate is finite. Introducing the following simplifying notation,

$$\begin{aligned}
A(\beta) &= \left(\beta^2 + k_m^2\right)^2 - k_p^4 & A_3(\beta) &= -e^{j\beta b} & A_6(\beta) &= j\beta e^{j\beta b}\\
A_1(\beta) &= \left(\beta^2 + 2k_m^2\right)e^{j\beta b} & A_4(\beta) &= 1. & A_7(\beta) &= -j\beta\left(\beta^2 + 2k_m^2\right)e^{j\beta b}\\
A_2(\beta) &= -\left(\beta^2 + 2k_m^2\right) & A_5(\beta) &= -j\beta & A_8(\beta) &= j\beta\left(\beta^2 + 2k_m^2\right)
\end{aligned} \qquad 98.$$

and

$$\begin{aligned}
X_1 &= W_m'(b) & X_4 &= W_m'''(0) & X_7 &= W_m(b)\\
X_2 &= W_m'(0) & X_5 &= W_m''(0) & X_8 &= W_m(0)\\
X_3 &= W_m'''(b) & X_6 &= W_m''(b)
\end{aligned} \qquad 99.$$

Substituting into equation (26),

$$A(\beta)\tilde{W}_m(\beta) = Q(\beta) + \frac{1}{B}\left[\tilde{P}_{s_{2_m}}(\beta) - \tilde{P}_{s_{1_m}}(\beta)\right] \qquad 100.$$

where the function $Q(\beta)$ is defined by,

$$Q(\beta) = -\frac{2}{B}\,\tilde{P}_{i_m}(\beta) + \sum_{i=1}^{i=8} X_i A_i(\beta) \qquad 101.$$

From equation (27) the Fourier transform of the pressure components also ranges from 0 to b. Therefore, the relationship is not in the form shown in equation (24). The relationship between $\tilde{P}_s(\beta)$ and $\tilde{W}_m(\beta)$ (derived in Appendix A), is given by,

$$\frac{1}{B}\tilde{P}_{s_{1_m}}(\beta) = \lambda_1 \int_{-\infty}^{+\infty} J_{1_m}(\beta')G(\beta - \beta')\tilde{W}_m(\beta')d\beta' \qquad 102.$$

$$\frac{1}{B}\,\tilde{P}_{s_{2_m}}(\beta) = -\lambda_2 \int_{-\infty}^{+\infty} J_{2_m}(\beta')G(\beta-\beta')\tilde{W}_m(\beta')d\beta' \qquad 103.$$

where $\lambda_1 = j\varrho_1\omega^2/(2\pi^2 aB)$, $\lambda_2 = j\varrho_2\omega^2/(2\pi^2 aB)$, $G(\beta) = e^{j\beta b} - 1/(j\beta)$ and J_{1_m} and J_{2_m} are defined in Appendix A.

Due to the finiteness of the plate, for each wavenumber β, the scattered pressure component is dependent on all of the plate displacement components. The fluid–plate coupling is represented by the parameters λ_1 and λ_2 and the functions J_{1_m} and J_{2_m}. The coefficients λ_1 and λ_2 are functions of the fluid loading parameters [1] α_1 and α_2 which are given by, $\alpha_1 = \omega^2\varrho_1/B$ and $\alpha_2 = \omega^2\varrho_2/B$.

The functions J_{1m} and J_{2m} represent the importance of the contribution of each plate wavenumber to the scattered pressure. In particular, the closer the wave number is to the wavenumber k_m, the more significant is the contribution, (see Appendix A).

Substituting equation (32) and (33) into equation (30),

$$A(\beta)\tilde{W}_m(\beta) = Q(\beta) + K(\tilde{W}_m)(\beta) \qquad 104.$$

where **K** is defined by,

$$K(\Phi)(\beta) = -\int_{-\infty}^{\infty} \left[\lambda_1 J_{1_m}(\beta') + \lambda_2 J_{2_m}(\beta')\right] G(\beta-\beta')\Phi(\beta')d\beta' \qquad 105.$$

The integral equation (34) represents the complete solution to the plate scattering problem. In evaluating this equation, it is still necessary to obtain the eight unknown functions X_i ($i = 1$ *to* 8), which are present in the function $Q(\beta)$. Eight simultaneous equations are required to solve for these unknowns. Four of the simultaneous equations can be obtained from the condition that whenever the polynomial $A(\beta)$ goes to zero, the first term in equation (34) also goes to zero and therefore the second term in equation (34) must also vanishes. Since $A(\beta)$ is a polynomial of degree four this condition gives four linear equations. The other four equations come from the boundary conditions.

Equation (34) is a Fredholm equation of the third kind. The main difficulty of solving this equation lies in finding an accurate representation for the operator **K**. Different techniques are available to evaluate **K** [4]. These include, (a) Iterative methods, (b) Quadrature methods, (c) Kernel approximation methods and (d) Projection methods.

The iterative methods are not applicable because of the large values of the parameters λ_1 and λ_2 The iterative algorithm in general does not converge. For the quadrature method a large number of points is required to cover the full range of integration which makes this technique very computationally intensive. Thus, only the Kernel approximation method and the projection method may be possible to use for obtaining a solution.

8. KERNEL APPROXIMATION METHOD

When the acoustic wavelength is less than the plate dimensions, the behavior of the plate can be assumed to be similar to that of an infinite plate. That is, the function G approaches a dirac delta function, $G(\beta) = 2\pi\delta(\beta)$. An approximation for the operator **K** can therefore be obtained as,

$$K(\Phi)(\beta) = -2\pi\left[\lambda_1 J_{1_m}(\beta) + \lambda_2 J_{2_m}(\beta)\right]\Phi(\beta) \qquad 106.$$

Substituting equation (36) into equation (34)

$$\tilde{W}_m(\beta) = \frac{Q(\beta)}{\left[A(\beta) + 2\pi\left(\lambda_1 J_{1_m}(\beta) + \lambda_2 J_{2_m}(\beta)\right)\right]} \qquad 107.$$

When determining the unknowns in the function $Q(\beta)$, four of the unknowns are determined from the condition that whenever the denominator in the equation (37) is equal to zero, the numerator must also vanish. This denominator is a sum of the polynomial $A(\beta)$ and a perturbation function. It can be assumed that the zeros of this denominator will be in the vicinity of the zeros K_1 and K_2 of the polynomial $A(\beta)$. The actual zeros can be found by an iterative process.

9. PROJECTION METHOD

The Fredholm integral equation of the third kind (equation 34) can be simplified to an integral equation of the second kind. This is done by determining the four unknowns of the function Q which are not determined by the boundary conditions.

Considering the case of the simply supported plate, from the boundary conditions, $X_5 = X_6 = X_7 = X_8 = 0$ and equation (31) becomes,

$$Q(\beta) = -\frac{2}{B}\,\tilde{P}_{i_m}(\beta) + \sum_{i=1}^{i=4} X_i A_i(\beta) \qquad 108.$$

The coefficients X_i ($i = 1$ *to* 4) can be obtained from equation (34), since when β is equal to one of the zeros of the polynomial, A ($\pm K_1$, $\pm K_2$), the left hand side of equation (34) goes to zero, the right hand side must also vanishes. Thus a set of four equations is obtained which can be solved for X_i ($i = 1$ *to* 4), that is

$$\sum_{i=1}^{i=4} X_i A_i(\bar{K}) = -K(\tilde{W}_m)(\bar{K}) + \frac{2}{B}\tilde{P}_{i_m}(\bar{K}) \qquad 109.$$

where $\bar{K}$ can take values $\pm K_1$ or $\pm K_2$. Solving this system of equations analytically, the result is of the form

$$\begin{aligned} X_1 &= X_{1A} + X_{1S} \qquad X_3 = X_{3A} + X_{3S} \\ X_2 &= X_{2A} + X_{2S} \qquad X_4 = X_{4A} + X_{4S} \end{aligned} \qquad 110.$$

where X_{1A}, X_{2A}, X_{3A}, X_{4A} represent the solutions of equation (39) when the scattering effects are neglected. These terms are given by,

$$X_{1A} = \frac{2}{\Delta B}\left\{\left[\tilde{P}_{i_m}(K_1) - \tilde{P}_{i_m}(-K_1)\right]\sin(K_2 b) - \left[\tilde{P}_{i_m}(K_2) - \tilde{P}_{i_m}(-K_2)\right]\sin(K_1 b)\right\} \qquad 111.$$

$$X_{2A} = \frac{2}{\Delta B}\left\{\left[\tilde{P}_{i_m}(K_1)e^{-jK_1 b} - \tilde{P}_{i_m}(-K_1)e^{jK_1 b}\right]\sin(K_2 b) - \left[\tilde{P}_{i_m}(K_2)e^{-jK_2 b} - \tilde{P}_{i_m}(-K_2)e^{jK_2 b}\right]\sin(K_1 b)\right\} \qquad 112.$$

$$X_{3A} = \frac{2}{\Delta B}\left\{\left[\tilde{P}_{i_m}(K_1) - \tilde{P}_{i_m}(-K_1)\right]\left(K_2^2 + 2k_m^2\right)\sin(K_2 b) - \left[\tilde{P}_{i_m}(K_2) - \tilde{P}_{i_m}(-K_2)\right]\left(K_1^2 + 2k_m^2\right)\sin(K_1 b)\right\} \qquad 113.$$

$$X_{4A} = \frac{2}{\Delta B}\left\{\left[\tilde{P}_{i_m}(K_1)e^{-jK_1 b} - \tilde{P}_{i_m}(-K_1)e^{jK_1 b}\right]\left(K_2^2 + 2k_m^2\right)\sin(K_2 b) - \left[\tilde{P}_{i_m}(K_2)e^{-jK_2 b} - \tilde{P}_{i_m}(-K_2)e^{jK_2 b}\right]\left(K_1^2 + 2k_m^2\right)\sin(K_1 b)\right\} \qquad 114.$$

X_{1S}, X_{2S}, X_{3S}, X_{4S} are the contributions from the scattering given by

$$X_{1S} = \frac{-1}{\Delta}\left\{\left[K(\tilde{W}_m)(K_1) - K(\tilde{W}_m)(-K_1)\right]\sin(K_2 b) - \left[K(\tilde{W}_m)(K_2) - K(\tilde{W}_m)(-K_2)\right]\sin(K_1 b)\right\} \qquad 115.$$

$$X_{2S} = \frac{-1}{\Delta}\left\{\left[K(\tilde{W}_m)(K_1)e^{-jK_1 b} - K(\tilde{W}_m)(-K_1)e^{jK_1 b}\right]\sin(K_2 b) - \left[K(\tilde{W}_m)(K_2)e^{-jK_2 b} - K(\tilde{W}_m)(-K_2)e^{jK_2 b}\right]\sin(K_1 b)\right\} \qquad 116.$$

$$X_{3S} = \frac{-1}{\Delta}\Big\{\Big[K(\tilde{W}_m)(K_1) - K(\tilde{W}_m)(-K_1)\Big]\sin(K_2 b)\big(K_2^2 + 2k_m^2\big) - \Big[K(\tilde{W}_m)(K_2) - K(\tilde{W}_m)(-K_2)\Big]\sin(K_1 b)\big(K_1^2 + 2k_m^2\big)\Big\} \quad 117.$$

$$X_{4S} = \frac{-1}{\Delta}\Big\{\Big[K(\tilde{W}_m)(K_1)e^{-jK_1 b} - K(\tilde{W}_m)(-K_1)e^{jK_1 b}\Big]\sin(K_2 b)\big(K_2^2 + 2k_m^2\big) - \Big[K(\tilde{W}_m)(K_2)e^{-jK_2 b} - K(\tilde{W}_m)(-K_2)e^{jK_2 b}\Big]\sin(K_1 b)\big(K_1^2 + 2k_m^2\big)\Big\} \quad 118.$$

where $\Delta = -4jk_p^2 \sin(K_1 b)\sin(K_2 b)$. Substituting these equations into equation (38)

$$Q(\beta) = -\frac{2}{B}\,\tilde{P}_{i_m}(\beta) + \sum_{i=1}^{4} X_{iA}A_i(\beta) + \sum_{i=1}^{4} X_{iS}A_i(\beta) \quad 119.$$

If the scattering terms are neglected in equation (49), then

$$A(\beta)\tilde{W}_{A_m}(\beta) = -\frac{2}{B}\,\tilde{P}_{i_m}(\beta) + \sum_{i=1}^{4} X_{iA}A_i(\beta) \quad 120.$$

where $\tilde{W}_{A_m}(\beta)$ is the Fourier transform of the plate displacement when the scattered pressure is neglected, given by the Fourier transform of equation (18). Substituting equations (41) to (48) into equation (49), the following expression (see Appendix B) is obtained.

$$Q(\beta) = A(\beta)\tilde{W}_{A_m}(\beta) + \int_{-\infty}^{+\infty}\Big[\lambda_1 J_{1_m}(\beta') + \lambda_2 J_{2_m}(\beta')\Big]\tilde{W}_m(\beta')K(\beta,\beta')d\beta' \quad 121.$$

where

$$K(\beta,\beta') = \frac{1}{\Delta}\Big\{(\beta^2 - K_2^2)\sin(K_2 b)\Big[G(K_1 - \beta')\big(e^{-jK_1 b} - e^{j\beta b}\big) - G(-K_1 - \beta')\big(e^{jK_1 b} - e^{j\beta b}\big)\Big] - (\beta^2 - K_1^2)\sin(K_1 b)\Big[G(K_2 - \beta')\big(e^{-jK_2 b} - e^{j\beta b}\big) - G(-K_2 - \beta')\big(e^{jK_2 b} - e^{j\beta b}\big)\Big]\Big\} \quad 122.$$

And substituting into equation (34), the Fourier transform of the plate displacement is then given by a Fredholm integral equation of the second kind,

$$\tilde{W}_m(\beta) = \tilde{W}_{A_m}(\beta) -$$

$$\frac{1}{A(\beta)} \int_{-\infty}^{+\infty} \left[\lambda_1 J_{1_m}(\beta') + \lambda_2 J_{2_m}(\beta')\right][G(\beta - \beta') + K(\beta,\beta')]\tilde{W}_m(\beta')d\beta' \qquad 123.$$

The displacement of the plate then consists of a displacement contribution obtained by neglecting the scattering terms and a corrective component introduced to account for the presence and influence of the fluid loading.

If the plate is under an edge moment excitation, a similar procedure as above can be followed to derive the dynamic response of the plate. The only change in the result being in the solution $\tilde{W}_{A_m}(\beta)$ to the plate displacement when the scattered terms are neglected. This solution will be referred to as $\tilde{W}_{M_m}(\beta)$. One can show that the constants X_1, X_2, X_3, X_4 in $\tilde{W}_{M_m}(\beta)$ are given by

$$X_{1M} = -\frac{2jM}{\Delta B}\left[K_1 \sin(K_2 b) - K_2 \sin(K_1 b)\right] \qquad 124.$$

$$X_{2M} = -\frac{2jM}{\Delta B}\left[K_1 \cos(K_1 b)\sin(K_2 b) - K_2 \cos(K_2 b)\sin(K_1 b)\right] \qquad 125.$$

$$X_{3M} = -\frac{2jM}{\Delta B}\left[K_1\left(K_2^2 + 2k_m^2\right)\sin(K_2 b) - K_2\left(K_1^2 + 2k_m^2\right)\sin(K_1 b)\right] \qquad 126.$$

$$X_{4M} = -\frac{2jM}{\Delta B}\left[K_1\left(K_2^2 + 2k_m^2\right)\sin(K_2 b)\cos(K_1 b) - K_2\left(K_1^2 + 2k_m^2\right)\sin(K_1 b)\cos(K_2 b)\right] \qquad 127.$$

where M is the edge moment, given by equation (23) and the dynamic response of the plate is given by an equation similar to equation (53) with $\tilde{W}_{0_m}(\beta)$ substituted for $\tilde{W}_{A_m}(\beta)$, where $\tilde{W}_{0_m}(\beta)$ is the plate response when the scattered pressure is neglected and which is equal to $\tilde{W}_{A_m}(\beta)$ in the case of acoustic excitation, $\tilde{W}_{M_m}(\beta)$ in the case of edge moment excitation, and $\tilde{W}_{A_m}(\beta) + \tilde{W}_{M_m}(\beta)$ in the case of both acoustic and edge moment excitation. $\tilde{W}_{0_m}(\beta)$ can be derived from equations (18).

Equation (53) is the general solution to the problem of scattering from a plate using a projection method. Projection methods include the Polynomial Collocation method, Galerkin's method, the Least Squares method, and others [4]. The polynomial collocation consists of approximating the solution to the integral equation using a set of polynomial basis and a set of

collocation points. The performance of this method depends on the choice of this set of points. For the problem considered here, the solution is highly oscillatory and the range of integration is between $-\infty$ and $+\infty$, making this approach inappropriate. The Least Squares method is also not suitable since it requires the calculation of multiple integrals. Galerkin's method consists of decomposing the solution using a basis and approximating the solution by truncating the decomposition. The performance of the method depends only on the choice of the basis. This method is the one used in the solution.

10. GALERKIN'S METHOD AND CHOICE OF BASIS

If the scattered pressure is neglected, the solution for the plate displacement is of the form $e^{\overline{K}y}$ (equations 19 and 20), where $\overline{K}$ can take any of the complex numbers, $\pm K_1, \pm K_2, K_y$. The form of the solution for the plate displacement including the influence of the fluid–loading will in general not significantly deviate from this form. Therefore, it can be assumed that the solution will still be of the form $e^{\overline{K}y}$, but with different values of $\overline{K}$. In the wavenumber domain, the solution will have a component of the form $G(\overline{K} + \beta)$. Using a Taylor expansion, $G(\overline{K} + \beta)$ can be written as,

$$G(\overline{K} + \beta) = \sum_{n=0}^{\infty} \frac{\overline{K}^n}{n!} \frac{d^n G(\beta)}{d^n \beta} \qquad 128.$$

Let $\phi_n(\beta) = d^n G(\beta)/d^n\beta$, these functions are a basis of the space of oscillatory functions. That is, any oscillatory function can be decomposed uniquely in terms of these functions. The evaluation of these functions is presented in Appendix C. The plate displacement in the wavenumber domain can therefore be decomposed in the form

$$\tilde{W}_m(\beta) = \sum_{n=0}^{\infty} a_n \phi_n(\beta) \qquad 129.$$

where the coefficients (a_n , $n = 0$ *to* ∞) are to be determined using equation (53). In the Galerkin's method $\tilde{W}_m$ is approximated using a finite summation, that is equation (58) is truncated for some value of N, which is chosen based on the desired level of accuracy. Substituting equation (58) into equation (53)

$$\tilde{W}_{0_m}(\beta) = \sum_{n=0}^{N} a_n[\phi_n(\beta) + \psi_n(\beta)] \qquad 130.$$

where

$$\psi_n(\beta) = \frac{1}{A(\beta)} \int_{-\infty}^{+\infty} \left[\lambda_1 J_{1_m}(\beta') + \lambda_2 J_{2_m}(\beta')\right][G(\beta - \beta') + K(\beta,\beta')]\phi_n(\beta')d\beta' \qquad 131.$$

The coefficients a_n (n = 0 to N) can be obtained by solving a set of equations of the form

$$\sum_{n=0}^{N} a_n\left[< \phi_n, \phi_l > + < \psi_n, \phi_l > \right] = < \tilde{W}_{0_m}, \phi_l > \qquad 132.$$

for $0 \leq l \leq N$, where

$$< u, v > = \int_{-\infty}^{+\infty} u(\beta)v^*(\beta)d\beta \qquad 133.$$

The asterisk indicates a complex conjugate. Substituting for $< \phi_n, \phi_l >$, $< \psi_n, \phi_l >$ and $< \tilde{W}_{o_m}, \phi_l >$ (see appendix C)

$$< \phi_n, \phi_l > = 2\pi b(-1)^l \frac{(jb)^{l+n}}{n + l + 1} \qquad 134.$$

$< \psi_n, \phi_l >$ and $< \tilde{W}_{0_m}, \phi_l >$ are computed using a numerical integration. When the fluid–loading effects are neglected, the term $< \psi_n, \phi_l >$ in equation (62) can be neglected. The solution to this system gives an approximation to the exact solution $\tilde{W}_{0_m}$ which is given by equation (50) or by equation (18). It has been found that N=5 gives an excellent approximation to $\tilde{W}_{0_m}$. It is therefore assumed that N=5 will give a good approximation to the exact solution when the scattering terms are included in the solution.

11. INPUT POWER

The power input to the plate is balanced by its dissipation through mechanical losses and acoustic radiation. From the equation of motion of the fluid–loaded plate,

$$-2P_i(x,y) = \frac{B}{j\omega}\left[\nabla^4 V(x,y) - k_p^4 V(x,y)\right] + P_{s_1}(x,y) - P_{s_2}(x,y) \qquad 135.$$

the power flow into the plate from the incident pressure is obtained by multiplying both sides of the above equation by $V^*(x,y)/2$ and taking the integral over the plate surface. The total input power to the plate is thus given by,

$$\Pi_i = -\frac{1}{2}\mathrm{Re}\left\{\int_0^a \int_0^b 2\ P_i(x,y)V^*(x,y)dxdy\right\} \qquad 136.$$

The factor of 2 in front of the incident pressure is included to take into account the reflected pressure contribution. Substituting for the displacement using equation (9) and using the notation of equation (12)

$$\Pi_i = \sum_{m=1}^{m=\infty} -\frac{a}{2}\mathrm{Re}\left\{\int_0^a P_{i_m}(y)V_m^*(y)dy\right\} \qquad 137.$$

The spatial integrals in the expression for the input power can be replaced by integral in the wavenumber domain using the complex Fourier spatial transforms. Therefore

$$\Pi_i = \sum_{m=1}^{m=\infty} -\frac{a}{4\pi}\mathrm{Re}\left\{\int_{-\infty}^{+\infty} \tilde{P}_{i_m}(\beta')\tilde{V}_m^*(\beta')d\beta'\right\} \qquad 138.$$

$\tilde{P}_{i_m}$ is the full–range Fourier transform of $P_{i_m}(y)$. From equation (12)

$$P_{i_m}(y) = j\frac{2P_0}{a}\ J_m\ e^{jk_y y} \qquad 139.$$

therefore

$$\tilde{P}_{i_m}(\beta') = j\frac{4\pi P_0}{a}\ J_m\ \delta(\beta' + k_y) \qquad 140.$$

and

$$\Pi_i = \sum_{m=1}^{m=\infty} -P_0\ Imag\left\{J_m\tilde{V}^*{}_m(-k_y)\right\} \qquad 141.$$

12. SCATTERED POWER

The scattered power is the power transferred to the fluid from the plate and is given by

$$\Pi_s = \frac{1}{2}\mathrm{Re}\left\{\int_0^a \int_0^b \left[P_{s_1}(x,y) - P_{s_2}(x,y)\right]V^*(x,y)dxdy\right\} \qquad 142.$$

In terms of modal contributions Π_s can be written as

$$\Pi_s = \sum_{m=1}^{m=\infty} \frac{a}{4} \mathrm{Re}\left\{ \int_0^a \left[P_{s_{1_m}}(y) - P_{s_{2_m}}(y) \right] V_m{}^*(y) dy \right\} \qquad 143.$$

From Appendix A, the relationships between the full–range Fourier transform of the scattered pressure components and the plate surface velocity are given by,

$$\tilde{P}_{s_{1_m}}(\beta') = 2\pi j \mu \varrho_1 J_{1_m}(\beta') \tilde{W}_m(\beta') = \frac{2\pi\mu\varrho_1}{\omega} J_{1_m}(\beta') \tilde{V}_m(\beta') \qquad 144.$$

$$\tilde{P}_{s_{2_m}}(\beta') = -2\pi j \mu \varrho_2 J_{2_m}(\beta') \tilde{W}_m(\beta') = -\frac{2\pi\mu\varrho_2}{\omega} J_{2_m}(\beta') \tilde{V}_m(\beta') \qquad 145.$$

Fourier transforming equation (73),

$$\Pi_s = \sum_{m=1}^{m=\infty} \frac{\omega}{8\pi^2} \int_{-\infty}^{+\infty} \mathrm{Re}\left[\varrho_1 J_{1_m}(\beta) + \varrho_2 J_{2_m}(\beta) \right] |\tilde{V}_m(\beta)|^2 d\beta \qquad 146.$$

From Appendix A, the real parts of $J_{1_m}(\beta)$ and $J_{2_m}(\beta)$ are not equal to zero only for the wavenumber satisfying $|\beta| \leq k$. Therefore only the components of the plate displacement corresponding to these wavenumbers contribute to the radiated sound power. The range of integration in equation (76) can be reduced to $-k \leq \beta \leq k$.

$$\Pi_s = \sum_{m=1}^{m=\infty} \frac{\omega}{8\pi^2} \int_{-k}^{+k} \mathrm{Re}\left[\varrho_1 J_{1_m}(\beta) + \varrho_2 J_{2_m}(\beta) \right] |\tilde{V}_m(\beta)|^2 d\beta \qquad 147.$$

To be consistent with the fundamental law of the conservation of energy, this scattered power must always be less than the input power to the plate. According to equations (74) and (75), the terms that mainly represents the influence of the fluid loading on the plate displacement are the integrals $J_{1_m}(\beta)$ and $J_{2_m}(\beta)$. It is shown in Appendix B that at a particular frequency of vibration, the form and associated physical nature, of the fluid loading represented by $J_{1_m}(\beta)$ depends upon how the plate wavenumber β in the Y direction is placed with respect to the acoustic wavenumber k. For $|\beta| \geq k$, the integral $J_{1_m}(\beta)$ is purely imaginary and is given by equation (A.12). This imaginary part represents the effective mass loading on the plate by the reactive component of the fluid loading. For $|\beta| \leq k$, the component $J_{1_m}(\beta)$ has both real and imaginary parts. The real part contributes to the far field radiation and it represents the resistive component of the fluid loading. This real part is present at all frequencies for a finite plate.

From Appendix A, equation (A.15), for any given wavenumber β, ($|\beta| \leq k$), the maximum value of the real part of $J_{1_m}(\beta)$ is reached when the mode wavenumber k_m is less than the value of V, given by $V = \sqrt{k^2 - \beta^2}$. In this case, the range of integration in the integral giving this real part includes the maximum value of the integrand. Thus when the wavenumbers of the plate in both the X and Y directions are less than the acoustic wavenumber, that is above critical frequency, the acoustic radiation will reach a maximum.

Of interest here is the radiation from a plate where none of the resonant modes excited in the plate are radiating as efficient acoustic radiators. That is when the plate is excited below the critical frequency. For a 6 mm thick steel plate in air the critical frequency is around 2 kHz. Therefore in the results the frequency range is limited to 1 kHz.

13. MECHANICAL LOSSES

The mechanical losses component of the power flow includes both the power lost due to the internal structural damping and the power transmitted across the junction if the plate is a component of a global structure. An explicit expression for the mechanical losses is given by,

$$\Pi_M = \sum_{m=1}^{m=\infty} \frac{-jaB}{4\omega} \int_0^b \left[\frac{d^4 V_m(y)}{dy^4} dy - 2k_m{}^2 \frac{d^2 V_m(y)}{dy^2} dy + \left(k_m{}^4 - k_p{}^4 \right) V(y) \right] V_m{}^*(y) dy \qquad 148.$$

Integrating by parts

$$\Pi_M = \sum_{m=1}^{m=\infty} \frac{-jaB}{4\omega} \Big\{ \omega^2 \big[X_3 X_7{}^* - X_4 X_8{}^* - X_6 X_1{}^* + X_5 X_2{}^* - 2k_m^2 (X_1 X_7{}^* - X_2 X_8{}^*) \big] + \int_0^b \frac{d^2 V(y)}{dy^2} \left(\frac{d^2 V(y)}{dy^2} \right)^* dy + 2k_m{}^2 \int_0^b \frac{dV(y)}{dy} \left(\frac{dV(y)}{dy} \right)^* dy + \left(k_m{}^4 - K_p{}^4 \right) \int_0^b |V(y)|^2 dy \Big\} \qquad 149.$$

where X_i , i = 1 to 8 are defined by equations (29). In the above equation, the spatial integrals can be transformed into the wavenumber domain as follows,

$$\int_0^b |V(y)|^2 dy = \frac{1}{2\pi}\int_{-\infty}^{+\infty} |\tilde{V}(\beta)|^2 d\beta \qquad 150.$$

and the Fourier Transform of the derivative of the velocity is,

$$\tilde{V}'(\beta) = j\omega\left(X_1 e^{j\beta b} - X_2\right) - j\beta\tilde{V}(\beta) \qquad 151.$$

Thus

$$\int_0^b \frac{dV(y)}{dy}\left(\frac{dV(y)}{dy}\right)^* dy = \frac{1}{2\pi}\int_{-\infty}^{+\infty} \left|\omega\left(X_1 e^{j\beta b} - X_2\right) - \beta\tilde{V}(\beta)\right|^2 d\beta \qquad 152.$$

Similarly for the second derivative of the velocity,

$$\int_0^b \frac{d^2V(y)}{dy^2}\left(\frac{d^2V(y)}{d^2y}\right)^* dy =$$

$$\frac{1}{2\pi}\int_{-\infty}^{+\infty} \left|j\omega\left(X_3 e^{j\beta b} - X_4\right) + \omega\beta\left(X_1 e^{j\beta b} - X_2\right) - \beta^2\tilde{V}(\beta)\right|^2 d\beta \qquad 153.$$

The mechanically dissipated power is thus,

$$\Pi_M = \sum_{m=1}^{m=\infty} \frac{-jaB\omega}{4}\left[X_5 X_2^* - X_6 X_1^*\right] +$$

$$\frac{aB}{8j\pi\omega}\int_{-\infty}^{+\infty} \left[\left|j\omega\left(X_1 e^{j\beta b} - X_2\right) - \beta^2\tilde{V}(\beta)\right|^2 + \left(k_m{}^4 + 2k_m{}^2\beta^2 - k_p{}^4\right)\left|\tilde{V}(\beta)\right|^2\right] d\beta$$

154.

In equation (84), the terms with X_5 and X_6 represent the transmitted power if the plate is connected to another plate. The rest of the terms represents the dissipation due to the structural damping.

In the case of a plate simply supported on all four edges, equation (84) reduces to,

$$\Pi_M = \sum_{m=1}^{m=\infty} \frac{aB}{8j\pi\omega}\int_{-\infty}^{+\infty} \left[\left|j\omega\left(X_1 e^{j\beta b} - X_2\right) - \beta^2\tilde{V}(\beta)\right|^2 + \left(k_m{}^4 - k_p{}^4 + 2k_m{}^2\beta^2\right)\left|\tilde{V}(\beta)\right|^2\right] d\beta \qquad 155.$$

For a plate with an edge moment at y =0 and with simple supports on the remaining edges, where the edge moment is due to the influence of another structure attached to the y=0 edge of the plate, the mechanical dissipation is

$$\Pi_M = \sum_{m=1}^{m=\infty} \frac{aB\omega}{4j} X_5 \, X_2^* +$$

$$\frac{aB}{8j\pi\omega} \int_{-\infty}^{+\infty} \left[\left| j\omega\left(X_1 e^{j\beta b} - X_2\right) - \beta^2 \tilde{V}(\beta) \right|^2 + \left(k_m^{\,4} - k_p^{\,4} + 2k_m^{\,2}\beta^2 \right) \left| \tilde{V}(\beta) \right|^2 \right] d\beta \qquad 156.$$

In this case, the transferred power is given by

$$\Pi_T = \sum_{m=1}^{m=\infty} \frac{aB\omega}{4\,j} X_5 \, X^*_2 \qquad 157.$$

14. RESULTS

Results have been obtained for a steel plate of dimension 1.m by 0.5 m and thickness 6.35 mm. The Young's Modulus of steel is E= 200 GN/m^2 and the Poisson's ratio is 0.3. Two structural loss factors are considered in the analysis 10^{-2} and 10^{-5}. The plate is excited by an incident acoustic waves with pressure amplitude 10^{-4} Pa and with angles of incidence of $\theta = 45^o$ and $\phi = 45^o$. Results are generated with and without the influence of the fluid loading. In generating these results, both the Kernel approximation method and the projection method are used.

The results for the input and transferred power are normalized with respect to the incident power on the plate, which is defined by

$$\Pi = \frac{P_0^2 ab}{2\varrho_1 c_1} \qquad 158.$$

The ratio of the input power, which is the power transmitted to the plate, to the incident power on the plate is a measure of the transmission coefficient T of the plate ($T = \Pi_i/\Pi$) and the ratio of the scattered power to the incident power on the plate is the portion of the power scattered to the far field and is defined as the reflection coefficient R, ($R = \Pi_s/PI$).

The results for different mode numbers and different levels of the internal loss factor are shown in figures (2) to (19).

14.1. AIR-LOADING

Figures (2) to (9) show the results for the transmission and reflection coefficients for different modes and loss factors using the two alternate solution methods presented in sections (5) and (6). It can

be observed from these figures that in the case of light fluid loading (air), the Kernel approximation method and the projection method give similar results, especially for high loss factors. At high frequencies the two methods give exactly the same results. At low frequencies there are some differences, especially in the results for the lower loss factor and these are expected since in the Kernel approximation method a short wavelength assumption is used. At low frequencies the infinite plate approximation does not hold. The kernel approximation method has a tendency to overestimate the input power to the plate. However for the scattered power from the plate, the results given by the kernel approximation and the projection method and results obtained with the fluid loading term neglected in the solution for the response of the plate, are the same. The main reason for this is that the plate response is hardly influenced by the light fluid loading

From these results one can conclude that even light fluid–loading has some influence on the transmission coefficient of the plate, at low mode numbers. The fluid loading increases the input power to the plate since some power is radiated into the acoustic medium. The influence of the fluid loading is also dependent on the structural loss factor. From figures (6) and (7) it can be observed that away from resonance frequencies, the scattered power is independent of the structural damping. On the other hand, the input power appears to increase with increased structural damping.

To show the importance of acoustic scattering, figures (8) and (9) show both the transmission and the reflection coefficients on the same plot. The input power into the plate is always greater than the scattered power from the plate. This is consistent with the requirement for the conservation of energy. The input power to the plate is balanced by the scattered power and the structural dissipation which is always positive, equation (86). At almost negligible loss factor, the input and the scattered power are almost equal.

When the structural damping is very low, the resonance peaks are very sharp and no modal interactions occur as the energy of the system is contained in very narrow, separate bands of frequencies. Thus, the acoustic field at any frequency is generated solely by the mode that is resonant at or near that frequency. The radiation damping is mainly due to the acoustic field generated by that mode. The total power flow can thus be obtained from the modal power flow for the plate. When the structural damping is large, the width of the resonance peaks increase, and each mode is excited over a wider frequency band. In this case to obtain the total power flow, a summation over excited modes is necessary.

14.2. WATER–LOADING

In the case of heavy fluid loading (water), figures (10) to (14), show that the results obtained by the Kernel approximation method become inconsistent with those given by the projection method. The

kernel approximation method has a tendency to overestimate the input power into the plate and underestimate the scattered power from the plate.

Both methods predict a strong fluid loading effect on both the transmission and reflection coefficients. The fluid loading significantly modifies the plate mode shapes. There is a decrease in the resonance frequencies from the in–vacuo resonances frequencies. This is because of the added mass entrained by the fluid and which is significant in the case of water. As for the light fluid loading, the structural loss factor has a significant influence on the power flow for the plate, figures (12) shows the influence of the structural damping on the transmission and reflection coefficients. As in the case of light fluid loading (air), the scattered power from the plate is always less than the input power (figure 13), however in the case of the heavy fluid loading (water), the plate scatters a significant portion of the power input to the plate.

From all the results for the heavy fluid–loaded plate, it can be observed that each resonance frequency is preceded by a minimum. The response of the plate is composed of an almost uniform driven response as the plate were infinite and an oscillating term due to the edge effects. Below a resonance frequency, there is a phase shift of π between the driven response and the oscillating term and cancellation occurs, which is responsible for the minimum value right before the resonance condition. At and above a resonance frequency, the two terms are in phase and their effects adds.

At the resonance frequencies, both the transmission dn reflection ratios have a huge peak. Near the resonance frequencies, the plate absorbs more power than is directly incident upon it. The plate absorbs power from the acoustic waves incident on the adjacent baffle. This energy is then scattered by the plate. At the resonance frequencies, the induced velocity field on the plate vibration becomes large and increases the level of scattering. These results are similar to those found by Photiadis [5] for a semi–infinite plate. Photiadis suggests that the plate grabs energy incident on the adjacent baffle to within a distance of $\lambda_0/2$, where λ_0 is the acoustic wavelength. In the case considered here, λ_0 is larger than the plate dimensions at all the considered frequencies. Thus the energy absorbed by the plate from the adjacent field is significant.

14.3. COMBINATION WATER AND AIR LOADING

Figure (15) shows the transmission and reflection coefficients computed using the Projection Method when the fluid loading on the excited side of the plate is water and the other side the fluid loading is air. The results for the mixed fluid loading are compared to other fluid loading conditions in figures (16) and (17). The scattered power is highest when the plate is water loaded on one side and air loaded on the other side. This increase in the scattered power is attributed to the way the plate interacts with the fluid loading and the excitation.

15. CONCLUSION

A solution has been obtained for the dynamic response and acoustic scattering from a fluid–loaded rectangular plate with arbitrary boundary conditions on two of the parallel edges of the plate. The solution takes into account the finiteness of the problem, especially when dealing with the scattered pressure. The influence of the finiteness of the scattered pressure is negligible for light fluid loading, however for heavy fluid loading it has a significant influence on the scattered pressure. The solution that is presented here can be used to analyze the response of coupled plate systems taken into account both the mechanical coupling and the acoustic coupling through the common acoustic medium.

16. REFERENCES.

1. Feit D., Liu Y. N., "The Nearfield Response of a Line Driven Fluid–Loaded Plate", Journal of the Acoustical Society of America, 78(2), 763–766, 1985.

2. Nayak P. R., "Line Admittance of Infinite Isotropic Fluid–Loaded Plates", Journal of the Acoustical Society of America, 47, 191–201, 1970.

3. Fahy F. J., "Sound and Structural Vibrations, Interaction, Transmission and Response", Academic Press, 1988.

4. Golberg M. A., "Solution Methods for Integral Equations: Theory and Applications", Plenum Press 1979.

5. Photiadis D. M, "The Scattering of Sound from Fluid–Loaded Plates",Journal of the Acoustical Society of America, 85 (6), 2440–2451, 1989.

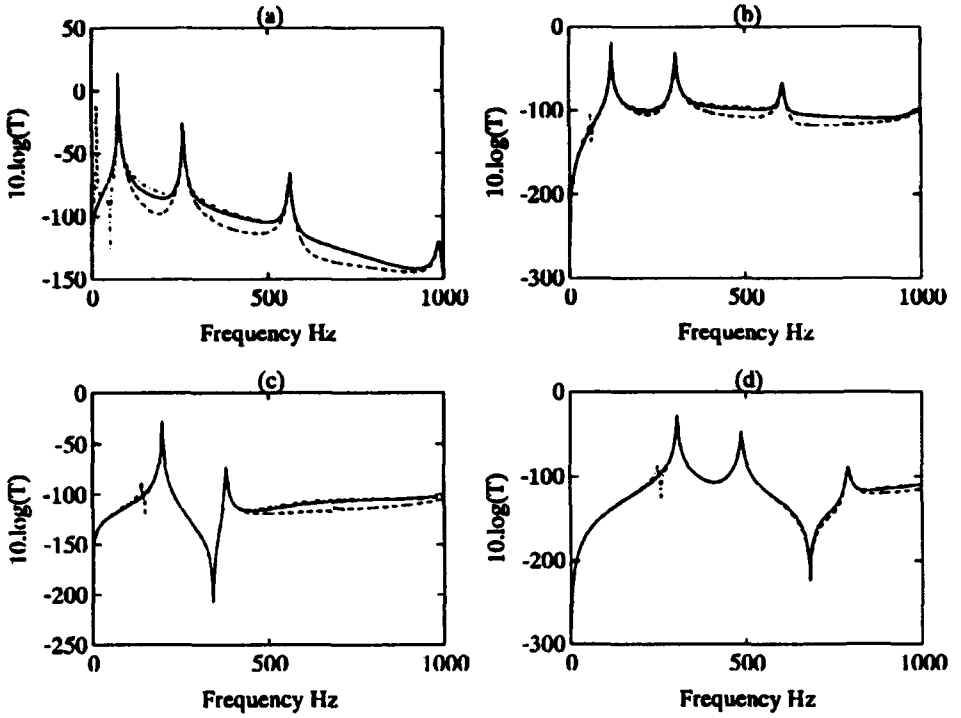

Figure 2. Transmission coefficient for a simply supported plate with air loading, loss factor 0.01, for different modes and different methods of solution. ———: Projection method; —— - -: Kernel approximation method; — — — —: No fluid loading. (a) mode 1; (b) mode 2; (c) mode 3; (d) mode 4.

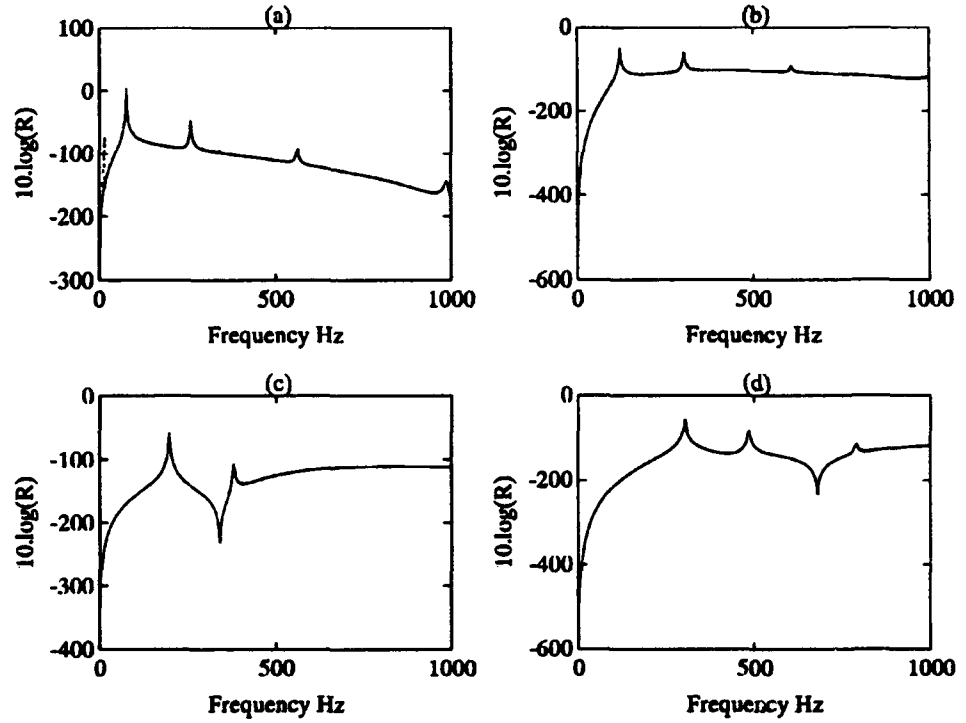

Figure 3. Reflection coefficient for a plate simply supported with air loading, loss factor 0.01, for different modes and different methods of solution. ———: Projection method; —— - -: Kernel approximation method; — — — —: No fluid loading. (a) mode 1; (b) mode 2; (c) mode 3; (d) mode 4.

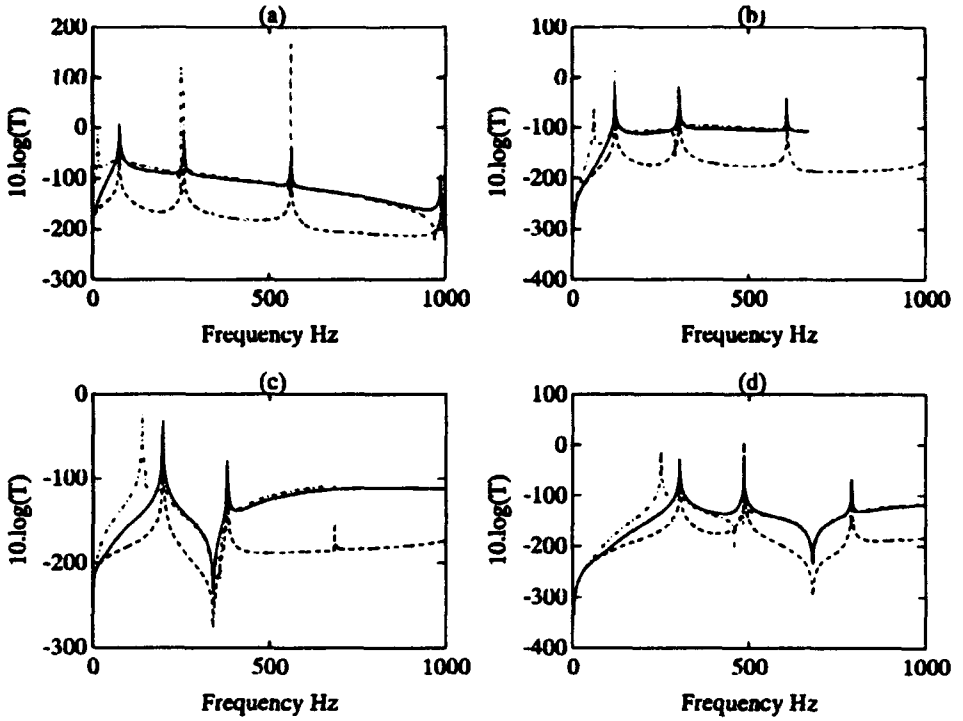

Figure 4. Transmission coefficient for a simply supported plate with air loading, loss factor 10^{-5}, for different modes and different methods of solution. ———: Projection method; — – –: Kernel approximation method; — — —: No fluid loading. (a) mode 1; (b) mode 2; (c) mode 3; (d) mode 4.

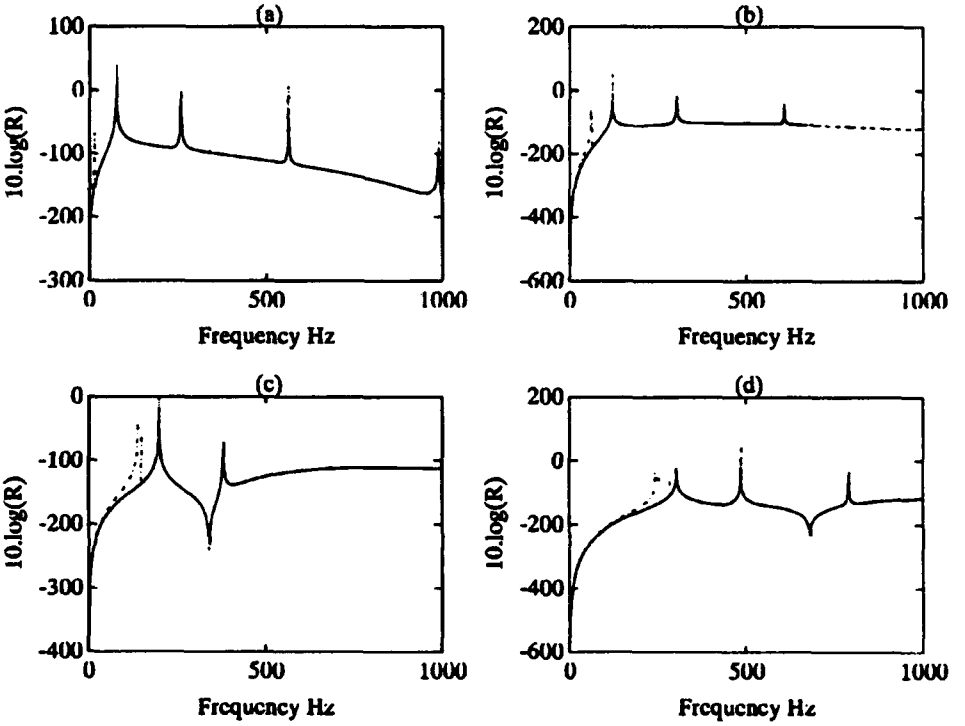

Figure 5. Reflection coefficient for a simply supported plate with air loading, loss factor 10^{-5}, for different modes and different methods of solution. ———: Projection method; — – –: Kernel approximation method; — — —: No fluid loading. (a) mode 1; (b) mode 2; (c) mode 3; (d) mode 4.

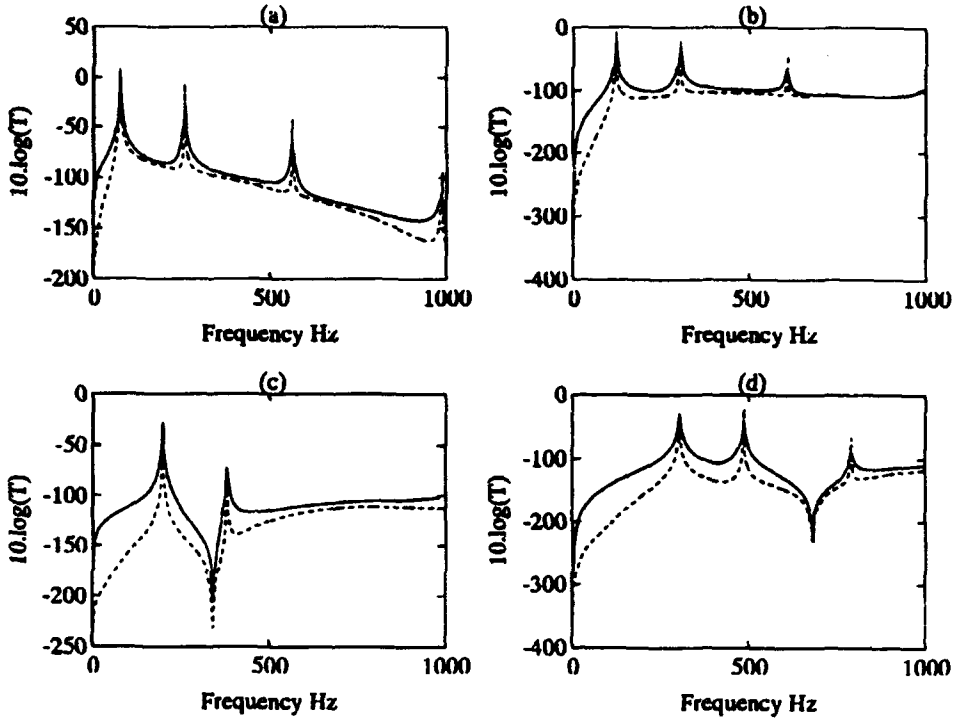

Figure 6. Transmission coefficient computed by the Projection method for a plate simply supported on all edges with air loading, for different modes and different structural loss factors. ———: Loss factor of 10^{-2}; – – – –: Loss factor of 10^{-5}. (a) mode 1; (b) mode 2; (c) mode 3; (d) mode 4.

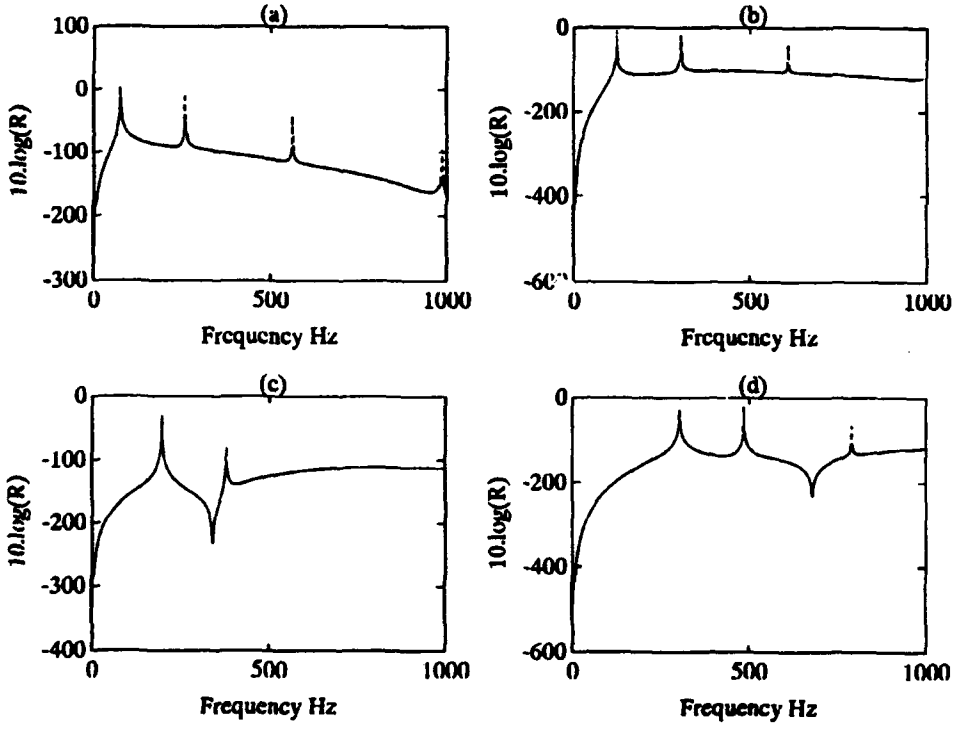

Figure 7. Reflection coefficient computed by the Projection method for a simply supported plate, for different modes and different structural loss factors. ———: Loss factor of 10^{-2}; – – – –: Loss factor of 10^{-5}. (a) mode 1; (b) mode 2; (c) mode 3; (d) mode 4.

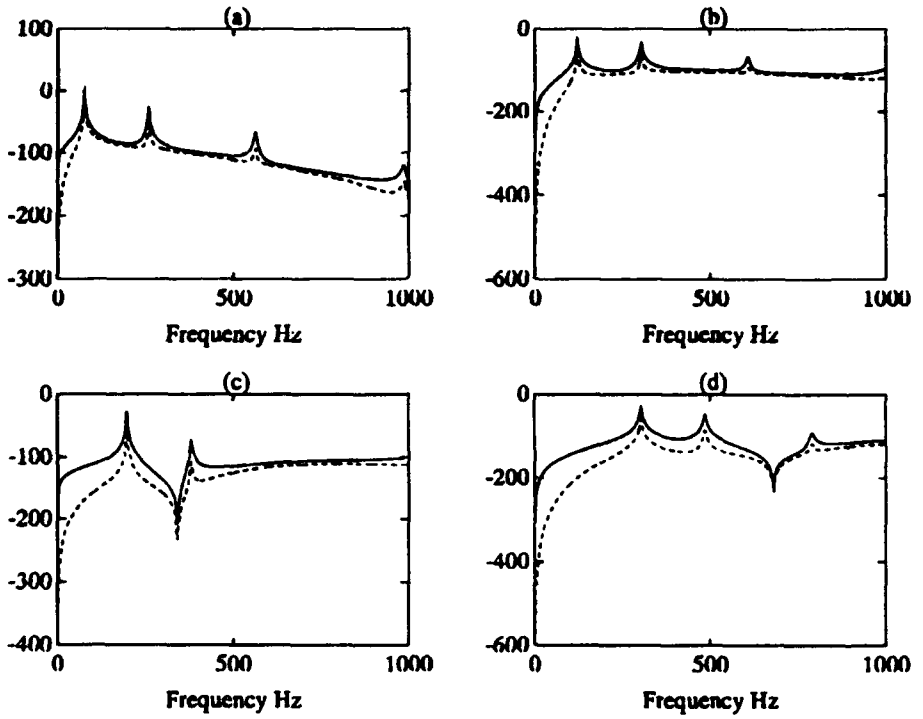

Figure 8. Transmission and Reflection coefficients computed by the Projection method for a simply supported plate with air loading, loss factor 0.01, for different modes. ———: Transmission coefficient; — — —: Reflection coefficient. (a) mode 1; (b) mode(2); (c) mode 3 and (d) mode 4.

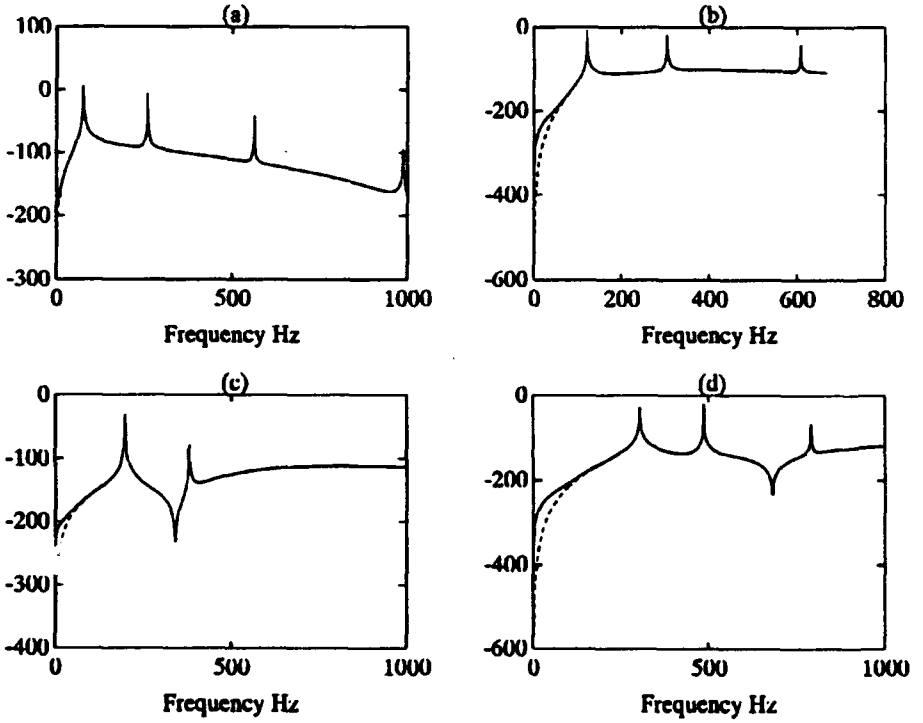

Figure 9. Transmission and Reflection coefficients computed by the Projection method for a plate simply supported with air loading, loss factor 10^{-5}, for different modes. ———: Transmission coefficient; — — —: Reflection coefficient. (a) mode 1; (b) mode(2); (c) mode 3 and (d) mode 4.

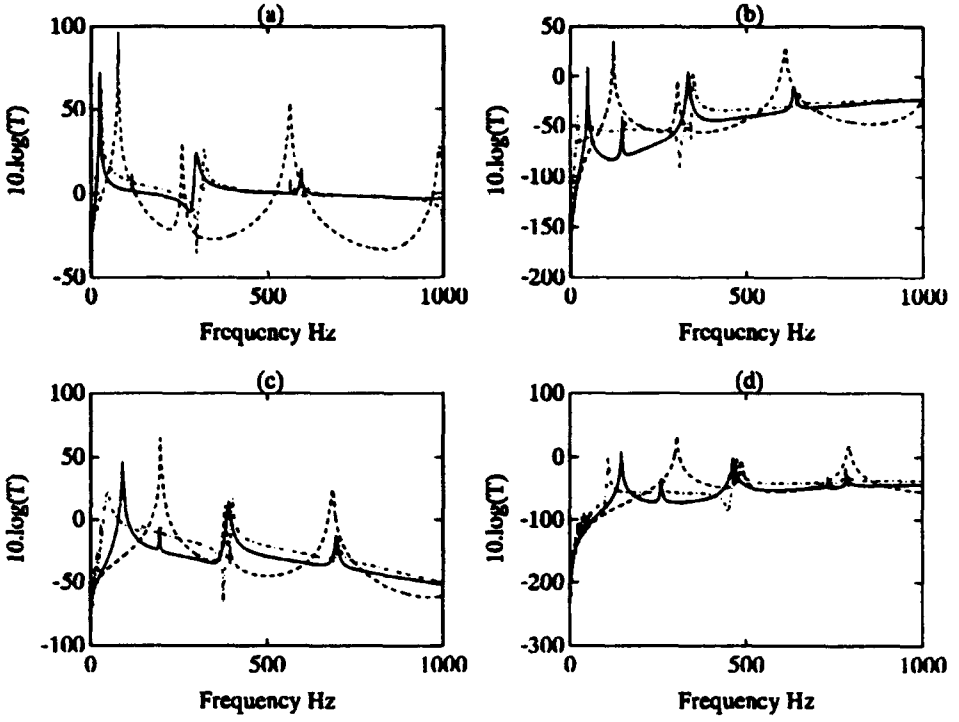

Figure 10. Transmission coefficient for a simply supported plate with water loading, loss factor 10^{-2}, for different modes and different methods of solution. ———: Projection method; — - -: Kernel approximation method; — — —: No fluid loading. (a) mode 1; (b) mode 2; (c) mode 3; (d) mode 4.

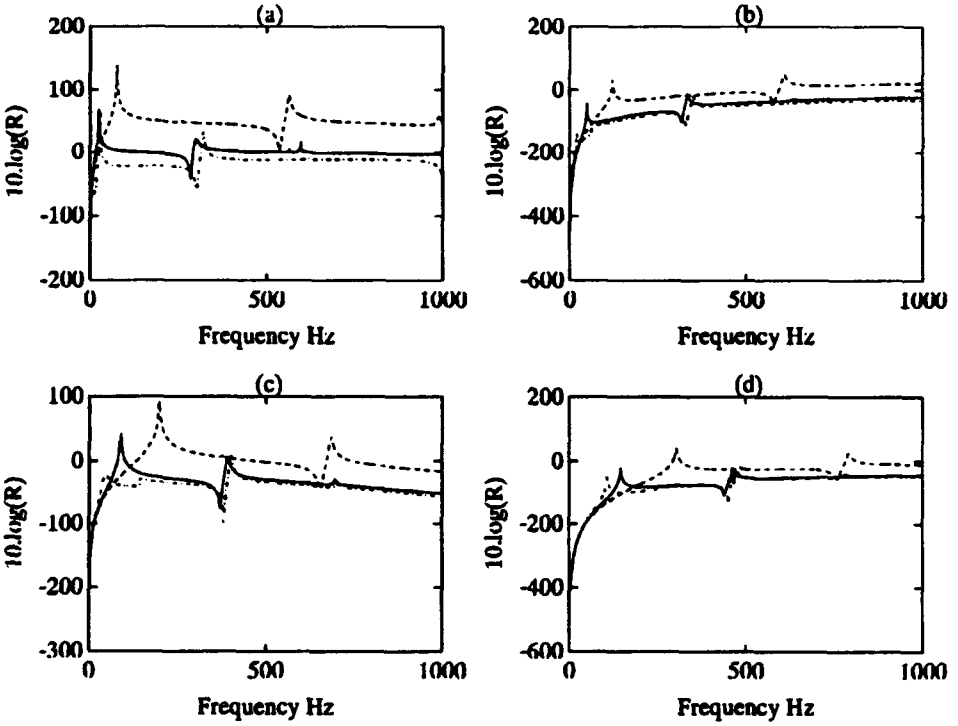

Figure 11. Reflection coefficient for a simply supported plate with water loading, loss factor 10^{-2}, for different modes and different methods of solution. ———: Projection method; — - -: Kernel approximation method; — — —: No fluid loading. (a) mode 1; (b) mode 2; (c) mode 3; (d) mode 4.

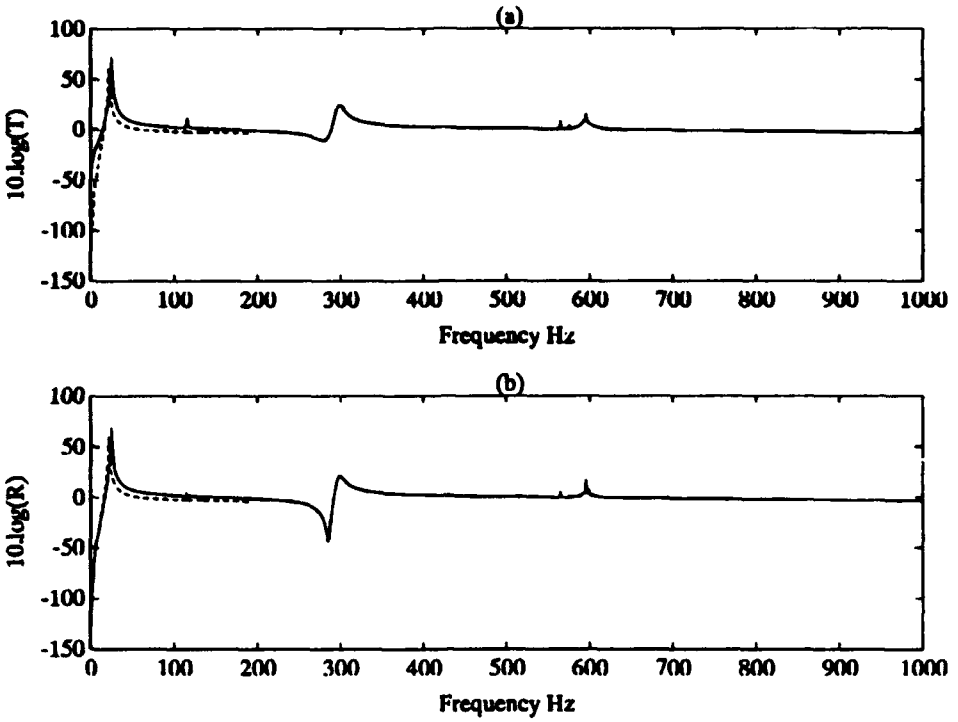

Figure 12. Transmission and reflection coefficients of mode 1 computed by the Projection method for a simply supported plate with water loading for different structural loss factors. ———: Loss factor of 10^{-2} ; – – – –: Loss factor of 10^{-5} . (a) Transmission coefficient; (b) Reflection coefficient.

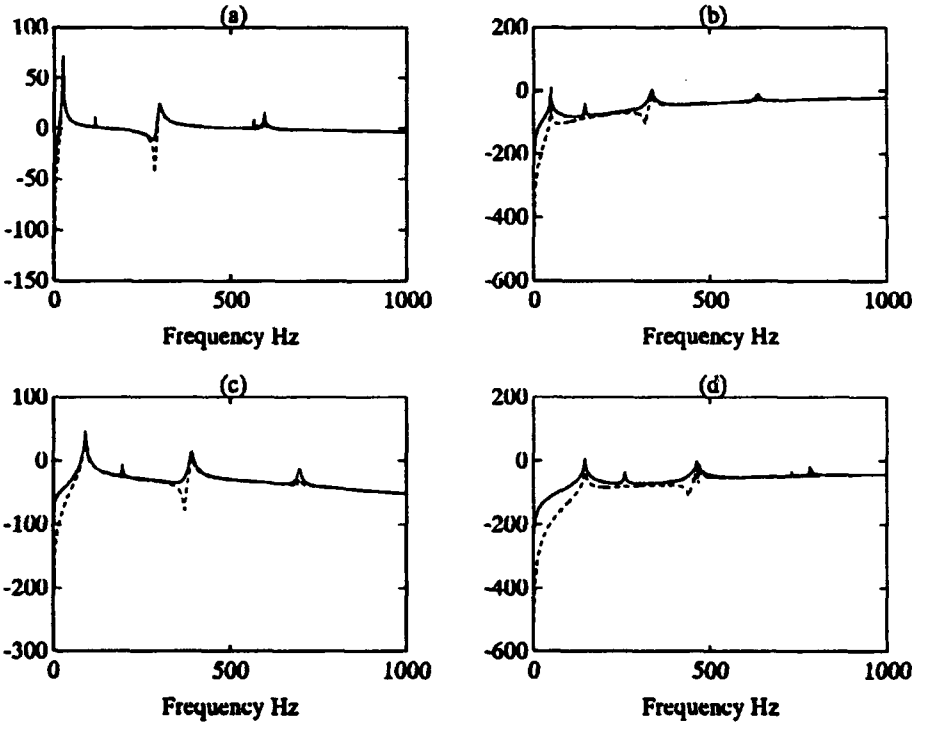

Figure 13. Transmission and Reflection coefficients computed by the Projection method for simply supported plate with water loading, loss factor 0.01, for different modes. ———: Transmission coefficient; – – – –: Reflection coefficient. (a) mode 1; (b) mode(2); (c) mode 3 and (d) mode 4.

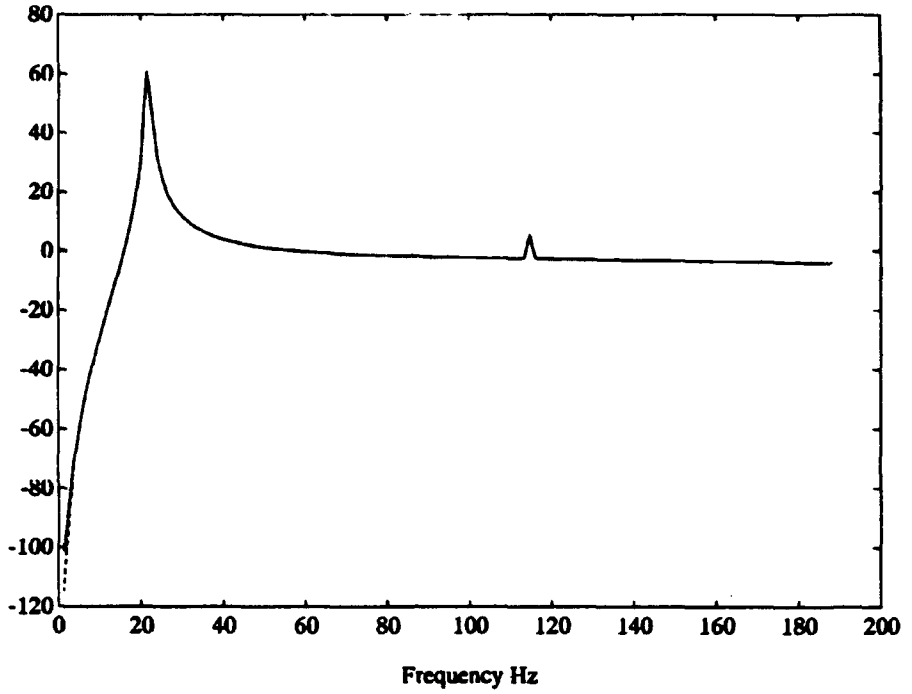

Figure 14. Transmission and Reflection coefficients of mode 1 computed by the Projection method for a simply supported plate with water loading, loss factor 10^{-5}. ———: Transmission coefficient; — — —: Reflection coefficient.

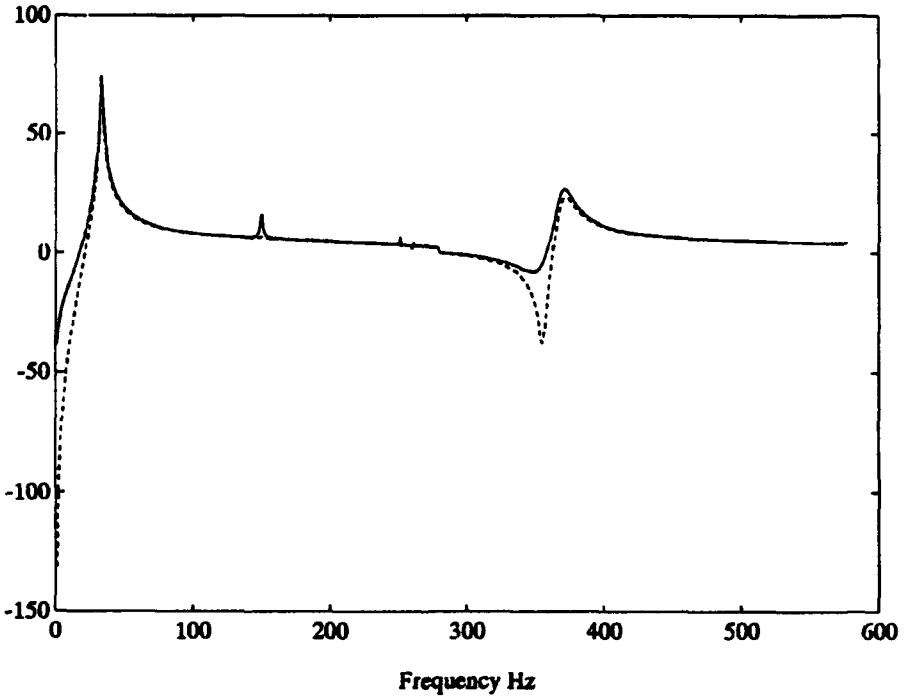

Figure 15. Transmission and Reflection coefficients for mode 1 for a simply supported plate with water/air loading, plate loss factor 10^{-2}. ——— :Transmission coefficient; — — —: Reflection coefficient.

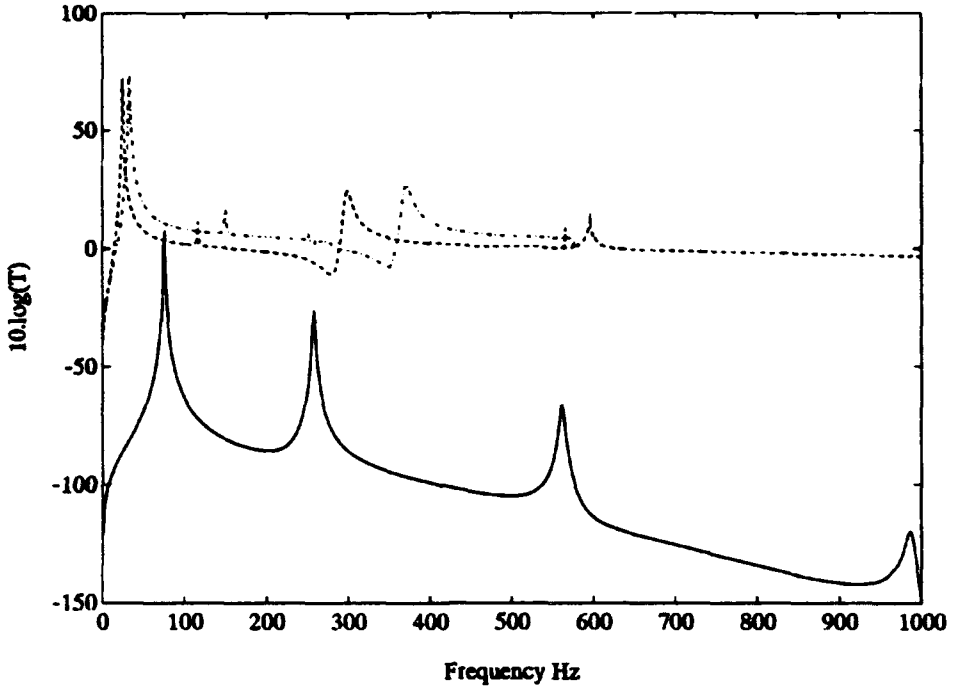

Figure 16. Transmission coefficient for mode 1 for a simply supported plate for different fluid loadings, loss factor 10^{-2}. ——— : Air loading; — — — -: Water loading; —— - -: Water/Air loading

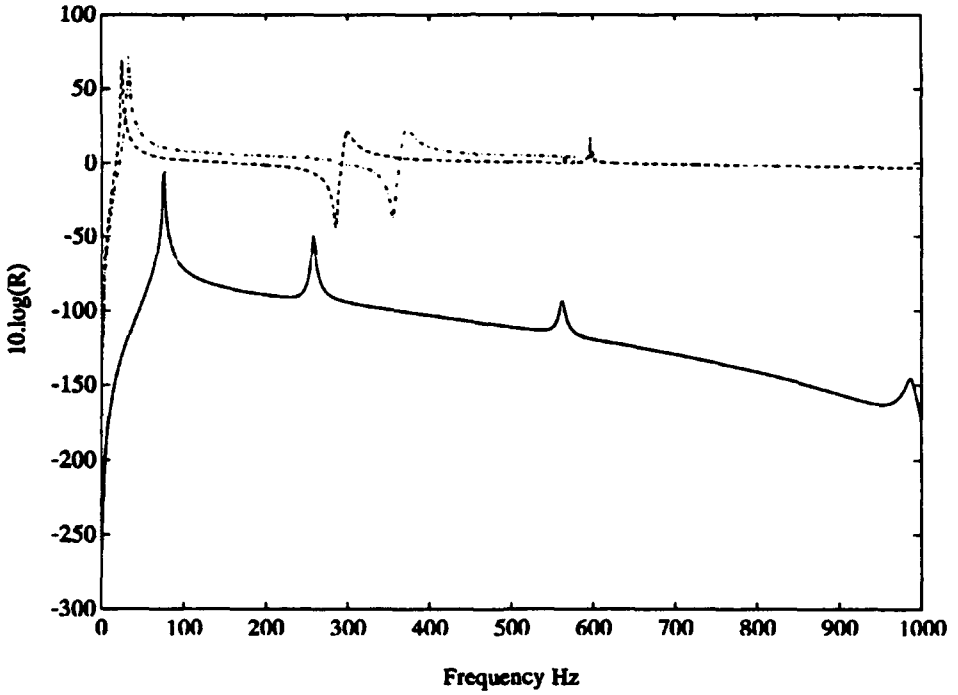

Figure 17. Reflection coefficient for mode 1 for a simply supported plate for different fluid loadings, loss factor 10^{-2}. ———: Air loading; — — — -: Water loading; —— - -: Water/Air loading

Appendix A

$$\tilde{P}_{s_{1_m}}(\beta) = \int_0^b P_{s_{1_m}}(y)e^{(j\beta y)}dy = \frac{2}{a}\int_0^a\left[\int_0^b P_{s_1}(x,y)e^{(j\beta y)}dy\right]\sin\left(\frac{m\pi x}{a}\right)dx \qquad \text{A.1.}$$

Using the inverse Fourier Transform

$$P_{s_1}(x,y) = \frac{1}{4\pi^2}\int_{-\infty}^{\infty}\int_{-\infty}^{\infty}\tilde{P}_{s_1}(\alpha',\beta')e^{-j\alpha' x - j\beta' y}d\alpha' d\beta' \qquad \text{A.2.}$$

$$\tilde{P}_{s_{1_m}}(\beta) = \frac{1}{2\pi^2 a}\int_{-\infty}^{\infty}\int_{-\infty}^{\infty}G(\beta-\beta')\tilde{P}_{s_1}(\alpha',\beta')S_m(-\alpha')d\alpha' d\beta' \qquad \text{A.3.}$$

where $G(\beta) = \int_o^b e^{j\beta y}dy = \frac{e^{j\beta b}-1}{j\beta}$ and $S_m(\alpha) = \int_o^a \sin\left(\frac{m\pi x}{a}\right)e^{j\alpha x}dx.$

$$W(x,y) = \sum_{n=1}^{n=\infty} W_n(y)\sin\left(\frac{n\pi x}{a}\right) \qquad \text{A.4.}$$

and

$$\tilde{W}(\alpha',\beta') = \sum_{n=1}^{n=\infty}\tilde{W}_n(\beta')S_n(\alpha') \qquad \text{A.5.}$$

Substituting into equation (24)

$$\tilde{P}_{s_1}(\alpha',\beta') = j\varrho_1\omega^2\sum_{n=1}^{n=\infty}\frac{\tilde{W}_n(\beta')S_n(\alpha')}{\gamma'} \qquad \text{A.6.}$$

and

$$\tilde{P}_{s_{1_m}}(\beta) = j\mu\varrho_1\sum_{n=1}^{n=\infty}\int_{-\infty}^{\infty}\tilde{W}_n(\beta')G(\beta-\beta')J_{1n,p}(\beta')d\beta' \qquad \text{A.7.}$$

where $\mu = \omega^2/(2\pi^2 a)$ and

$$J_{1m,n}(\beta') = \int_{-\infty}^{\infty} \frac{S_n(\alpha')S_m(-\alpha')}{\gamma'} d\alpha' \qquad \text{A.8.}$$

Similarly

$$\tilde{P}_{s_{2_m}}(\beta) = -j\mu\varrho_2 \sum_{n=1}^{n=\infty} \int_{-\infty}^{\infty} \tilde{W}_n(\beta')G(\beta - \beta')J_{2m,n}(\beta')d\beta' \qquad \text{A.9.}$$

The negative sign is introduced in equation (A.9) because the scattered pressure waves are propagating in the negative z direction.

In equations (A.7) and (A.9), the terms of the summation for which $p \neq m$ represent the intramodal interaction. This coupling has been shown to be negligible when the fluid loading is light and the modal density of the structure is low [4]. If the intramodal coupling is neglected,

$$J_{1_m}(\beta) = 2k_m^2 \int_{-\infty}^{+\infty} \frac{\left[1 - (-1)^m \cos(\alpha a)\right]}{(\alpha^2 - k_m^2)^2 \gamma} d\alpha \qquad \text{A.10.}$$

where $\gamma = \pm \sqrt{k^2 - \beta^2 - \alpha^2}$. The sign of the square root term is chosen according to the radiation condition, that is the scattered pressure is equal to zero at infinity.

If $k < \beta$, γ is imaginary, $\gamma = -j\sqrt{\beta^2 - k^2 + \alpha^2}$

If $k > \beta$, $\gamma = \begin{cases} \sqrt{k^2 - \beta^2 - \alpha^2} & \text{for } \alpha \leq k^2 - \beta^2 \\ -j\sqrt{\alpha^2 - k^2 + \beta^2} & \text{for } \alpha \geq k^2 - \beta^2. \end{cases}$

If $k = \beta$, γ is imaginary, $\gamma = -j\alpha$.

In equation (A.10), the integrand is an even function of α and therefore

$$J_{1_m}(\beta) = 4k_m^2 \int_{0}^{+\infty} \frac{\left[1 - (-1)^m \cos(\alpha a)\right]}{(\alpha^2 - k_m^2)^2 \gamma} d\alpha \qquad \text{A.11.}$$

Also $J_{1_m}(\beta)$ is an even function of β, and therefore the integral in equation (A.10) can be limited to $\beta \geq 0$. The solution for different ranges of k and β is as follows:

Case $k < \beta$:

$$J_{1_m}(\beta) = 4k_m^2 j \int_0^{+\infty} \frac{f(a)}{\sqrt{V^2 + a^2}} da \qquad \text{A.12.}$$

Case $\beta = k$:

$$J_{1_m}(k) = 4k_m^2 j \int_0^{+\infty} \frac{f(a)}{a} da \qquad \text{A.13.}$$

At zero, the integrand goes to infinity when m is odd and equals to zero when m is even. However the integrand is also an odd function for odd values of m and therefore the value of the integral always goes to zero for odd values of m.

Case $0 < \beta < k$:

$$J_{1_m}(\beta) = 4k_m^2 \left[\int_0^V \frac{\left[1 - (-1)^m \cos(aa)\right]}{(a^2 - k_m^2)^2 \sqrt{V^2 - a^2}} da + j \int_V^{+\infty} \frac{\left[1 - (-1)^m \cos(aa)\right]}{(a^2 - k_m^2)^2 \sqrt{a^2 - V^2}} da \right] \qquad \text{A.14.}$$

$$J_{1_m}(\beta) = 4k_m^2 \left[\int_0^{\frac{\pi}{2}} f(V \cos X) dX + j \int_0^{+\infty} f(V ch X) dX \right] \qquad \text{A.15.}$$

In equations (A.12), (A.13) and (A.14), $V = \sqrt{|k^2 - \beta^2|}$, and

$$f(a) = \frac{\left[1 - (-1)^m \cos(aa)\right]}{(a^2 - k_m^2)^2} \qquad \text{A.16.}$$

The function f is a smooth function and is not singular at k_m. For $a = k_m$) $f(k_m) = a^2/(8m^2\pi^2)$.

In equation (A.15), the substitutions, $x = a/V$, and $x = \cos(X)$ for the first integral and $x = ch(X)$ for the second integral have been used.

The integrands in these integrals are smooth functions and therefore can be directly evaluated numerically.

Appendix B

From equation (28), $A_1(\beta) = A_2(\beta)\ A_3(\beta)$ and $A_4(\beta) = 1$

$$\sum_{i=1}^{i=4} X_{iA}A_i(\beta) = A_2(\beta)\left[A_3(\beta)X_{1A} + X_{2A}\right] + A_3(\beta)X_{3A} + X_{4A} \qquad \text{B.1}$$

From equation (20):

$$A_3(\beta)X_{1A} + X_{2A} = -\frac{1}{\Delta}$$
$$\left\{\sin(K_2b)\left[\left(e^{-jK_1b} - e^{j\beta b}\right)K(\tilde{W}_m)(K_1) - \left(e^{jK_1b} - e^{j\beta b}\right)K(\tilde{W}_m)(-K_1)\right] -\right.$$
$$\left.\sin(K_1b)\left[\left(e^{-jK_2b} - e^{j\beta b}\right)K(\tilde{W}_m)(K_2) - \left(e^{jK_2b} - e^{j\beta b}\right)K(\tilde{W}_m)(-K_2)\right]\right\} \qquad \text{B.2}$$

$$A_3(\beta)X_{3A} + X_{4A} = -\frac{1}{\Delta}\left\{\sin(K_2b)\left(K_2^2 + 2k_m^2\right)\right.$$
$$\left[\left(e^{-jK_1b} - e^{j\beta b}\right)K(\tilde{W}_m)(K_1) - \left(e^{jK_1b} - e^{j\beta b}\right)K(\tilde{W}_m)(-K_1)\right] -$$
$$\sin(K_1b)\left(K_1^2 + 2k_m^2\right)\left[\left(e^{-jK_2b} - e^{j\beta b}\right)K(\tilde{W}_m)(K_2) -\right.$$
$$\left.\left.\left(e^{jK_2b} - e^{j\beta b}\right)K(\tilde{W}_m)(-K_2)\right]\right\} \qquad \text{B.3}$$

$$\sum_{i=1}^{i=4} X_{iA}A_i(\beta) = \frac{1}{\Delta}\left\{\sin(K_2b)\left(\beta^2 - K_2^2\right)\right.$$
$$\left[\left(e^{-jK_1b} - e^{j\beta b}\right)K(\tilde{W}_m)(K_1) - \left(e^{jK_1b} - e^{j\beta b}\right)K(\tilde{W}_m)(-K_1)\right] -$$
$$\left.\sin(K_1b)\left(\beta^2 - K_1^2\right)\left[\left(e^{-jK_2b} - e^{j\beta b}\right)K(\tilde{W}_m)(K_2) - \left(e^{jK_2b} - e^{j\beta b}\right)K(\tilde{W}_m)(-K_2)\right]\right\} \qquad \text{B.4}$$

Substituting for function K

$$\sum_{i=1}^{i=4} X_{iA}A_i(\beta) = -\int_{-\infty}^{+\infty}\left[\lambda_1 J_{1_m}(\beta') + \lambda_2 J_{2_m}(\beta')\right]\tilde{W}_m(\beta')K(\beta,\beta')d\beta' \qquad \text{B.5}$$

where

$$K(\beta,\beta') = \frac{1}{\Delta}\Big\{(\beta^2 - K_2^2)\sin(K_2 b)$$
$$\Big[G(K_1 - \beta')\Big(e^{-jK_1 b} - e^{j\beta b}\Big) - G(-K_1 - \beta')\Big(e^{jK_1 b} - e^{j\beta b}\Big)\Big]$$
$$(\beta^2 - K_1^2)\sin(K_1 b)\Big[G(K_2 - \beta')\Big(e^{-jK_2 b} - e^{j\beta b}\Big) - G(-K_2 - \beta')\Big(e^{jK_2 b} - e^{j\beta b}\Big)\Big]\Big\}$$

B.6

Appendix C

Functions ϕ_n are defined by $\phi_m(\beta) = d^n G(\beta)/d^n\beta$, where $G(\beta) = e^{j\beta b} - 1/(j\beta)$.

The recurrence relation for ϕ_n may be obtained by operating on the series, (3.27).

$$G(z + \beta) = \sum_{n=0}^{\infty} \frac{z^n}{n!}\phi_n(\beta) \qquad \text{C.1}$$

Using the definition for $G(\beta)$

$$e^{j(\beta+z)b} - 1 = j(\beta + z)\sum_{n=0}^{\infty} \frac{z^n}{n!}\phi_n(\beta) \qquad \text{C.2}$$

Differentiating this equation with respect to z and then with respect to β

$$jb^2 e^{j(\beta+z)b} = \sum_{n=0}^{\infty} \frac{z^n}{n!}\left[(n + 2)\phi_{n+1}(\beta) + \beta\phi_{n+2}(\beta)\right] \qquad \text{C.3}$$

where use was made of the relationship, $\phi_{m+1}(\beta) = d\phi_m(\beta)/(d\beta)$

Substituting for the exponential term

$$\phi_{n-1}(\beta) = \frac{1}{jbn}\left[(n + 1 - j\beta b)\phi_n + \beta\phi_{n+1}\right] \qquad \text{C.4}$$

Given ϕ_0 and ϕ_1 any other ϕ_n can be computed. For high value of n and small values of β, $\phi_n(\beta)$ is very small and numerical problems occur. A better way to compute these functions is to use Miller's algorithm applying the recurrence downward [4 page 142 and 28]. The method of computing $\phi_n(\beta)$ consists of starting from some arbitrary value $\phi_M(\beta) = \varepsilon$ with M >> n and ε a small number, and making use of the recurrence downward. All the $\phi_n(\beta)$ thus computed have a common normalizing factor given by

$$\phi_n(0) = \frac{b}{n + 1}(jb)^n \qquad \text{C.5}$$

$$b = \sum_{0}^{\infty} \frac{(-\beta)^n}{n!}\phi_n(\beta) \qquad \text{C.6}$$

Appendix D

In computing $< \phi_n, \phi_l >$,

$$< \phi_n, \phi_l > = \int_{-\infty}^{+\infty} \phi_n(\beta)\phi_l{}^*(\beta)d\beta \qquad \text{D.1}$$

where $\phi_n(\beta) = d^nG(\beta)/d\beta^n$. The function G can be expressed as an integral

$$G(\beta) = \int_0^b e^{j\beta y}dy \qquad \text{D.2}$$

and therefore

$$\phi_n(\beta) = \int_0^b (jy)^n e^{j\beta y}dy \qquad \text{D.3}$$

$$< \phi_n, \phi_l > = \int_0^b \int_0^b (jy_1)^n (jy_2)^l \left[\int_{-\infty}^{+\infty} e^{j\beta(y_1 - y_2)}d\beta \right] dy_1 dy_2 = 2\pi b(-1)^l \frac{(jb)^{n+l}}{l+n+1} \qquad \text{D.4}$$

since

$$\int_{-\infty}^{+\infty} e^{j\beta(y_1 - y_2)}d\beta = 2\pi\delta(y_1 - y_2) \qquad \text{D.5}$$

In computing $< \psi_n, \phi_l >$

$$< \psi_n, \phi_l > = \int_{-\infty}^{+\infty} \psi_n(\beta)\phi_l{}^*(\beta)d\beta \qquad \text{D.6}$$

and substituting for $\psi_n(\beta)$ from equation (61) and interchanging the order of integration,

$$< \psi_n, \phi_l > = \int_{-\infty}^{+\infty} \left[\lambda_1 J_{1_-}(\beta') + \lambda_2 J_{2_-}(\beta')\right] \phi_n(\beta') \theta_l(\beta') d\beta' \qquad \text{D.7}$$

$$\theta_l(\beta') = \int_{-\infty}^{+\infty} \frac{1}{A(\beta)} [G(\beta - \beta') + K(\beta, \beta')] \phi^*_l(\beta) d\beta \qquad \text{D.8}$$

A contour integral can be used to evaluate equation (D.8). Substituting for $\phi_l^*(\beta)$ from equation (D.3) and substituting for $G(\beta - \beta')$ from equation (D.2).

$$\theta_l(\beta') = (-j)^l \int_0^b y^l \left[\int_{-\infty}^{+\infty} \frac{1}{A(\beta)} G(\beta - \beta') e^{-j\beta y} d\beta + \int_{-\infty}^{+\infty} \frac{1}{A(\beta)} K(\beta, \beta') e^{-j\beta y} d\beta \right] dy \qquad \text{D.9}$$

$$\int_{-\infty}^{+\infty} \frac{1}{A(\beta)} G(\beta - \beta') e^{-j\beta y} d\beta = \int_0^y \left[\int_{-\infty}^{+\infty} \frac{e^{j\beta(y_1 - y)}}{A(\beta)} d\beta \right] dy_1 + \int_y^b \left[\int_{-\infty}^{+\infty} \frac{e^{j\beta(y_1 - y)}}{A(\beta)} d\beta \right] dy_1 \qquad \text{D.10}$$

$$\int_0^y \left[\int_{-\infty}^{+\infty} \frac{e^{j\beta(y_1 - y)}}{A(\beta)} d\beta \right] dy_1 = 2\pi \left[\frac{e^{jK_1 y} - e^{-j\beta' y}}{(K_1 + \beta') A'(K_1)} + \frac{e^{jK_2 y} - e^{-j\beta' y}}{(K_2 + \beta') A'(K_2)} \right] \qquad \text{D.11}$$

$$\int_y^b \left[\int_{-\infty}^{+\infty} \frac{e^{j\beta(y_1 - y)}}{A(\beta)} d\beta \right] dy_1 = 2\pi \left[\frac{e^{j(K_1 - \beta')b} e^{-jK_1 y} - e^{-j\beta' y}}{(K_1 - \beta') A'(K_1)} + \frac{e^{j(K_2 - \beta')b} e^{-jK_2 y} - e^{-j\beta' y}}{(K_2 - \beta') A'(K_2)} \right] \qquad \text{D.12}$$

And

$$(-j)^l \int_0^b y^l \left[\int_{-\infty}^{+\infty} \frac{1}{A(\beta)} K(\beta, \beta') e^{-j\beta y} \right] dy = (-1)^l 2\pi \frac{j}{\Delta} \left[\frac{e^{jbK_1} \phi_l(-K_1)}{A'(K_1)} H_1(\beta') + \frac{e^{jbK_2} \phi_l(-K_2)}{A'(K_2)} H_2(\beta') + \frac{\phi_l(K_1)}{A'(K_1)} H_3(\beta') + \frac{\phi_l(K_2)}{A'(K_2)} H_4(\beta') \right] \qquad \text{D.13}$$

where

$$
\begin{aligned}
H_1(\beta') &= -2k_p^2 \sin(K_2 b)\left[G(-K_1-\beta') - G(K_1-\beta')\right] \\
H_2(\beta') &= -2k_p^2 \sin(K_1 b)\left[G(-K_2-\beta') - G(K_2-\beta')\right] \\
H_3(\beta') &= -2k_p^2 \sin(K_2 b)\left[e^{-jK_1 b}G(K_1-\beta') - e^{jK_1 b}G(-K_1-\beta')\right] \\
H_4(\beta') &= -2k_p^2 \sin(K_1 b)\left[e^{-jK_2 b}G(K_2-\beta') - e^{jK_2 b}G(-K_2-\beta')\right]
\end{aligned}
\qquad \text{D.14}
$$

$\phi_l(\overline{K})$, for $\overline{K} = \pm K_1$, and $\pm K_2$, can be evaluated using equation (D.3).

In computing $< \tilde{W}_{0_m}, \phi_l >$

$$
< \tilde{W}_{0_m}, \phi_l > = \int_{-\infty}^{+\infty} \tilde{W}_{0_m}(\beta)\phi^*_l(\beta)d\beta \qquad \text{D.15}
$$

Using equation (D.3)

$$
< \tilde{W}_{0_m}, \phi_l > = \int_0^b (-jy)^l \left[\int_{-\infty}^{+\infty} \tilde{W}_{0_m}(\beta)e^{-j\beta y}d\beta \right] dy \qquad \text{D.16}
$$

Inverse Fourier transforming the integral between the brackets

$$
< \tilde{W}_{0_m}, \phi_l > = 2\pi \int_0^b (-jy)^l w_{m_0}(y)dy \qquad \text{D.17}
$$

STRUCTURAL INTENSITY MEASUREMENTS

There are a variety of wave modes which can propagate in a vibrating structure. Some waves can propagate almost unaffected past energy dissipation or isolation mechanisms meant for other wave modes. This has the effect of 'short circuiting' the reduction mechanism(s) for vibrational energy propagation. One example is the case of in–plane and out–of–plane waves propagating in a structure. The in–plane waves propagate past the isolators and damping layers used to reduce the propagation of bending waves. Furthermore, some wave types are more efficient acoustic radiators than others, and can be the dominant sources of radiation from a vibrating structure. For example, subsonically propagating out–of–plane waves radiate inefficiently in water, in contrast with the supersonic in–plane waves which are efficient radiators.

The scattering of propagating waves by discontinuities in their paths can alter their relative energy content. For instance, the energy of incident bending waves can be redistributed into in–plane longitudinal and/or in–plane shear waves when the waves encounter discontinuities. The scattering process(es) can thus lead to an increase in the acoustic radiation from a structure. That is, the radiated noise is a function of the(se) scattering process(es). Thus, the relationship between the nature of the discontinuities and the various wave scattering mechanisms needs to be better understood. This would enable the governing parameters of the power exchange between various wave modes to be quantitatively identified.

A useful tool to describe the dynamic behavior of structures, is the concept of *structural intensity*. In general, the instantaneous structural intensity (or Poynting) vector at a point with position vector $\bar{r}$, in an isotropic, lossless, elastic medium, is defined [1] as,

$$\bar{I}(\bar{r},t) = -\frac{\partial \bar{s}(\bar{r},t)}{\partial t}.\sigma(\bar{r},t) \qquad 17.$$

where $\bar{s}(\bar{r},t)$ is the displacement vector and $\sigma\ (\bar{r},t)$ is the stress tensor

The magnitude of the structural intensity vector is thus the power associated with the waves propagating in the elastic medium, and the direction of the vector is the direction of propagation of this power. For the more realistic case of losses existing in the elastic medium, there will be a phase lag 'ϕ' between the stress and displacement. Thus, material damping is accounted for by incorporating this phase lag in the time dependent parts of the expression for the structural intensity.

It is of interest to consider two simplifications of this definition [2]. Firstly, the instantaneous intensity can be *time–integrated* (for transient waves) or *time–averaged* (for steady–state waves). This yields a frequency–domain (using Parseval's theorem) description of the net energy flow or time–averaged power flow respectively, $\bar{I}\ (\bar{r}, \omega)$, which are useful for source/sink localization. The second simplification involves specialization to two–dimensional structures such as plates and

shells. In this case, it is usual to assume that the displacement vector $\bar{s}(\bar{r}, t)$ can be expanded in a series in the thickness direction, about the middle surface of the cross–section. Substitution in the expression for the intensity vector, and integration over the thickness of the structure, leads to the simplification of the intensity as an *intensity resultant per unit length.*

It can also be shown that upon rearrangement of the expressions, one obtains the intensity resultant vector as a product of the stress resultant tensor and the corresponding velocity vector. It is thus possible to decompose the total structural intensity resultant vector $\bar{P}$, into the (scalar) power flow contributions associated with each wave–type and/or direction. For two–dimensional structures, these contributions would come from the in–plane shear, in–plane longitudinal and out–of–plane waves. Each of these wave–types has different dispersion characteristics with corresponding propagation wavenumbers, for the in–plane shear waves, $k_S = 2\pi f/\left(\sqrt{G/\varrho}\right)$, for the in–plane longitudinal waves, $k_L = 2\pi f/\left(\sqrt{E/\varrho}\right)$ and for the out–of–plane (transverse) waves $k_T \approx \sqrt{2\pi f}\left(Eh^2/(\varrho)\right)^{-1/4}$.

The component wavenumbers each have a specific dependence on frequency and the medium's inertial & elastic properties. Thus, a wavenumber decomposition of the structural intensity would enable identification of the contributions from the various propagating waves. This decomposition can lead to a better understanding of the mechanisms of scattering by discontinuities, modal energy conversion & distribution and modal coupling. This understanding is of importance in the investigation of the dynamic response of, and acoustic radiation from, fluid–loaded structures consisting of coupled complex substructures.

This paper deals with the theoretical analysis of structural intensity measurement schemes for thick plate structures. Firstly, the frequency–wavenumber domain structural intensity is defined. Then, the various intensity components for the case of thick structures are described. Next, a scheme is described for measuring the frequency–wavenumber domain structural intensity, which uses finite difference approximations for the various spatial derivatives required. The proposed scheme's performance is considered for the practical case of relatively small data sets, and for various levels of Signal–to–Noise Ratio (SNR). To study the limits of applicability of the structural intensity measurement scheme, it's performance is characterized. Finally, the results of experiments using the proposed measurement scheme are also presented in order to illustrate the various issues involved.

Frequency – Wavenumber Analysis

From the definition of structural intensity in equation (1), the intensity resultant over a surface of area S is defined at an instant of time t as,

$$\overline{P}(\overline{r},t) = \frac{1}{S}\int_S \overline{F}(\overline{r},t).\overline{v}(\overline{r},t).\hat{n}_r.dS \qquad 18.$$

where $\overline{r}$ is the position vector, and $\hat{n}_r$ is the unit normal to S and $\overline{r}$, and $\overline{F}(\overline{r},t)$ and $\overline{v}(\overline{r},t)$ are the generalized force and velocity vectors.

The time–averaged (time–integrated) structural intensity for the case of real, steady–state (transient) time–series, is given from an application of the power theorem [1] by,

$$\tilde{\overline{P}}(\overline{r},\omega) = Real\ [\tilde{\overline{F}}(\overline{r},\omega).\tilde{\overline{v}}^{*}(\overline{r},\omega)] \qquad 19.$$

where $\tilde{\overline{F}}(\overline{r},\omega)$ and $\tilde{\overline{v}}(\overline{r},\omega)$ are respectively the force and velocity vectors in the transformed frequency – space domain and * represents a complex conjugate.

For the analogous case of spatial transformation to the wavenumber domain, it is useful to consider a general vector spatial field, where the position of a point is defined by a vector $\overline{r}$. The field consists of a generalized force $\overline{F}$ and a generalized velocity $\overline{v}$ which vary with both space and time. The cross–correlation R_{Fv} of the force and the velocity is defined using the expectation operator $E\{\ \}$ as,

$$R_{\overline{F}\overline{v}}\ (\overline{r},\overline{\xi},t,\tau) = E\ \{\ \overline{F}(\overline{r},t).\overline{v}(\overline{r}+\overline{\xi},\ t+\tau)\ \} \qquad 20.$$

The force–velocity cross–spectrum $S_{F\,v}$, given by the Fourier transformation of the cross–correlation over time t and space $\overline{r}$, gives the frequency–wavenumber domain structural intensity. For a stationary field, the cross–correlation $R_{F\,v}$ (and every higher statistical moment in time) is independent of the absolute observation time t , and depends only on the observation time difference τ. Similarly, for a homogeneous field, the cross–correlation (and every higher statistical moment in space) is independent of the absolute spatial position $\overline{r}$, and depends only on the spatial separation vector $\overline{\xi}$. As steady–state phenomena are of greater interest in the present study, temporal stationarity is assumed. The structural discontinuities are of interest however, and consequently, spatial homogeneity is *not* assumed. For the homogeneous case, the cross spectrum has a dependency only on the wavenumber $\overline{k}$ and the frequency ω, thus yielding $S_{F\,v}(\overline{k},\ \omega)$. However, for the inhomogeneous case, there is an additional dependency on the absolute spatial position $\overline{r}$, apart from the wavenumber $\overline{k}$ and the frequency ω, which yields $S_{F\,v}(\overline{k},\ \omega,\ \overline{r})$. This additional dependency on the absolute position is resolved by *spatial averaging* the cross–spectrum over sections of the domain of interest for which the spatial field can be considered homogeneous. This gives the frequency–wavenumber domain cross–spectrum. Thus, taking a spatial average (integral)

over the domain of the structure, the structural intensity in the frequency–wavenumber domain is, again from the power theorem [1] given by,

$$\tilde{\bar{P}}(\bar{k},\omega) = Real\left[\tilde{\bar{F}}(\bar{k},\omega).\tilde{\bar{v}}^{*}(\bar{k},\omega)\right] \qquad 21.$$

If a section in the spatial domain cannot be identified for which the response field can be considered homogeneous, then the frequency–wavenumber spectrum of the structural intensity would be given by the convolution integral,

$$\tilde{\bar{P}}(\bar{k},\omega) = Real\int_{-\infty}^{\infty}\left[\tilde{\bar{F}}(\bar{k}',\omega).\tilde{\bar{v}}^{*}(\bar{k}-\bar{k}',\omega)\right]d\bar{k}' \qquad 22.$$

Structural Intensity Components and Their Estimation.

The intensity components to be considered in a structure of interest depend upon the approximation to exact elasticity theory used to describe the structure. In thick plate structures where the out–of–plane motion is significantly affected by the transverse shear and rotary inertia, the Timoshenko–Mindlin theory [2] is appropriate. Based on this theory, there are waves associated with the shear, bending, and twisting moments for the flexural motion. The corresponding structural intensity components associated with the out–of–plane waves in the x–direction are listed below.

The out–of–plane shear force component is

$$I_{qx} = \frac{1}{2}\ Real\left[G'h\left(\frac{\partial w}{\partial x} + \psi_x\right) j\omega w^{*}\right] \qquad 23.$$

The out–of–plane bending moment component is

$$I_{mx} = \frac{1}{2}\ Real\left[D\left(\frac{\partial \psi_x}{\partial x} + \nu\frac{\partial \psi_y}{\partial y}\right) j\omega\psi_x{}^{*}\right] \qquad 24.$$

The out–of–plane twisting moment component is

$$I_{tx} = \frac{1}{2}\ Real\left[(1-\nu)D\left(\frac{\partial \psi_x}{\partial y} + \frac{\partial \psi_y}{\partial x}\right) j\omega\psi_y{}^{*}\right] \qquad 25.$$

where ν, D, G', E and h are respectively the poisson's ratio, the flexural rigidity, the corrected shear modulus, the modulus of elasticity and the thickness. u, v, and w are the x, y, z direction displacements and $\psi_x = \partial w/\partial x$ and $\psi_y = \partial w/\partial y$.

The expressions for the y–direction components are similar but with x and y interchanged. In structures where the coupling between the in–plane extensional and shearing modes significantly affects the in–plane motion, an approach along the lines of Kane & Mindlin [3], Mindlin and Medick [4] and Dubbelday [5] needs to be considered. The present analysis will consider the approach of Kane & Mindlin for the in–plane motion, in conjunction with the Mindlin thick–plate formulation for out–of–plane motion. The corresponding x–direction components of structural intensity, associated with the in–plane waves are listed below

The in–plane longitudinal force component is

$$I_{nx} = \frac{1}{2}\ Real\left[\frac{Eh}{(1-\nu^2)}\left(\frac{\partial u}{\partial x} + \nu\frac{\partial v}{\partial y}\right) j\omega u^*\right] \qquad 26.$$

The in–plane shear force component is

$$I_{sx} = \frac{1}{2}\ Real\left[\frac{Eh}{2(1+\nu)}\left(\frac{\partial u}{\partial y} + \frac{\partial v}{\partial x}\right) j\omega v^*\right] \qquad 27.$$

The expressions for the y–direction components are similar.

The hybrid approach used above has the implication that there is no direct coupling between the in–plane and the transverse motion. However, there is an indirect relationship between the flexural and extensional displacements [6] that comes from the generalized plane stress assumption for the in–plane motion. For plates lying in the x, y plane, this implies that

$$\varepsilon_z = -\frac{\nu}{1-\nu}(\varepsilon_x + \varepsilon_y) \qquad 28.$$

Substituting the plate displacements for the strains in equation (12), the out–of–plane motion contribution from in–plane waves in each orthogonal direction is

$$w_{in-plane,\,i} = -\frac{\nu h}{2(1-\nu)}(k_i u_i) \qquad 29.$$

where i =x or y. Thus, equations (7) to (11) can all be obtained in terms of the out–of–plane displacement 'w'.

3. Estimation of the Spatial Derivatives

One method of obtaining the spatial derivative (and consequently intensity) in the wavenumber domain follows from Fourier transform properties [1]. Thus, the first order derivative(s) would be given by

$$\nabla w(\bar{r},\omega) = \mathcal{F}^{-1}[(j\bar{k}).w(\bar{k},\omega)] \qquad 30.$$

where $w(\bar{k},\omega)$ is the spatial Fourier transform ($\mathcal{F}$) of $w(\bar{r},\omega)$

The higher order derivatives are obtained by further application of eq.(12). In the presence of noise, these estimates have been shown by Pate et al [7] to degrade progressively as the order of the derivative(s) increases, due to the uncertainty in wavenumber components k_x and k_y. Instead of this, finite difference approximations for the derivatives can be used, as suggested by Paviç [8]. Thus, we have for the the first order spatial derivative(s) of the displacement in the 'i' direction using transducers spaced a distance 'Δ_i' apart,

$$\frac{\partial w(\bar{r},\omega)}{\partial r_i} \approx \frac{w(\bar{r} + \Delta_i, \omega) - w(\bar{r} - \Delta_i, \omega)}{2\Delta_i} \qquad 31.$$

The higher order derivatives required to compute the various generalized forces and velocities can thus be similarly approximated using finite differences, in terms of the signals from an array of transverse displacement transducers. The highest order of spatial derivatives in equations (7) to (11) for thick plates is 2. Consequently, the number of measurements required in the array are 9, to enable approximation of all the partial and mixed spatial derivatives. Thus the array geometry shown in figure (1), can be used to estimate all of the spatial derivatives up to order two, thus enabling measurement of in–plane wave intensity as well as the thick–plate out–of–plane wave intensity.

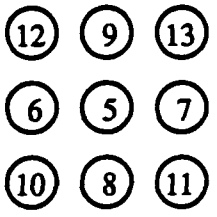

Figure 1. Array geometry with 9 channels for measuring structural intensity using a finite difference approximation for the derivatives.

From equations (7) to (11), the structural intensity components can be obtained by either evaluating convolution integrals of the form of equation (6). The elements in the convolution integral are obtained directly from the spatial transforms of the response and its derivatives. Alternatively, if the response field over a section of the structure can be considered homogeneous, as would be the case under resonant behavior, then using equation (5) and substituting the finite difference estimates for the required partial derivatives leads to expressions for the frequency wavenumber intensity components 'i' associated with the different wave–types and/or directions as

a linear combination of frequency–wavenumber cross–spectra 'S_{lm}' of the signals from the array transducer channels 'l' and 'm', as follows ,

$$\tilde{P}_i(\bar{k},\omega) = \sum_{lm} a_{lm}.\tilde{S}_{lm}(\bar{k},\omega) \qquad 32.$$

where 'a_{lm}' are the coefficients of the cross–spectra 'S_{lm}' introduced from the finite difference approximation and the relationships between forces and measured responses. l and m can take values from 1 to 9.

This procedure is graphically represented in figure (2).

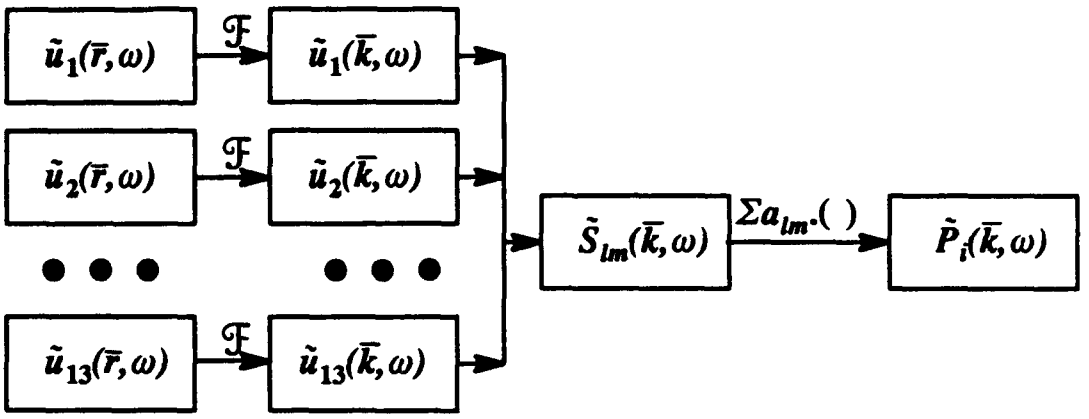

Figure 2. Measurement procedure for the frequency–wavenumber domain structural intensity. The wavenumber transform is taken over a spatial region of the structure (length or area).

Whether using the space averaged result or the convolution approach, the structural intensity estimates are only subject to finite–difference errors, provided phase and magnitude errors in the measurement have been eliminated or minimized. The finite difference errors can be limited by choosing the array dimensions appropriately [8,9]. The expressions for the x–components of the finite–difference based approximations of the piece wise space averaged structural intensity components associated with the various wave–types, in terms of the velocity cross–spectra are listed below.

The out–of–plane shear force component is

$$I_{qx} = \frac{1}{2}\, Imag\left[\frac{G'h}{\Delta\omega}(S_{32} - S_{12})\right] \qquad 33.$$

The out–of–plane bending moment component is

$$I_{mx} = \frac{1}{2}\, Imag \left[\frac{D}{4\omega\Delta^3} \{ (S_{33} - S_{11} - 2S_{23} + 2S_{21}) + \nu\,(S_{83} - S_{81} + S_{53} - S_{51} - 2S_{23} + 2S_{21}) \} \right] \quad 34.$$

The out–of–plane twisting moment component is

$$I_{tx} = \frac{1}{2}\, Imag \left[\frac{(1-\nu)D}{8\omega\Delta^3} (S_{98} - S_{95} + S_{48} - S_{45} - S_{78} + S_{75} - S_{68} + S_{65}) \right] \quad 35.$$

The in–plane longitudinal component is

$$I_{nx} = \frac{1}{2}\, Imag \left[\frac{Eh}{2\Delta\omega(1-\nu^2)} \{ (S^{uu}{}_{32} - S^{uu}{}_{12}) + \nu (S^{uv}{}_{82} - S^{uv}{}_{52}) \} \right] \quad 36.$$

The in–plane shear component is

$$I_{sx} = \frac{1}{2}\, Imag \left[\frac{Eh}{4(1+\nu)\Delta\omega} (S^{uv}{}_{82} - S^{uv}{}_{52} + S^{vv}{}_{32} - S^{vv}{}_{12}) \right] \quad 37.$$

where S_{ij} is the velocity cross–spectrum between channels 'i' and 'j'. The superscripts refer to the in–plane velocity components. The *y*–direction expressions are similar. Each of the cross spectra are functions of frequency and wavenumber.

Measurement Limits for Structural Intensity.

The transformation of the frequency–space domain structural intensity to the frequency–wavenumber domain involves the wavenumber spectrum estimation from the space–domain data. There are a number of methods available for this, including Fast Fourier Transform (FFT), Auto Regressive (AR), Moving Average (MA), Auto Regressive Moving Average (ARMA), Pisarenko Harmonic Decomposition (PHD), Maximum Entropy Method (MEM) and Maximum Likelihood Method (MLM).

The usual method for estimating the spectrum of discretely sampled deterministic and stochastic processes is based on the FFT. This approach has the advantage of being computationally efficient and is valid for a large class of signal processes. The most prominent limitation of the FFT approach is that of relatively low spectral resolution. A second limitation inherent in the method is the energy leakage in the spectral domain from the main lobe of the spectral response to the sidelobes. These two limitations have an especially detrimental effect when only short data record lengths are available.

The windowing of data is the fundamental factor that restricts the FFT's frequency resolution. This is a consequence of the implicit assumption that the finite length of measured data

is obtained by multiplying an infinite length of the sampled data sequence by a window function which is zero outside the measurement interval. This multiplication of the actual time–series by a windowing function implies that the overall transform is the convolution of the desired transform of the actual time–series with the transform of the windowing function. This convolution results in the spreading of a narrow–bandwidth signal into adjacent frequencies. This is the leakage phenomenon, which distorts the spectrum estimate from the desired true spectrum.

The most narrow spectral response of the transform estimate is limited to that of the main–lobe width of the window's transform, and is independent of the data. It is proportional to the reciprocal of the length of data being transformed. The type of window function chosen depends on the desired compromise between reducing leakage and increasing resolution. This trade–off occurs because when windows with tapered ends are used to obtain lower sidelobes, the main lobe width increases, reducing resolution.

The various alternative methods listed previously have been proposed to alleviate the inherent limitations of the FFT. These methods are often more restricted in the class of signals to which they are applicable. They can provide a substantial improvement in the spectral resolution and signal detectability. These performance advantages however, are strongly dependent on the Signal to Noise Ratio (SNR). It has been shown in previous studies [10] that for low enough SNRs, the alternative spectral estimates often provide no improvement over conventional FFT–based estimates. They have the further disadvantage of higher computational requirements. The structural intensity measurements can involve SNR values as low as –10 dB. At such low values of SNR, it is clearly advantageous to consider an FFT implementation of the space–wavenumber transformation. This provides a conservative estimate of the measurement limits, which can then be improved using alternative methods if necessary.

Of the two FFT–based spectral estimation techniques available, this analysis will consider the periodogram method in preference to the autocorrelation method. This is because the autocorrelation estimate can sometimes yield negative values for the PSD, which is physically unrealistic. Thus, when measured data is available only for samples $w_0, w_1, w_2, \ldots, w_{N-1}$, equally spaced Δx apart, the estimate of the spectrum is given by,

$$\tilde{W}_{PER}(k) = E\left\{\left(\frac{1}{N\Delta x}\right)\Delta x \sum_{n=0}^{N-1} w_n\, e^{-(j\,2\pi\, k_n \Delta x)}\right\} \qquad 38.$$

which is defined for the spectral interval $-1/(2\,\Delta x) \le k \le 1/(2\,\Delta x)$. It is to be noted that the expectation operator still needs to be applied. The use of the FFT thus permits evaluation of the

$\tilde{W}_{PER}$ (k) at a discrete set of N equally spaced spectral points $k_m = m\ \Delta k$ where m = 0, 1, ..., N–1 and $\Delta k = 1/(N\ \Delta x)$.

For the frequency–wavenumber domain structural intensity measurement using finite and small–length data sets, the wavenumber resolution is the limiting factor. The dispersion curves for the various wave–types approach each other as the frequency approaches zero. Consequently, there is a lower wavenumber limit, k_{min}, below which the wavenumber separation is lower than the available wavenumber resolution Δk . The frequency corresponding to this wavenumber is the lower frequency limit. Below this lower frequency bound, the FFT–based measurement cannot distinguish between the dispersion curves associated with the various wave–types. The upper frequency bound is the frequency corresponding to the maximum wavenumber that can be measured, and is given by the Nyquist criterion to be $k_{max} = \pi/(\Delta x)$. Above this wavenumber, aliasing phenomena will cause errors in the estimation of the spectrum.

Experimental Analysis

Experiments were performed using the proposed approach, on a Plexiglass model of a semi–infinite beam, 0.0254m thick, 1.17m long and 0.05m wide. One end of the beam was embedded in sand to provide an anechoic termination, as shown in figure (3). The excitation was provided using an electrodynamic shaker attached to the beam by direct threading at the free end.

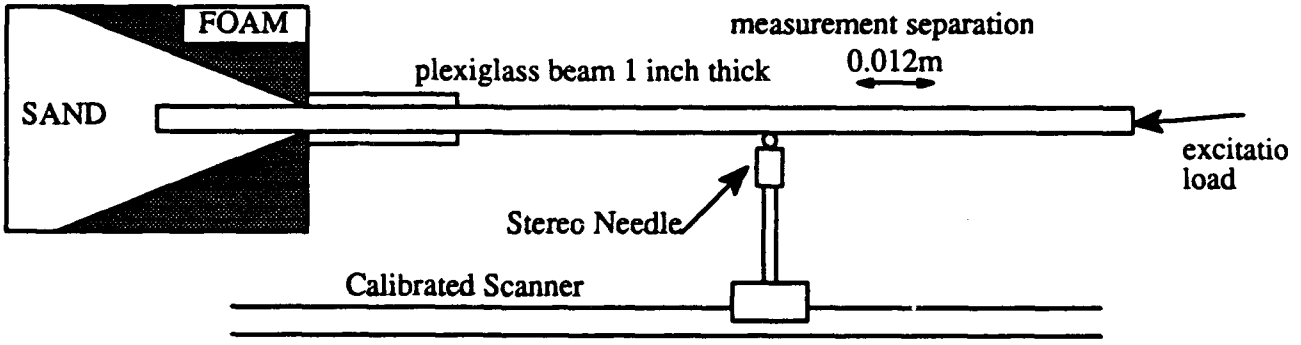

Figure 3. Experimental set–up for frequency–wavenumber intensity measurements

The frequency–wavenumber spectrum was obtained by measuring the response at 179 locations spaced 0.012m apart. The sample record was zero–padded to 256 points, and spatial–transformed. The limiting wavenumber is given by

$$k_{\max} < \frac{\pi}{\Delta} = \frac{\pi}{0.012} = 261.7m^{-1} \qquad 39.$$

where Δ is the measurement spacing. The beam–response measurement was performed using a Radio Shack stereophone cartridge as a velocity transducer. The model used had an operational upper frequency limit of 18 kHz. The excitation was consequently limited to 20 kHz. The frequency response estimate at each measurement location on the beam was obtained as a cross–spectrum between the acceleration at that location and the input load. The spatial transformed results for the acceleration and its spatial derivatives (obtained using finite differences) were then used to compute the structural intensity in the frequency–wavenumber domain..

The approach used is that based on a homogeneous spatial field. That is the structural intensity components are evaluated using expressions of the form of equations (17) to (21). This assumption is not quite correct in the case of the semi–infinite beam. and as will be shown later the results reflect this. The results of the analysis are shown in figure (4). The two intensity components observed correspond to the in–plane waves (the linear frequency–wavenumber relation) and the out–of–plane waves (the non–linear frequency–wavenumber relation). The horizontal axis corresponds to positive and negative wavenumbers bounded by the maximum value computed above. The vertical axis corresponds to the frequency axis with the 18kHz upper limit mentioned previously.

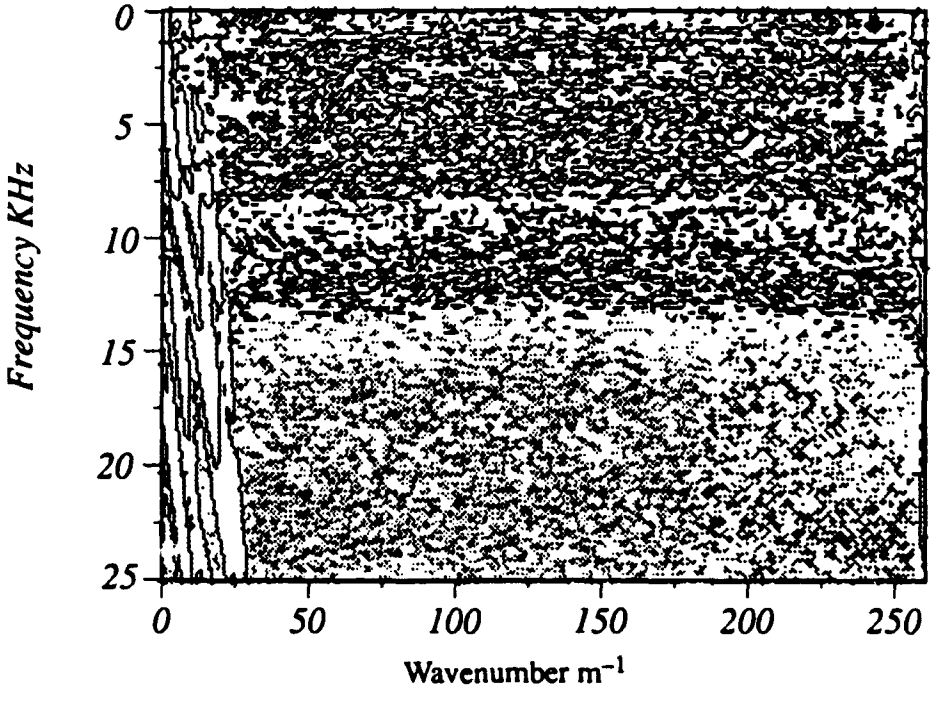

Figure 4. Experimentally measured frequency–wavenumber–domain intensity

Careful examination of the results in figure (4) reveals that while the general trends of the two components of intensity are as expected followed, the curves show some features which cannot be attributed to physical phenomena. For example, upon expansion of the wavenumber region containing the two curves it is observed that one of the curves does not start from the origin. These inaccuracies are attributed to the fact that for a semi–infinite beam, the response and structural intensity are monotonically decreasing away from the input. Therefore the approximation of a piecewise homogeneous spatial field is not appropriate. In this case a convolution approach to evaluate the structural intensity components from the estimates of the response and its derivatives should be used.

Conclusion

A method for discriminating between the components of the structural intensity propagating through a structure has been developed. The dependency of the measurement method and the evaluation of the structural intensity as a frequency–wavenumber function for both homogeneous and non–homogeneous response fields have been explored. The effects of expected noise and damping levels, as well as the relatively short data sets, on the measurements have been considered to obtain an understanding of the governing factors that control the quality and resolution of the results.

The proposed approach has been implemented on a semi–infinite beam, using the assumption of a homogeneous spatial response field. In this case, while the expected general trends can be observed in the results, there are inaccuracies which can only be attributed to the homogeneous field assumption. Analysis of the data without using this assumption will be explored in the future together with the analysis of the structural intensity for the beam if a structural discontinuity is introduced some distance away from the excitation point.

REFERENCES

22. Bracewell. "The Fourier transform and its applications". McGraw–Hill. second edition. 1978.
23. Mindlin R. D., "Influence of Rotary Inertia and Shear on Flexural Motions of Isotropic Plates", Journal of Applied Mechanics, Vol: 18, 31–38, 1951.
24. Kane T. R., Mindiin R. D., "High Frequency Extensional Vibration of Plates", Journal of Applied Mechanics, Vol: 23, 277–283, 1956.
25. Mindlin R. D., Medick M. A., "Extensional Vibration of Elastic Plates", Journal of Applied Mechanics, Vol: 26, 561–569, 1959.
26. Dubbleday P. S., "Effective Shear Modulus for Flexural and extensional waves in an Unloaded Thick Plate", Naval Research Lab report 8372, Orlando, Fl 1980.
27. L.Cremer, M. Heckl, and E. Ungar. "Structure–borne sound". Springer Verlag. second edition. 1989.
28. A. L. Pate et al. "Determination of structure–borne intensity in plates from acoustic imaging". Proc. of the third international congress on intensity techniques, 1990, 189–196.
29. G. Pavic'. "Structural surface intensity: an alternative approach in vibration analysis and diagnostics". JSV 1987, 115(3), 405–422.
30. W. Redman–White. "The measurement of structural wave intensity". 1983. Ph. D dissertation, Univ. of Southampton.
31. S. M. Kay and S. L. Marple. "Spectrum analysis– A modern perspective". Proc. IEEE 69 (11), Nov. 1981, 1380–1419.